NASA/TP-1999-209698

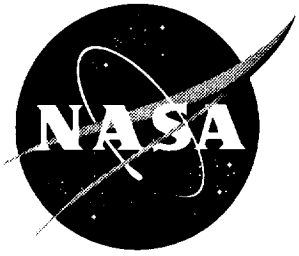

Piloted Simulation Study of a Dual Thrust-Cutback Procedure for Reducing High-Speed Civil Transport Takeoff Noise Levels

Donald R. Riley
Langley Research Center, Hampton, Virginia

Louis J. Glaab
Lockheed Engineering & Sciences Company, Hampton, Virginia

Jay M. Brandon and Lee H. Person, Jr.
Langley Research Center, Hampton, Virginia

Patricia C. Glaab
Unisys Corporation, Hampton, Virginia

December 1999

The NASA STI Program Office . . . in Profile

Since its founding, NASA has been dedicated to the advancement of aeronautics and space science. The NASA Scientific and Technical Information (STI) Program Office plays a key part in helping NASA maintain this important role.

The NASA STI Program Office is operated by Langley Research Center, the lead center for NASA's scientific and technical information. The NASA STI Program Office provides access to the NASA STI Database, the largest collection of aeronautical and space science STI in the world. The Program Office is also NASA's institutional mechanism for disseminating the results of its research and development activities. These results are published by NASA in the NASA STI Report Series, which includes the following report types:

- TECHNICAL PUBLICATION. Reports of completed research or a major significant phase of research that present the results of NASA programs and include extensive data or theoretical analysis. Includes compilations of significant scientific and technical data and information deemed to be of continuing reference value. NASA counterpart of peer-reviewed formal professional papers, but having less stringent limitations on manuscript length and extent of graphic presentations.

- TECHNICAL MEMORANDUM. Scientific and technical findings that are preliminary or of specialized interest, e.g., quick release reports, working papers, and bibliographies that contain minimal annotation. Does not contain extensive analysis.

- CONTRACTOR REPORT. Scientific and technical findings by NASA-sponsored contractors and grantees.

- CONFERENCE PUBLICATION. Collected papers from scientific and technical conferences, symposia, seminars, or other meetings sponsored or co-sponsored by NASA.

- SPECIAL PUBLICATION. Scientific, technical, or historical information from NASA programs, projects, and missions, often concerned with subjects having substantial public interest.

- TECHNICAL TRANSLATION. English-language translations of foreign scientific and technical material pertinent to NASA's mission.

Specialized services that complement the STI Program Office's diverse offerings include creating custom thesauri, building customized databases, organizing and publishing research results . . . even providing videos.

For more information about the NASA STI Program Office, see the following:

- Access the NASA STI Program Home Page at ***http://www.sti.nasa.gov***

- Email your question via the Internet to help@sti.nasa.gov

- Fax your question to the NASA STI Help Desk at (301) 621-0134

- Telephone the NASA STI Help Desk at (301) 621-0390

- Write to:
  NASA STI Help Desk
  NASA Center for AeroSpace Information
  7121 Standard Drive
  Hanover, MD 21076-1320

NASA/TP-1999-209698

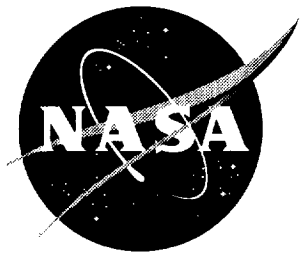

Piloted Simulation Study of a Dual Thrust-Cutback Procedure for Reducing High-Speed Civil Transport Takeoff Noise Levels

Donald R. Riley
Langley Research Center, Hampton, Virginia

Louis J. Glaab
Lockheed Engineering & Sciences Company, Hampton, Virginia

Jay M. Brandon and Lee H. Person, Jr.
Langley Research Center, Hampton, Virginia

Patricia C. Glaab
Unisys Corporation, Hampton, Virginia

National Aeronautics and
Space Administration

Langley Research Center
Hampton, Virginia 23681-2199

December 1999

Available from:

NASA Center for AeroSpace Information (CASI)
7121 Standard Drive
Hanover, MD 21076-1320
(301) 621-0390

National Technical Information Service (NTIS)
5285 Port Royal Road
Springfield, VA 22161-2171
(703) 605-6000

Summary

As part of a NASA and industry effort that addresses the potential airport-community noise problem of a High-Speed Civil Transport (HSCT), a piloted simulation study was performed for the purpose of indicating the noise reduction benefits and piloting performance that could occur for a typical 4-engine HSCT configuration during takeoff when a dual thrust-cutback procedure was employed with throttle operation under direct computer control. Two sequential thrust cutbacks were employed with the first cutback performed while the vehicle was accelerating on the runway and the second cutback performed at a distance farther downrange. Added vehicle performance improvements included the incorporation of high-lift increments into the aerodynamic database of the vehicle and the use of limited engine oversizing. Four single-stream turbine bypass engines that had no noise suppression of any kind were used with this configuration. This approach permitted establishing the additional noise suppression level that was needed to meet Federal Air Regulation (FAR) Part 36 Stage 3 noise levels for subsonic commercial jet aircraft. Noise level results of the study presented herein indicate 7 EPNdB less noise suppression was required to meet the FAR noise standards with the dual thrust-cutback procedure than with the standard takeoff procedure in FAR Part 36. Noise level differences due to variations in human piloting performance were less than 3/4 EPNdB in over 95 percent of the takeoffs performed. Noise level results were calculated with the jet mixing and shock noise modules of the Aircraft Noise Prediction Program (ANOPP) that was developed at Langley.

Introduction

As part of the NASA High-Speed Research Program, a six-degree-of-freedom piloted simulation study was undertaken at the Langley Research Center to address the potential problem of airport-community noise generated by a future High-Speed Civil Transport (HSCT) and the piloting issues involved. Reducing the high level of noise during takeoffs is one of several technological problems that must be solved before the HSCT can be certified for operation by the commercial airlines. In an attempt to reduce the noise level at the Federal Air Regulation (FAR) sideline noise certification location during HSCT takeoffs, a dual thrust-cutback procedure was postulated and examined. Two independent reduced-thrust levels were selected and arranged sequentially to reduce noise levels at the sideline and the centerline FAR Part 36 measurement locations, respectively. The dual thrust-cutback procedure coupled with a high-lift increment that was added to the configuration aerodynamics and the use of engine oversizing are included in the noise level assessment. The aircraft had four single-stream turbine bypass engines with no noise suppressors. Differences between the EPNdB levels presented herein and the levels mandated in FAR Part 36 Stage 3 indicate the amount of noise suppression needed to meet current noise certification standards. The basic premise of this study was the reduction of takeoff levels of jet mixing and shock noise at the sideline and the centerline flyover FAR measurement locations by reducing engine exhaust jet velocities through the use of reduced throttle settings.

The high-speed transport configuration used in this study was developed during the Supersonic Cruise Aircraft Research (SCAR) program of the 1970's. The configuration was used because of its representative HSCT character, the existence of a large wind-tunnel database, and the availability of the full six-degree-of-freedom piloted simulation program of reference 1. This aircraft was chosen because it provided a baseline configuration against which to compare some of the proposed technology advances for future HSCT configurations. (See refs. 2 and 3.) The engines of the configuration of reference 1 were replaced with turbine bypass engines for this study. This power plant is one of several candidate engines under consideration for the HSCT because of the high level of efficiency of the engine during cruise. References 4 and 5 provide additional information on airport-community noise levels produced during takeoff for several of the HSCT configurations considered herein.

Background

The FAR Part 36 Stage 3 requirements for subsonic commercial jet aircraft noise certification for the takeoff maneuver given in reference 6 require that the maximum sideline noise level following wheel liftoff from the runway surface, expressed in EPNdB, be less than a specified value that varies with aircraft takeoff gross weight. These Stage 3 noise levels may also be applied to future HSCT aircraft. The certification takeoff procedure allows the landing gear to be raised shortly after liftoff, but permits no throttle reductions to be made until the aircraft has reached an altitude of 689 ft. This latter requirement results in the microphones along the Stage 3 noise evaluation line in the vicinity of the measurement location for sideline noise certification to be exposed to engine full-throttle operation, and thus, very high noise levels. One possibility for reducing these large sideline noise values is to reduce engine thrust before the aircraft reaches wheel liftoff. A dual thrust-cutback procedure is employed in the study presented herein. The first thrust cutback is performed while the aircraft is still accelerating on the runway. The second thrust cutback is performed a short time later at a point further along the

trajectory, but before the aircraft passes over the centerline measuring station. The final throttle setting is selected so that the aircraft can maintain a constant-speed 4-percent climb gradient. Although the dual thrust-cutback procedure violates current FAR Part 36 regulations, the use of a fully automated throttle operation with an automatic throttle under direct computer control with the pilot out-of-the-loop may be an acceptable alternative to the present FAR Part 36 takeoff requirements when applied to future HSCT aircraft. The final 4-percent climb gradient part of the trajectory meets the present FAR Part 36 regulations.

Nomenclature

The aerodynamic force and moment coefficients are illustrated in figure 1 with the body system of axes that were used for motion calculations. A dot over a symbol represents a derivative with respect to time. The symbols and abbreviations are defined as follows:

b	wing span, ft
C_D	drag coefficient, (Aerodynamic drag)/$q_\infty S_W$
C_L	lift coefficient, (Aerodynamic lift)/$q_\infty S_W$
C_l	rolling moment coefficient, (Aerodynamic rolling moment)/$q_\infty S_W b$
C_m	pitching moment coefficient, (Aerodynamic pitching moment)/$q_\infty S_W \bar{c}_w$
C_n	yawing moment coefficient, (Aerodynamic yawing moment)/$q_\infty S_W b$
C_T	thrust coefficient, (thrust)/$q_\infty S_W$
C_y	side force coefficient, (Aerodynamic side force)/$q_\infty S_W$
C_μ	BLC blowing coefficient, (Thrust produced by BLC)/$q_\infty S_W$
$\bar{c}_w$	wing mean aerodynamic chord, ft
D	aerodynamic drag, lb
DLδA	aileron deflection limit, deg
DLδAI	inboard flaperon deflection limit, deg
DLδAO	outboard flaperon deflection limit, deg
DLδR	rudder deflection limit, deg
EPNdB	effective perceived noise in decibels
G_{ENG}	engine dynamics gain value
g	acceleration due to gravity, 32.17 ft/sec^2
h	altitude, ft
IAS	indicated airspeed, knots
I_x, I_y, I_z	moments of inertia about body axes, slug-ft^2
I_{xz}	product of inertia, slug-ft^2
K	control system gain (subscript specifies use)
K_{ARI}	aileron and rudder interconnect gain, deg/deg
K_{ay}	lateral acceleration feedback gain, deg/g units
K_p	roll rate gain, deg/(deg/sec)
K_{pc}	roll rate command gain, (deg/sec)/deg
K_{PY}	roll rate feedback gain, deg/(deg/sec)
K_q	rate command scaling gain, deg/(deg/sec)
K_{q_c}	rate command gain, (deg/sec)/deg
K_r	yaw rate feedback gain, deg/(deg/sec)
K_{r_ϕ}	coordination gain, deg/deg
K_{size}	engine sizing factor
K_{WL}	wings leveler gain, deg/deg
$K_{\dot{\beta}}$	estimator feedback gain, deg/(deg/sec)
$K_{\delta a}$	aileron control gearing, deg/deg
$K_{\delta afi}$	inboard flaperon control gearing, deg/deg
$K_{\delta afo}$	outboard flaperon control gearing, deg/deg
K_θ	pitch attitude command gain, deg/deg
$K_{\delta PED}$	pedal to rudder gearing, deg/in.
K_{θ_H}	pilot attitude command gain, deg/(deg/sec)
K_ϕ	bank angle feedback gain, deg/deg
K_{ϕ_2}	SCAS gain, deg/deg
$K_{\phi_{TC}}$	wings leveler rate gain, (deg/sec)/deg
L	aerodynamic lift, lb
L_{ARI}	aileron and rudder interconnect gain authority limit, deg
L/D	lift drag ratio
$(L/D)_{max}$	maximum lift drag ratio
LPR	pedal to rudder gearing limit, deg
LSA	control system authority limit, deg
LSR	stability augmentation system authority limit, deg
M	Mach number
$Ny_{p.s.}$	lateral acceleration at pilot station, g units
P_{RAH}	wings leveler, RAH switching criterion, deg/sec
PLA	engine power lever angle (throttle deflection), deg
PLA_{pilot}	pilot throttle input

PLAF1	throttle position for flight idle
PLAG1	throttle position for ground idle
PLAMAX	throttle position for maximum thrust
PLAMRT	throttle position for maximum reverse thrust
PLδht	horizontal tail deflection limit, deg
p, q, r	angular velocities about body axes, deg/sec
PCL	pitch control system limit, deg
PSL	pitch rate command authority limit, deg
q_∞	dynamic pressure, lb/ft^2
RAH	roll attitude hold
RL$^+$, RL$^-$	engine dynamics rate limits
RLδA	aileron rate limit, deg/sec
RLδAI	inboard flaperon rate limit, deg/sec
RLδAO	outboard flaperon rate limit, deg/sec
RLδht	horizontal tail deflection rate limit, deg/sec
RLδR	rudder deflection rate limit, deg/sec
S	Laplace variable
S_W	wing area, ft^2
SASR	rudder stability augmentation system
SCAS	stability and control augmentation system
T	total thrust force on vehicle, lb
T_{DRAG}	engine ram drag, lb
$T_{DRAG_{REF}}$	reference engine ram drag, lb
T_G	engine gross thrust, lb
T_{GC}	commanded engine gross thrust, lb
T_{GMAX}	full-throttle engine gross thrust, lb
T_{GMIN}	flight-idle engine gross thrust, lb
T_{GREF}	reference engine gross thrust, lb
T_{GRC}	engine gross thrust ratio command
T_{GROSS}	engine gross thrust, lb
T_{NET}	engine net thrust, lb
T_0	thrust at brake release, percent
T_1	thrust after first cutback, percent
T_2	thrust after second cutback, percent
V	airspeed, knots
V_c	climb speed, knots
V_R	rotation speed, knots
V_j	exhaust jet velocity, ft/sec
$V_{j_{max}}$	exhaust jet velocity at full-throttle setting ft/sec
W	airplane weight, lb
$X_B, Y_B, Z_B,$	Cartesian coordinate system of body axes with origin located at vehicle center of gravity
X	longitudinal distance from brake release, ft
X_1	initiate first thrust cutback
X_2	end first thrust cutback
X_3	initiate second thrust cutback
X_4	end second thrust cutback
α	angle of attack, deg
β	angle of sideslip, deg
$\dot{\beta}_{LIM}$	estimator authority limit, deg/sec
γ	flight-path angle, deg
Δ	an increment
ΔPLA	computer commanded autothrottle input, deg
δ_a	aileron deflection, deg
$\delta_{a\ trim}$	aileron trim deflection, deg
δ_{ac}	commanded aileron deflection, deg
δ_{afi}	inboard flaperon deflection, deg
δ_{afo}	outboard flaperon deflection, deg
$\delta_{c_{pilot}}$	pilot hand controller pitch input, deg
δ_f	trailing-edge flap deflection, deg
δ_{ht}	horizontal tail deflection, deg
δ_{htc}	commanded horizontal tail deflection, deg
$\delta_{ht_{trim}}$	pilot horizontal-tail trim input, deg
δ_{PED}	rudder pedal deflection, in.
δ_r	rudder deflection, deg
δ_{rc}	commanded rudder deflection, deg
$\delta_{r\ trim}$	trim rudder deflection, deg
$\delta_{W\ pilot}$	pilot hand controller roll input, deg
δ_{WRAH}	wings leveler, RAH switching criterion, deg
θ	vehicle pitch attitude, deg
θHLIM	attitude command limit, deg
θ_{trim}	vehicle pitch-attitude trim setting, deg
τ	time constant (subscript specifies use), sec
τ_r	yaw rate feedback time constant, sec
τ_w	hand controller roll time constant, sec
ϕ	vehicle roll angle, deg
ϕ_{WL}	wings leveler, bank angle switching criterion, deg

Abbreviations:

ANOPP	Aircraft Noise Prediction Program
AOA	angle of attack
ARI	aileron-rudder interconnect
BLC	boundary-layer control
CGI	computer generated image
CL	centerline
CRT	cathode ray tube
c.g.	center of gravity
DAC	digital-to-analog converter
DOT	Department of Transportation
EADI	electronic attitude director indicator
EPNL	effective perceived noise level
FAA	Federal Aviation Administration
FAR	Federal Air Regulation
FCS	flight control system
HSCT	High-Speed Civil Transport
HSI	horizontal situation indicator
HUD	heads-up display
MAC	mean aerodynamic chord
Ref	reference
SL	sideline
TBE	turbine bypass engine
VMS	Langley Visual/Motion Simulator
VSCE	variable stream control engine

Description of Simulated Aircraft

The supersonic transport concept that was used in this study is designated AST-105-1 and is the same configuration that was used in the piloted simulation study reported in reference 1. The configuration was originally designed to transport 273 passengers in 5 abreast seating at a Mach number of 2.62 for a distance of 4500 miles. A detailed description of the vehicle that includes a summary of the aerodynamic database is given in reference 7. Some additional details are provided in reference 1. A three-view sketch of the simulated airplane is given in figure 2. Vehicle weight, moments of inertia, and geometric characteristics are given in table I.

The aircraft design employs an arrow-shaped wing that incorporates leading-edge sweep angles of 74°, 70.84°, and 60° across each semispan. A sketch of the left semispan that indicates the various control elements is given in figure 3. For takeoff, the outboard flaperons and ailerons are deflected down 5° from the neutral position to provide additional lift. The apex and the Krueger flaps are deflected 30° and 45°, respectively, and remain fixed during the initial climb out. In addition, wing spoilers and a speed brake are available during landing approaches. An all-movable vertical tail provides directional control and an all-movable horizontal tail with a geared elevator provides pitch control. The rigid outboard vertical fins shown in figures 1 and 2 were employed to improve the directional stability of the configuration. For this study the c.g. of the vehicle was located in the plane of symmetry and positioned longitudinally at 60.1 percent of the wing mean aerodynamic chord. This c.g. location was also used in the study reported in reference 1 and was the most aft location chosen for this design, as noted in reference 7. For this c.g. position, the vehicle was statically unstable longitudinally with a static margin of −3.7 percent, and thus, required an upload on the horizontal tail for trim. When positioned on the runway, the longitudinal axis of the vehicle was pitched downward 5°. For improved pilot visibility in the terminal area, the vehicle nose was deflected downward an additional 12°.

The landing gear consisted of left and right main units and nose wheels. The mathematical model in the simulation of this arrangement was extensive and included the complete strut deflections and strut dynamics for each landing gear unit to provide realistic vehicle motion response. The runway mathematical database included runway crown and surface roughness.

The engines chosen for this study were scaled versions of a single-stream turbine bypass engine (TBE) that was designed for a cruise Mach number of 2.4 and modeled with the Navy-NASA Engine Program of reference 8. The four engines were scaled to provide a thrust-to-weight ratio of 0.295 for takeoff at sea level. The engines as designed had no noise suppressors or acoustic treatment of any kind. Engine transient response times used herein were approximately 4.8 sec for acceleration from flight idle to maximum thrust and 3.4 sec from maximum to flight idle. A computer programmable automatic throttle option was available in the simulation and was employed for all takeoffs that used the dual thrust-cutback procedure. Additional engine details are contained in appendix A.

For the study reported herein, the Pratt and Whitney VSCE engines of the AST-105-1 original design discussed in reference 1 were replaced by TBE-M2.4 engines. No readjustments to the aerodynamic database and no resizing of the configuration to optimize for the cruise condition were undertaken because the study was limited to the takeoff flight phase.

Description of Apparatus

The tests were performed in the Langley Visual/ Motion Simulator (VMS), which is a hydraulically operated, six-degree-of-freedom, six-legged synergistic motion base. (See fig. 4.) Six computed leg positions were used to drive the motion base. The transformation equations that computed the leg extensions, the filter characteristics that smoothed the computed drive signals from the DAC outputs, and the performance limits of the VMS are given in references 9, 10, and 11, respectively. The washout system used to present the motion-cue commands to the motion base was the coordinated adaptive washout system reported in references 12 and 13 with some adjustment of the parameter values to improve base response for this study.

The pilot's compartment consisted of a general purpose transport type arrangement with CRT displays to provide normal flight information to the pilot. A photograph of the cockpit is shown in figure 5. Duplicate EADI and HSI are provided to the pilot and the copilot and two center CRT displays provided identical engine information. Figure 6 shows an enlarged sketch of the EADI that identifies the various elements used during a takeoff. A CGI system generates the out-of-the-window visual scenes, which were displayed to the pilots by color monitors that were viewed through beam splitters and infinity optics. Forward and side window views were available to the pilot and the copilot. Engine throttle controls, located on the center console, are visible forward of the pilot's right hand in figure 5. These throttle controls could be either operated manually or driven by the computer programmable autothrottle feature that is available in this simulation. Flap, spoiler, and speed brake controls are also located on the center console. A two-axis hand controller located on the left side permitted the pilot to make pitch and roll control inputs to the simulated vehicle. Rudder pedals permitted directional control inputs to be made. Force-feel characteristics were programmed for both axes of the hand controller and also the rudder pedals. The control system employed was a rate-command attitude-hold system. Details of the hand controller, rudder pedals, and flight control systems are contained in appendix B.

The VMS is driven by a real-time digital simulation system that uses a Control Data CYBER 175 series computer. The dynamics of the simulated airplane were calculated by using six-degree-of-freedom nonlinear equations of motion computed at an iteration rate of 32 frames per sec.

Description of Noise Level Computations

Figure 7 briefly outlines the overall information flow of this study. The pilot in the simulator cockpit utilizes the hand and foot controllers, the panel instruments, the out-of-the-window visual scene, and the motion cues supplied by the six-degree-of-freedom motion base to fly various takeoff trajectories. Several flight control systems were available, as well as automated throttle controls. The resulting flight trajectories coupled with the appropriate engine characteristics serve as the information input to the Aircraft Noise Prediction Program (ANOPP). The calculations performed in ANOPP (ref. 14) generate the corresponding ground noise contours, as well as provide the numerical values for the noise levels at the centerline, sideline, and approach certification measuring locations. The values are calculated as EPNL in EPNdB (effective perceived noise level in decibels) as specified by the FAR Part 36 regulations. Note that the noise values presented herein are the combined value for jet-mixing and shock noise only and were calculated for a standard day. Noise calculations in ANOPP (ref. 14) were made with the module for jet-mixing noise described in reference 15 and the module for shock noise described in references 16 and 17. Other noise sources, such as engine-inlet noise, and airframe noise, were not included in this study. Although of much smaller magnitudes, these noise sources should be considered when determining the total overall noise levels. All microphones in this study were placed at a height of 4 ft above ground level.

Basic Considerations

The basic approach used herein to reduce noise levels at the sideline and the centerline measurement locations was to reduce exhaust jet velocities by lowering throttle settings at specified times during the takeoff and the initial climb-out maneuver. The various means employed to accomplish this task are briefly described in the following sections.

Dual Thrust-Cutback Procedure

Thrust reductions during the takeoff maneuver were commanded by the computer and based on the distance of the aircraft from the brake release point as shown in figure 8. Distances X_1 and X_2 were selected to provide large reductions in the sideline noise level. Distances X_3 and X_4 were chosen to provide reductions in the centerline noise level. The thrust value commanded at location X_2 was chosen to permit the aircraft to accelerate along the flight path to approach 250 knots at location X_3. The thrust value chosen depended on the constant flight-path climb gradient to be flown between locations X_2 and X_3. The thrust value chosen at location X_4 permitted the aircraft to stabilize on a 4-percent climb gradient at a constant IAS of 250 knots.

High-Lift Aerodynamic Increments

To address the impact of high-lift aerodynamic improvement on the sideline and the centerline noise levels during takeoff, two lift increments were added to the aerodynamic database. One increment was obtained from wind-tunnel test data of a model of the AST-105-1 configuration with and without blowing boundary-layer control over the upper surface of the two inboard flap elements on each wing semispan. A larger increment ($\Delta C_L = 0.10$) was included to represent a potentially achievable value for future HSCT configurations. Airframe noise was assumed negligible and noise generated from producing the additional lift increment was not accounted for in the study. An indication of the performance improvement of the aircraft configuration due to the addition of the high-lift increments is shown in figure 9. This figure presents the L/D curves for the baseline and the two high-lift configurations. The improvements shown in L/D, and particularly $(L/D)_{max}$, due to the addition of high-lift increments permit a reduction in thrust settings, and thus, a corresponding reduction in noise level. Observe that the final climb segment to be performed at an IAS of 250 knots has the configuration operating in the vicinity of $(L/D)_{max}$. Also, 250 knots is the maximum speed permitted by the FAA for flight operations under an altitude of 10 000 ft. Further discussion with additional details on the effect of the two high-lift increments is contained in appendix C. It should be noted that the aerodynamic increments due to flap BLC are used in this paper only as an example of a realistic achievable improvement in high-lift aerodynamic performance and not proposed as a HSCT high-lift application. The magnitudes of the added lift increments that are used here can undoubtedly be obtained by other means. For this reason, the engine sizes in this study did not incorporate the bleed-air requirement for providing flap BLC.

Engine Oversizing

At higher throttle settings, the major contributor to both sideline and centerline EPNdB values is jet-mixing noise. Jet-mixing noise, in turn, is exponentially dependent on the magnitude of the exhaust jet velocity. As a consequence, any reduction that can be made in exhaust jet velocity will have a large impact on the EPNdB values. For this reason, limited amounts of engine oversizing can be considered as a possible means of obtaining lower exhaust jet velocities and yet maintain a given level of thrust. As throttle settings are reduced, shock noise becomes a larger percentage of the total noise, and thus, can become more of a contributor to the total EPNdB value. However in this instance, engine oversizing reduces the combined value of jet-mixing and shock noise. As used herein, engine oversizing is simply an increase in the mass flow through the engine by increasing the original jet cross-sectional area. All values of the thermodynamic properties, as well as jet exhaust velocity at any given throttle setting, are retained. Thus, the increased thrust from increased mass flow permits lower throttle settings to achieve the same thrust at a given flight condition.

Test Subjects

Three pilots participated in this study. One pilot was a senior NASA research pilot with extensive experience in multiengine aircraft, which includes the position of principle pilot of the NASA Boeing 737 research aircraft. Another pilot (pilot B) was a multiengine-rated flight instructor and the remaining pilot (pilot G) was instrument-rated. All three pilots had extensive flight simulator experience. During this study, all three pilots flew simulated takeoffs with the baseline configuration both with and without the aerodynamic high-lift additions and the engine oversizing.

Task of the Pilot

The pilot's task was to set the trailing-edge flaps to 20° for takeoff, select the automatic throttle mode for engine operation, release the brakes, start the takeoff roll, and steer the aircraft down the runway. At a V_R of 200 knots, the pilot initiated rotation with a pitch rate of about 3 deg/sec and performed the liftoff. The pilot set the desired vehicle pitch attitude using the command bar guidance on the EADI that provided the instantaneous pitch attitude for a desired climb gradient to be flown. He then maintained the climb gradient indicated by the command bar for the remainder of the flight. The landing gear was raised shortly after takeoff and the aircraft was permitted to accelerate along the climb gradient until the IAS reached 250 knots. Automatic throttle operation commanded the proper thrust level at the appropriate longitudinal distance from brake release during the takeoff and the initial climb-out procedure. The FAR noise certification procedures require flight trajectories to be aligned with the extended runway centerline with deviations within specified limits. Pilots monitored vehicle lateral position with the localizer display. Simulation flights were terminated when the airplane reached a distance of 8.5 n.mi. from brake release.

Presentation of Results

Results of this study are presented in three main parts. Part I presents and discusses noise levels that result from varying a single takeoff task parameter in an attempt to determine parameter values that achieve the lowest sideline and/or centerline EPNdB levels. Part II provides an overall noise level reduction assessment of the dual thrust-cutback procedure for takeoff by comparing noise levels of the dual thrust-cutback procedure with

those from the single thrust-cutback of the FAA noise certification procedure. Finally, Part III presents some observations concerning pilot variability on noise level values and some comments on flight safety and piloting by the participating NASA research pilot.

Five appendixes (A through E) are included in this paper. Appendix E, entitled "Further Noise Reductions and Operational Constraints," contains additional information relevant to this study.

Results and Discussion

Noise characteristics of the simulated HSCT were obtained during takeoff at the sideline and the downrange centerline locations and during landing at the approach location as specified in reference 6 and indicated in figure 10. Only a few landing flights were performed for the purpose of establishing the approach EPNdB value for use in the noise trades considered herein. In addition, calculations were carried out with ANOPP that provided noise level distributions for various takeoffs; however only the values at the FAR certification measuring locations are presented in this paper. To provide some indication of data variability, a number of repeat simulator takeoff flights were performed for a given set of test conditions and these results appear as multiple data points on the various figures.

Part I: Basic Parameter Variations

Effect of location of first thrust cutback. A number of preliminary runs were made to determine the thrust level that established the aircraft on a constant-speed 4-percent climb gradient and then permitted selection of the final thrust-cutback distances X_3 and X_4 that minimized the EPNdB centerline flyover noise value. Distances of 18240 ft (X_3) and 20672 ft (X_4) were determined to yield near minimum noise levels at the FAR Part 36 centerline noise measurement location. These values were used for all simulation runs with only one exception. With these X_3 and X_4 values held constant, a series of takeoffs were then performed for different longitudinal positions of first thrust cutback. Results for both thrust settings and noise levels are given in figure 11. The data show that a reasonable reduction in the sideline EPNdB value can be achieved when first thrust cutback is initiated at a distance along the runway between 7000 and 8000 ft from brake release. Thrust cutbacks performed earlier produced larger sideline EPNdB values because of the larger thrust settings needed to accelerate the aircraft to reach 250 knots after the second cutback was complete. Thrust cutbacks performed later in the takeoff resulted in more of the higher full-throttle engine noise to be measured by the sideline microphone. In contrast, centerline noise levels, as might be expected, show little influence of the first thrust-cutback location. Figures 11(a), 11(b), and 11(c) show the results for the baseline vehicle alone and with the two aerodynamic lift additions. All data sets show that a minimum sideline noise level exists and that the lowest sideline noise level was obtained when the computer-commanded thrust values were reduced over approximately a 2000-ft distance. The results in figure 11 are shown as a function of X_1 for convenience. The major influence is, of course, the position of the thrust-cutback distances X_1 and X_2 with respect to the wheel liftoff location. It is interesting to observe that for the results shown in figure 11, the vehicle rotation point falls between X_1 and X_2 for sideline noise levels that were near the minimum. Thus, the first thrust cutback is initiated before vehicle rotation occurs and ends after rotation is in progress. Finally, the data in figure 11 indicate that for a given configuration, some latitude exists in selecting a thrust-reduction distance ($X_2 - X_1$) because the minimum sideline noise level for each of the three data curves is within 1 EPNdB of the others.

Effect of high lift. The data in figure 11 for $X_2 - X_1$ = 2000 ft for the different configurations are presented in figure 12 and indicate the effect of adding aerodynamic high-lift capability to the basic aircraft. Adding flap boundary-layer control or the $\Delta C_L = 0.10$ increment to the baseline configuration reduces the sideline noise level because of the reduction in the thrust level required at the first thrust cutback. In addition, the longitudinal position of the minimum EPNdB value occurs closer to the brake release point because of the reduced airplane angle of attack needed for liftoff. As expected, centerline noise levels also are reduced with the addition of aerodynamic high-lift capability. The effect on thrust settings and noise levels of adding high lift to the basic aircraft configuration for all thrust reduction distances considered is shown in figure 13. The figure shows that providing improved aerodynamic lift reduces both the throttle settings required for takeoff and the sideline and the centerline noise levels. For the configuration with $\Delta C_L = 0.10$, a noise reduction of 2.1 EPNdB for the sideline and 4.6 EPNdB for the centerline appears achievable. The noise values presented in figure 13 are the minimum levels presented in figures 11 and 12. (Some operational requirements of FAR Part 25 that impact these takeoffs are considered in appendix D.)

Effect of engine oversizing. Oversized engines that provide increased mass flow while maintaining the same full-throttle exhaust jet velocities as the standard engines can be used to provide limited reductions in both sideline and centerline noise levels during takeoff. The oversized engine capability can be employed in one of two distinctly different ways. One way is to utilize

full-throttle operation at brake release, and thus, capitalize on the additional thrust to shorten the takeoff roll. A larger thrust cutback on the runway can be used because of the presence of a longer distance $X_3 - X_2$, which results in a lower sideline noise level. In addition, a shortened takeoff roll results in the aircraft acquiring more altitude over the centerline microphone, which yields a lower flyover noise level. The alternate way is to use a reduced throttle setting at brake release to provide the identical thrust profile and flight trajectory as obtained with the standard engines, but with lower exhaust jet velocities over the entire takeoff maneuver. Engine oversizing used in this manner provides reduced noise levels at all locations surrounding the flight path. Noise results and corresponding net-thrust levels as a function of the engine sizing factor K_{size} for the configuration with $\Delta C_L = 0.10$ for both methods are presented in fig- ures 14(a) and 14(b), respectively.

For takeoffs with full throttle applied at brake release (fig. 14(a)), first thrust-cutback distance X_1 has been shortened to obtain minimum noise levels for the oversized engines. Unfortunately a reduced X_1 distance of 6000 ft penalizes the configuration with the standard engine ($K_{size} = 0.773$) because larger thrust settings are required at first thrust cutback, and hence, larger noise levels are obtained than the minimum levels given in all previous figures. As a consequence, an additional data set is presented for the standard engines for $X_1 = 7000$ ft, which gives a sideline noise level near the minimum. Figure 14(b) provides the results for the three engines sizes for a single X_1 distance. The throttle settings for the different engine sizes were adjusted to produce the same thrust values at all points along the takeoff trajectory. The results indicated in both figures show that increasing engine size reduces both sideline and centerline noise levels. In addition the results indicate that the use of 10-percent oversized engines, under consideration by both Boeing Commercial Airplanes and Douglas Aircraft Company for possible use on a future HSCT, can provide approximately 2 EPNdB reduction in both sideline and centerline noise levels.

To provide an indication of the effect of varying the downrange location of the second thrust-cutback location, an additional flight was made for the configuration with the 10-percent oversized engines. These results are indicated by the diamond symbols on figure 14(a). Sideline and centerline noise levels appear nearly coincident and result from an earlier second thrust-cutback location. Sideline noise levels increase because of the increased thrust, which is required when reducing the distance defined by $X_3 - X_2$; whereas, flyover noise levels are reduced because of the increased distance from the centerline microphone station when second thrust cutback occurs. Thus, it appears that limited adjustment in the magnitudes between the sideline and the centerline noise levels is available through selective positioning of the second thrust-cutback location.

For completeness and to provide an additional comparison, noise levels and thrust values as a function of first thrust-cutback location X_1 are presented in figure 15 for the following three configurations: the baseline configuration, the configuration with the $\Delta C_L = 0.10$ addition, and the configuration with the $\Delta C_L = 0.10$ addition and 10-percent engine oversizing. The data shown in figure 15 illustrate the reduction in sideline and centerline noise levels due to added lift increase and engine over-sizing. The results also show the reduction in the X_1 value for minimum sideline noise level as the additions are made to the baseline configuration. Finally, individual results are provided for two of the pilots to illustrate the consistency of the piloting performance.

Effect of first climb gradient. A number of simulator flights were made in which the initial climb gradient was varied from 4 percent to 8 percent to achieve higher aircraft altitudes over the centerline microphone station, and thus, lower centerline noise levels. These simulated flights were made for the aircraft configuration with the $\Delta C_L = 0.10$ high-lift addition and 10-percent oversized engines. The results are presented in figure 16 for two sets of throttle-programmable distances for X_1 through X_4. Both data sets are included to illustrate the effect of first climb gradient. Note that the climb gradient after second thrust cutback was always 4 percent as specified by the FAR Part 36 requirements. Examination of the figure shows that increasing the first climb gradient above 4 percent increased the sideline noise level because of the increase in net thrust required for the higher climb rate. Also, increasing the first climb gradient above 4 percent decreased the centerline noise level because of the higher altitude achieved over the centerline microphone station. The results point out the desirability of using a 4-percent climb gradient after the first thrust cutback. A comparison of the numerical values for both noise levels and thrust values for the 4-percent climb gradient given on figure 16 differ from those in all the preceding figures because of differences in the computer programmable thrust-cutback distances X_1 through X_4.

Effect of reduced initial thrust. A few simulator flights were made with a different takeoff procedure to assess the sideline noise reduction potential when throttle settings for the basic engine were set at a value less than maximum at brake release. Following brake release, the vehicle was permitted to accelerate down the runway until it reached the same runway location for rotation that was encountered during full-throttle takeoffs with the dual thrust-cutback procedure. Thus, this takeoff scheme

utilized the same available ground roll distance. The automatic throttles were programmed to eliminate the first thrust cutback and maintain a constant thrust setting. Rotation was then initiated at a speed less than 200 knots and a 4-percent climb gradient was established. The vehicle was permitted to accelerate until it reached 250 knots at the downrange location of the second thrust-cutback point where thrust was reduced to establish the constant-speed 4-percent climb gradient. Noise levels and corresponding thrust values were obtained for the basic aircraft configuration and the configuration with the high-lift additions. The results are given in table II. Also shown are the values for the dual thrust-cutback procedure. An examination of the table shows sideline noise levels are lower by between 3 and 4 EPNdB for the dual thrust-cutback procedure than for the reduced initial thrust procedure. As a consequence, further consideration of lower initial thrust settings of the basic engine at brake release for noise abatement was not undertaken. The reduced-thrust procedure did, however, provide lower noise levels than those produced by a full-throttle takeoff with no thrust cutback.

Part II: Noise Reduction Assessment

An overall noise reduction evaluation for takeoffs with the dual thrust-cutback procedure can be made by comparing the EPNdB value of the noise suppressors that must be installed on the aircraft to meet the FAR Part 36 Stage 3 noise standards for the dual thrust-cutback procedure and that for the standard operating procedure. The addition of the high-lift $\Delta C_L = 0.10$ increment and 10-percent engine oversizing are included for both takeoff procedures. Assessment results are shown in figure 17.

As a point of reference, a full-throttle takeoff was performed and the resulting noise levels are listed on the left side of the figure under "Standard Operating Procedure" in figure 17. For this takeoff, the pilot commanded full throttle at brake release, accelerated the vehicle down the runway, performed the rotation, and then the liftoff. The landing gear was then retracted and the pilot pitched the aircraft to acquire a 4-percent climb gradient. The vehicle was permitted to accelerate until the airspeed reached 250 knots, which is the maximum speed permitted by the FAA for flight operations under an altitude of 10 000 ft. At this time the pilot pitched the aircraft to maintain 250 knots. The run was terminated at 8.5 n.mi. from brake release. The EPNdB noise levels calculated by ANOPP and shown in figure 17 for this takeoff are very large as expected. For comparison note the certification standards given in the lower center of the figure.

The FAR Part 36 regulations of 1993 permit a single thrust reduction to be made for noise certification but only after the aircraft passes an altitude of 689 ft. The pilot's task for the single thrust-cutback procedure is similar to the full-throttle case until a preselected cutback altitude is acquired. At the preselected altitude, the copilot reduces engine thrust and the pilot pitches the vehicle down to establish a constant-speed 4-percent climb gradient. The noise results in figure 17 indicate that a large reduction occurred in the centerline noise level. No change, however, occurred in the sideline noise level because the thrust cutback was performed sufficiently downrange of the sideline certification location to have little impact on the sideline noise level.

The addition of high-lift aerodynamics ($\Delta C_L = 0.10$) reduces the centerline noise level, as would be expected, because of the lower thrust setting required at cutback, but has little influence on sideline noise for the same reason as discussed previously. One possibility of reducing sideline noise is to employ engine oversizing as suggested by both Boeing Commercial Airplanes and Douglas Aircraft Company. By increasing the mass flow while retaining the same jet velocity magnitude, the pilot can command the same takeoff thrust by using less than maximum throttle deflection. Thus, the same thrust profile can be flown as for the single thrust-cutback case, but with a lower exhaust jet velocity, and hence, lower noise levels. The sideline noise levels in figure 17 show about a 2 EPNdB improvement in noise level for the configuration using the oversize engines. Combining high lift and 10-percent engine oversizing yields the lowest values for the noise level with the FAA single thrust-cutback procedure. Differences between the noise levels thus obtained and the FAR Part 36 Stage 3 certification standards provide the minimum untraded noise level reduction that must be contributed by the engine noise suppressors. If it is assumed that the maximum noise value of 2 EPNdB can be applied to the sideline noise values, then the results indicate 22 EPNdB of noise reduction must be provided by the engine noise suppressors to meet the FAR Part 36 Stage 3 certification standards. This is beyond the demonstrated capability of present day suppressor technology.

For flights with dual thrust-cutback procedures, the engine throttles were computer driven with thrust reduction programmed as a function of distance from brake release. Two sequential thrust cutbacks were employed. The first cutback was initiated prior to vehicle rotation while the aircraft was still accelerating on the runway. The second cutback was performed a short distance before reaching the centerline microphone station. The thrust levels were programmed prior to brake release so that the pilot simply established and maintained a 4-percent climb gradient after wheel liftoff to run termination.

A comparison of noise levels for full throttle with the noise levels for dual thrust-cutback procedures for the vehicle with baseline aerodynamics points out the large reduction in sideline EPNdB values that occur when thrust levels are reduced prior to vehicle wheel liftoff. Adding high lift to the configuration or employing 10-percent oversized engines reduces both the centerline and the sideline noise levels. Larger noise level reductions are obtained when high lift and engine oversizing are simultaneously employed. Differences between these values and the values required by the FAR noise certification standards yield the untraded noise levels that must be provided by engine noise suppressors and other acoustical treatments. Applying the maximum noise trade value of 2 EPNdB to the sideline noise values, as was done for the standard operating procedure calculation, the result indicates that 15 EPNdB of noise reduction must be provided by the engine noise suppressors to meet the FAR Part 36 Stage 3 noise certification standards.

An assessment of the use of advanced operating procedures is thus reduced to the difference between 22 EPNdB and 15 EPNdB. This 7 EPNdB difference is the benefit achieved by using the dual thrust-cutback procedure. Note, however, that an improved configuration employing high-lift aerodynamics and engine oversizing is required.

Noise trades. Several landing approach simulator flights for the baseline aircraft were made following the FAR Part 36 noise certification procedures and the approach noise levels were calculated. The computed value of 105.9 for the standard 3° approach at 158 knots exceeded the 105 EPNdB value specified as the certification standard for subsonic jet aircraft with gross weights of 617 300 lb or more. Recall that the present aircraft configuration had no noise suppression devices of any kind. With a noise suppressor installed, noise levels below 103 EPNdB would be expected for the approach noise level. With the addition of high lift and some level of noise suppression even lower thrust settings would be employed, which would result in lower approach noise levels. Thus, the use of the 2 EPNdB trade value previously applied for establishing the amount of noise suppression capability required appears reasonable. It should be pointed out, however, that fan noise and airframe noise were not included in the noise calculations for these approach flights and should be considered because they may not be negligible during landing approaches.

Part III: Some Piloting Considerations

Pilot-variability effects. Differences in vehicle trajectory and noise levels may occur because of individual pilot differences in performing the following three tasks:

1. Initiation of vehicle rotation at the desired airspeed

2. Achieving the specified maximum pitch rate during rotation

3. Acquiring and tracking the 4-percent climb gradient

Because the throttle commands were computer controlled for the dual thrust-cutback procedure, the pilot must be particular in meeting the 200 knot rotation speed because first and second thrust-cutback settings were preset prior to initiating the takeoff roll. Deviation in rotation speed either early or late affects the sideline and the centerline noise levels. Figure 18 provides an indication of incremental noise level changes due to rotation speed differences. Airspeed errors up to 10 knots were used to generate the data reported in figure 18 and are believed to represent the maximum range of pilot variability for initiating rotation for takeoff maneuvers.

Sideline noise levels for an early rotation approaching −10 knots show the rapid noise increase due to the influence of engine operation at full throttle. In addition, figure 18 also presents the airspeed differences from the desired 250 knots at 8 n.mi. downrange from brake release (just prior to run termination point). The results presented in figure 18 were obtained by a single pilot who flew several runs for each test point. To establish how well a given pilot can perform vehicle rotation at the specified airspeed of 200 knots, rotation speed errors for the simulator flights made by pilots B and G are presented in figure 19. Also presented is the cumulative frequency distribution for their combined data. This latter result indicates about 95 percent of all simulator flights were within ±5 knots of the desired 200 knot rotation speed. The influence on sideline and centerline noise levels due to a 5 knot error in rotation speed is of the order of 1/2 EPNdB or less. In addition, variations from the maximum desired pitch rate of 3 deg/sec as commanded by the different pilots during rotation also can influence the noise levels, as indicated on figure 20. Slower pitch rates affect noise levels similar to late rotation rates. Finally, the piloting error in tracking the 4-percent climb gradient indicated by the command bar can influence the noise levels, but mainly those at the downrange centerline location. The combined influence of the three contributions on sideline and centerline noise levels due to pilot variability appears to be of the order of 1/2 to 3/4 EPNdB or less, which is well within the accuracy of the noise calculations.

Pilot comments. Several pilots flew the simulated takeoff maneuvers as described herein. A comparison of the sideline and the centerline noise levels obtained by the pilots were found to be in excellent agreement and

similar to those presented in figures 11 to 17. Comments from the pilots were qualitatively similar to those of the NASA research pilot, but much less detailed. The NASA research pilot commented that the airplane response to pilot control inputs was good. Likewise he also thought the aircraft stability characteristics with the pilot out-of-the-control-loop was good. He gave a Cooper-Harper pilot rating of 2 for the handling qualities of the longitudinal control system for the specific takeoff task simulated. (See fig. 21.) Takeoffs using the dual thrust-cutback procedure with the programmed automatic throttle engaged provided no concern for this pilot. He indicated the takeoffs were easy to perform and appeared acceptable for normal flight operations. In addition, simulator flights incorporating a critical engine-out condition at the point of first cutback posed no piloting or safety difficulties because more than adequate thrust remained to complete the takeoff. For this engine-out condition with ample thrust available, the research pilot preferred not to command full thrust on the remaining three engines, but rather for the three engines to spool up to provide the same total thrust as would be obtained from four engines. Benefits from using this technique are

1. Less yawing moment that requires pilot compensation
2. Essentially unchanged climb profile
3. Manageable although increased workload

The research pilot suggested several desirable additions to the EADI used in the study reported herein that would immediately indicate the presence of an inoperable engine. (See fig. 6.) Although not incorporated in this study, such additions might possibly be available on an HSCT production aircraft.

Another desirable improvement would be to reprogram the command bar logic to provide some guidance during the rotation maneuver to permit the pilot to smoothly capture the 4-percent climb gradient, and thus, eliminate the pitch angle overshoots presently encountered. The command bar logic for the present tests provided the instantaneous vehicle pitch attitude for a 4-percent climb gradient at the instantaneous airspeed of the vehicle. To reduce overshoots, the research pilot pitched the aircraft to a preselected pitch angle that differed for each configuration and waited until the capture of the command bar could be more easily accomplished. Also for flight operations, some information on the EADI should be provided on a HUD to reduce the time spent on the instruments, and thus permit additional time for out-of-the-window surveillance for other aircraft during the takeoff. Finally, this research pilot commented that the motion cues provided by the simulator during the takeoff were realistic, and in particular, the ground roll cues were representative of those experienced by actual transport aircraft.

Conclusions

As part of a NASA and industry effort that addresses the airport-community noise problem of a High-Speed Civil Transport (HSCT), a piloted simulation study was made for the purpose of indicating the noise reduction benefits that could occur for a typical 4-engine HSCT configuration during a pilot-controlled takeoff and initial climb-out maneuver when a dual thrust-cutback procedure was employed. Additional vehicle performance improvements included incorporation of high-lift increments into the aerodynamic database of the vehicle and limited engine oversizing. The vehicle simulated was the AST-105-1 configuration designed during the mid-1970's for supersonic flight and is representative of HSCT designs of the 1990's. Four single-stream turbine bypass engines that had no suppressors or noise attenuation devices of any kind were selected for use with the configuration in this study. This approach permitted establishing the additional noise suppression that was needed to meet the FAR Part 36 Stage 3 standards for noise levels for subsonic commercial jet aircraft. All throttle adjustments for the dual thrust-cutback procedure were made by an automatic throttle under direct computer control. The pilot used a rate-command attitude-hold control system. A number of simulated takeoff flights with rotation speeds of 200 knots were carried out. Noise levels were calculated with the jet mixing and shock noise modules of ANOPP. Results of the study are as follows:

1. Use of a dual thrust-cutback procedure with initiation of the first thrust cutback occurring while the aircraft is accelerating on the runway and the second thrust cutback occurring prior to reaching the downrange centerline measuring station can provide lower sideline noise levels than obtained when using the FAR Part 36 specified takeoff and initial climb-out procedures.

2. Additional reductions in EPNdB noise values of the baseline configuration at the FAR sideline and downrange centerline measuring locations can be obtained by incorporating high-lift capability in the aerodynamic design of the aircraft and/or employing oversized engines to reduce exhaust jet velocities.

3. A dual thrust-cutback procedure with the addition of high-lift increments and 10-percent engine oversizing needed 7 EPNdB less noise suppression to meet the FAR Part 36 Stage 3 noise certification standards than the FAR Part 36 specified takeoff procedure.

4. Simulation results for the takeoff maneuver employing the dual thrust-cutback procedure indicated

that noise levels at the centerline and the sideline FAR Part 36 measurement stations varied less than 3/4 EPNdB due to differences in human piloting performance in over 95 percent of the takeoffs.

5. The dual thrust-cutback procedure that employed a computer-controlled automatic throttle was found by the NASA research pilot to be acceptable as an operational takeoff procedure. Simulation takeoffs in still air with the critical engine inoperative were accomplished with little difficulty and no flight safety concerns.

NASA Langley Research Center
Hampton, VA 23681-0001
May 19, 1995

Table I. AST-105-1 Physical Characteristics

Geometric data:

Reference wing area, ft^2	8366
Wing span ft	126.22
Wing leading-edge sweep, deg	74.00, 70.84, and 60.00
Reference mean aerodynamic chord, ft	88.16
Center of gravity, percent MAC	60.10
Distance from nose to c.g., ft	173.96
Static margin, percent	−3.7
Wing fin area (exposed), ft^2	196
Horizontal tail area (exposed), ft^2	620
Vertical tail area (exposed), ft^2	358

Weight and moments of inertia:

Takeoff gross weight, lb	686 000
I_x, slug-ft^2	7 540 000
I_y, slug-ft^2	54 910 000
I_z, slug-ft^2	60 730 000
I_{xz}, slug-ft^2	−1 540 000

Control surface deflections:

δ_{ht}, deg	±20
δ_f, deg	0 to 30
δ_a, deg	±35
δ_{afo}, deg	±30
δ_{afi}, deg	±10
δ_r, deg	±25

Table II. Noise Data for Single and Dual Thrust-Cutback Procedures

[Ground roll distance to vehicle rotation point held constant]

Configuration	Net thrust at—			IAS at—		EPNdB at—		Engine K_{size}	Engine T/W
	T_0, percent	T_1, percent	T_2, percent	V_R, knots	V_c, knots	CL	SL		
Single thrust-cutback procedure with reduced initial thrust									
With $\Delta C_L = 0.10$	80	80	41	180	251	123.0	124.3	0.773	0.295
With flap BLC	83	83	45	183	252	124.4	124.7	0.773	0.295
Baseline	86	86	51	188	249	126.1	125.5	0.773	0.295
Full throttle									
Baseline	100	100	100	200	250	128.8	127.2	0.773	0.295
Dual thrust-cutback procedure[a]									
With $\Delta C_L = 0.10$	100	58	42	200	250	121.7	119.8	0.773	0.295
With flap BLC	100	63	45	200	250	123.4	121.3	0.773	0.295
Baseline	100	67	52	200	250	126.3	121.8	0.773	0.295

[a]With automatic throttle distance settings of X_1 = 8000 ft, X_2 = 10000 ft, X_3 = 18240 ft, and X_4 = 20672 ft.

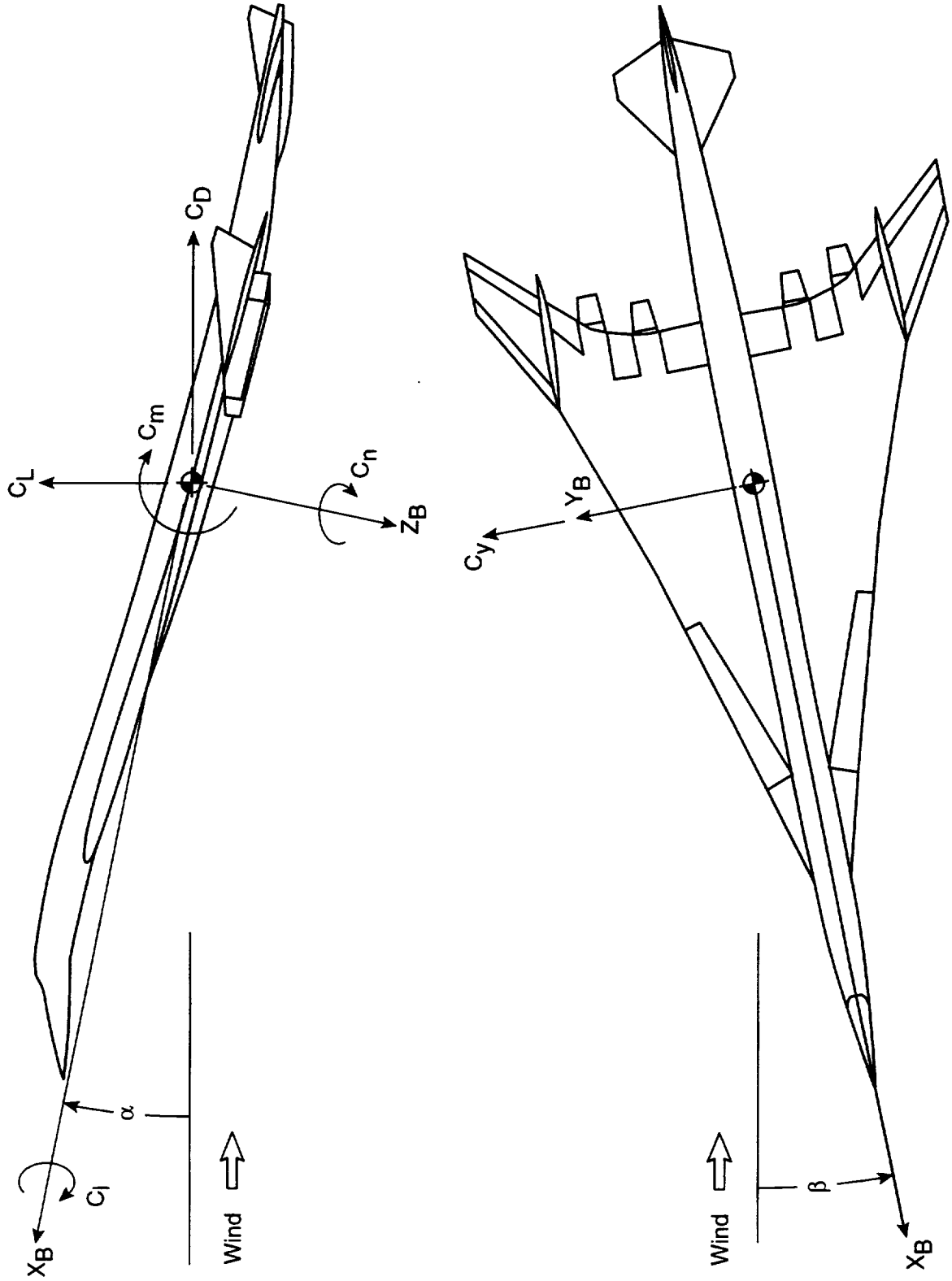

Figure 1. Aerodynamic coefficients and body system of axes.

Four TBE-M2.4 engines
4500 n.mi. range
273 passengers
Takeoff weight = 686 000 lb
Landing weight = 392 250 lb
c.g. = 60.1 percent MAC
T/W = 0.295
W/S = 82 psf

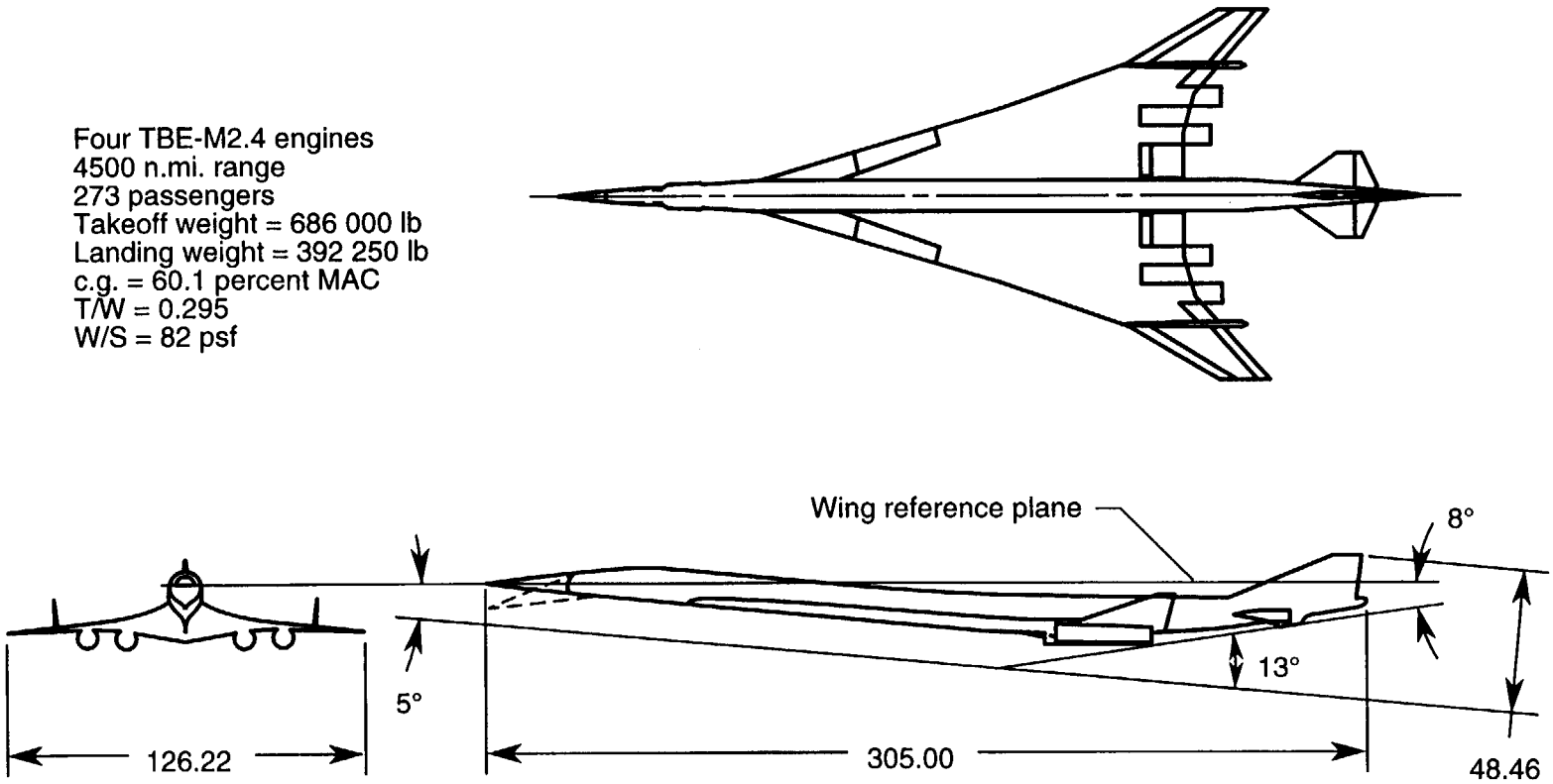

Figure 2. AST-105-1 configuration. All linear dimensions are in feet.

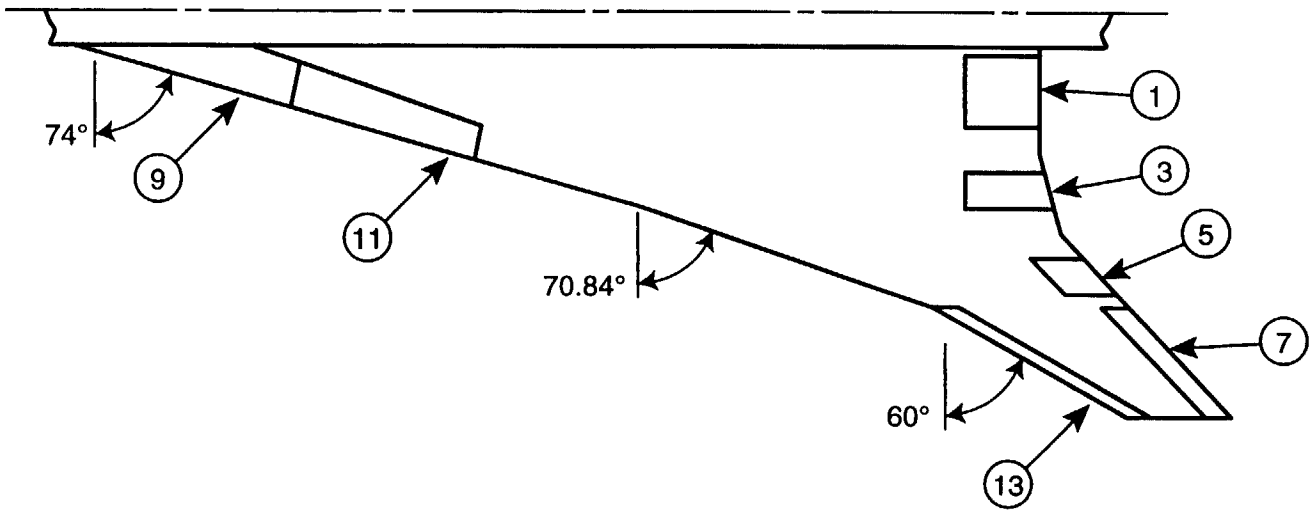

Number[a]	Area, ft^2 each	Surface definition	Longitudinal input symbol	Lateral input symbol
1-2	126.3	Flap	δ_f	
3-4	87.2	Inboard flaperon	δ_f	δ_{afi}
5-6	50.5	Outboard flaperon		δ_{afo}
7-8	82.5	Aileron		δ_a
9-10	166.2	Inboard apex flap		
11-12	176.5	Outboard apex flap		
13-14	91.0	Krueger flap		

[a]Odd numbers left wing, even numbers right wing.

Figure 3. Wing control surfaces.

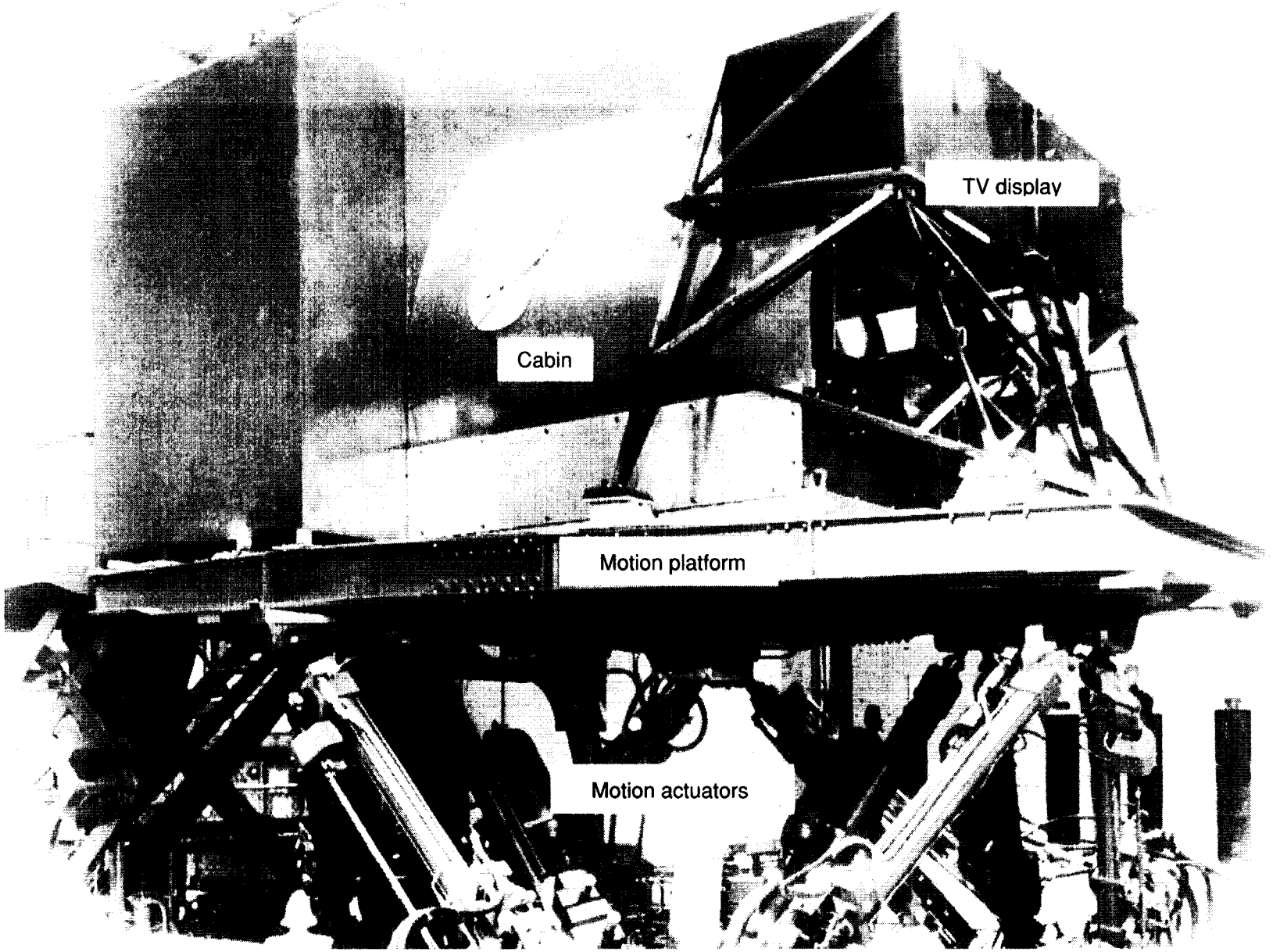

L-73-7163.1

Figure 4. Six-degree-of-freedom Langley Visual/Motion Simulator.

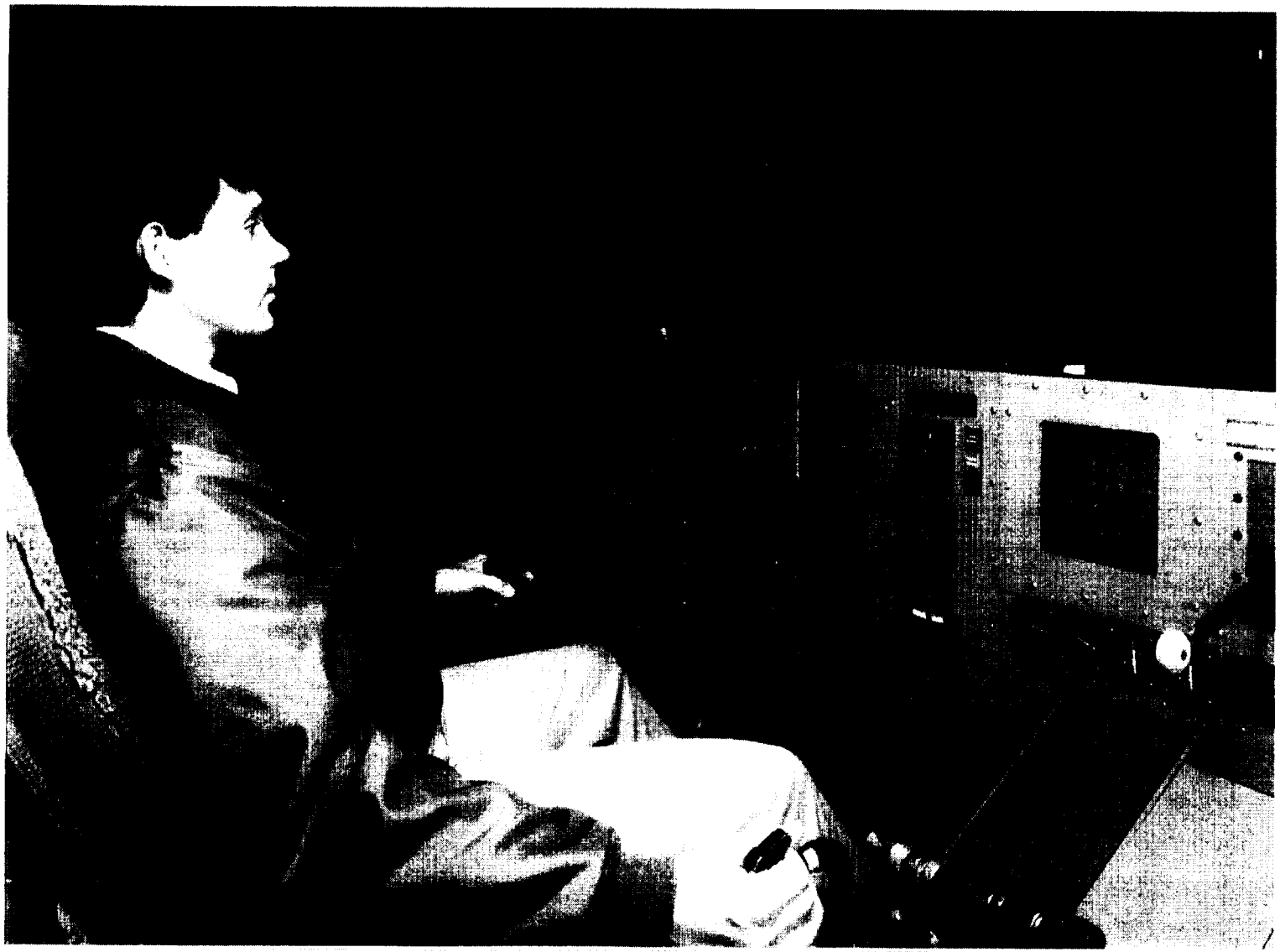

L-90-13683

Figure 5. Langley Visual/Motion Simulator flight deck.

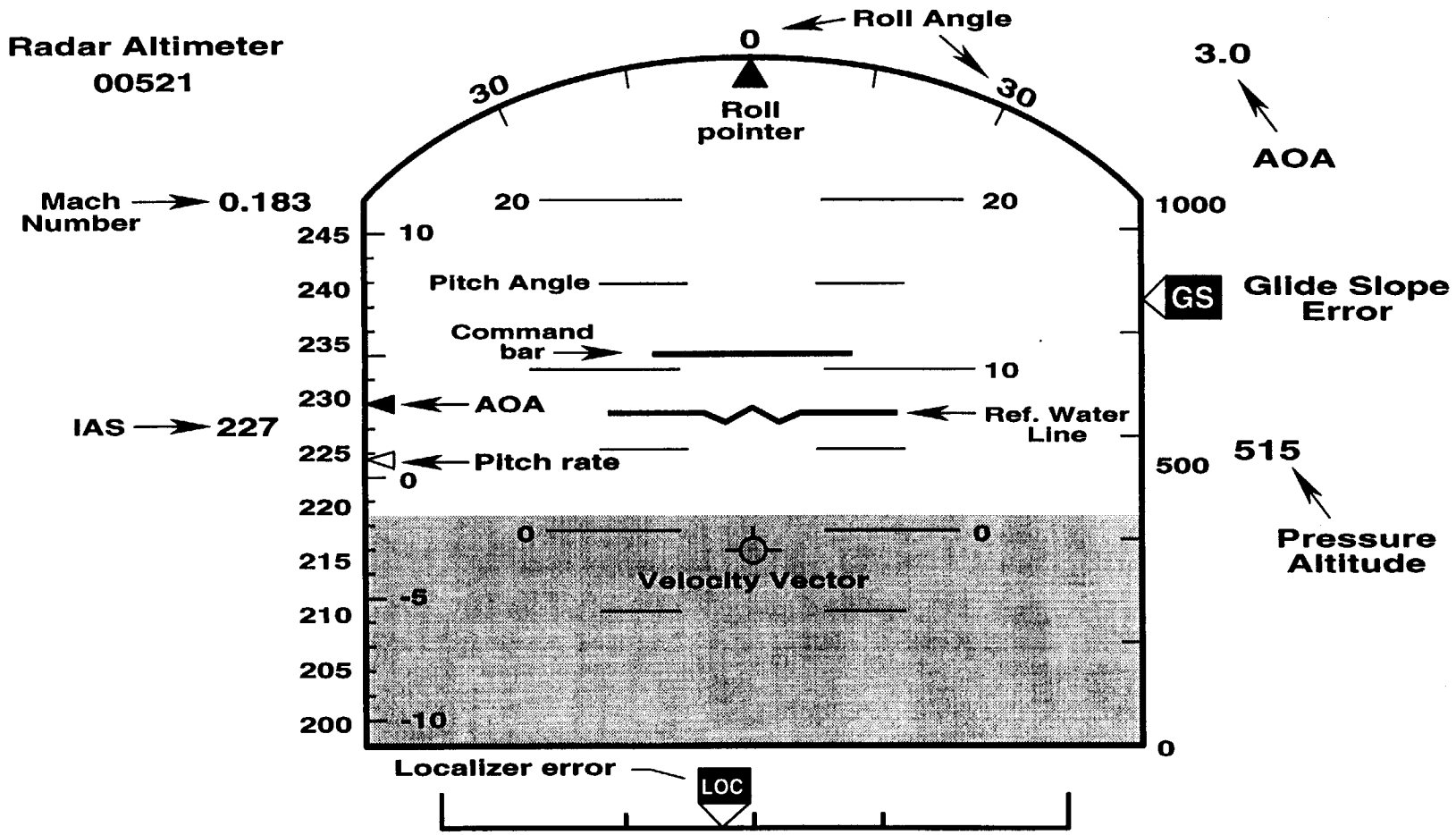

Figure 6. Electronic attitude director indicator (EADI).

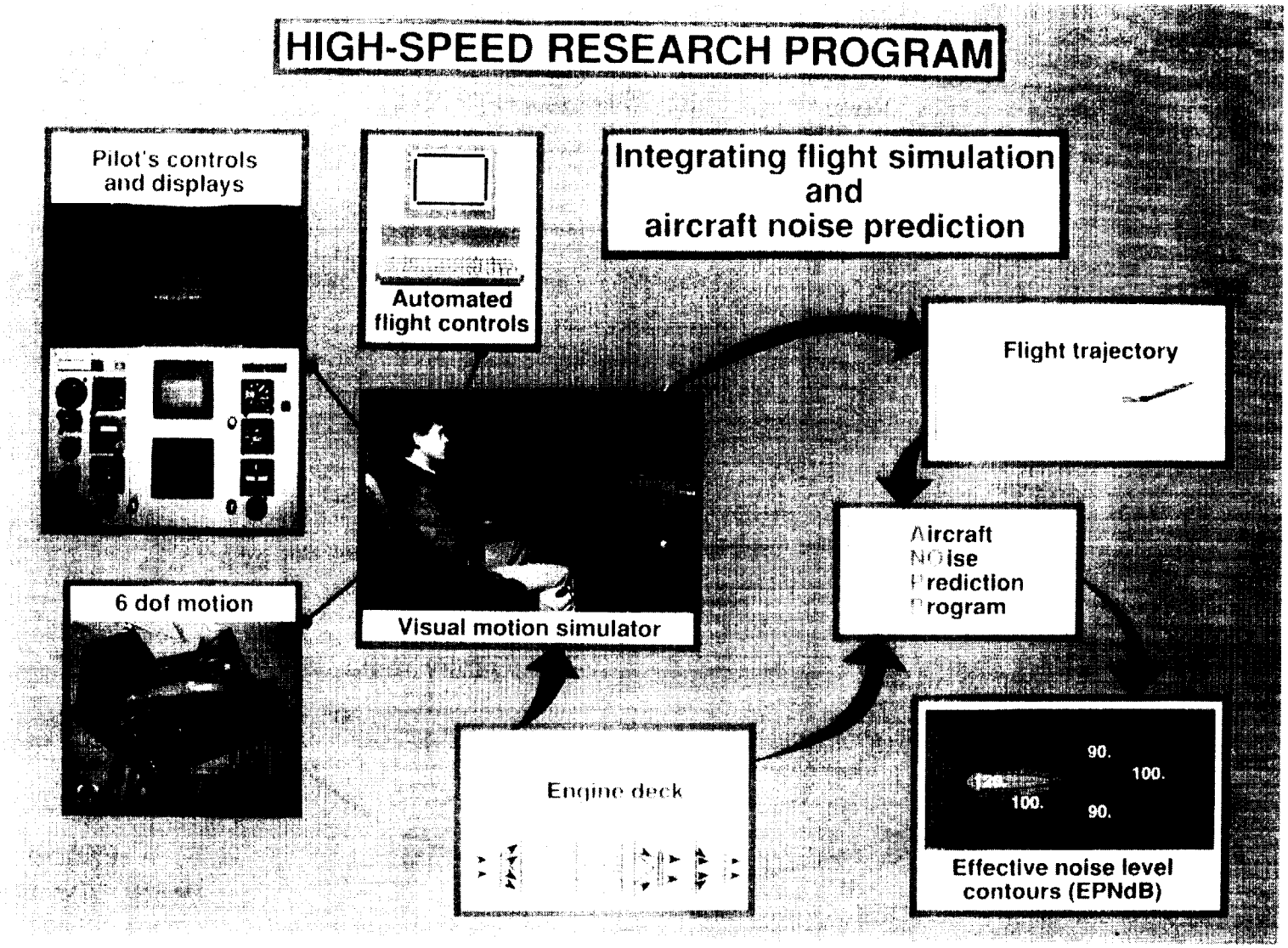

L-91-7372

Figure 7. Information flow of VMS/ANOPP simulation.

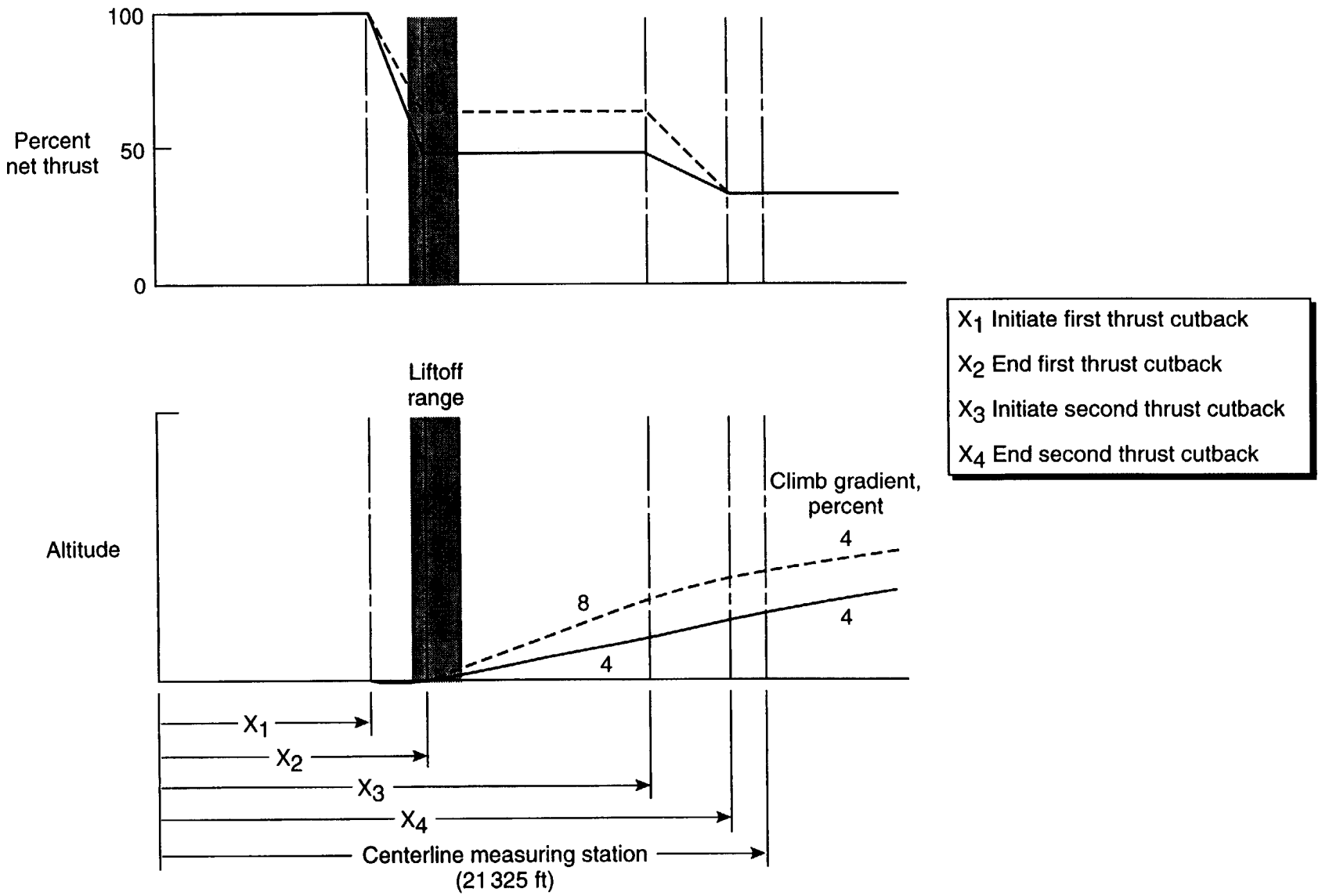

Figure 8. Dual thrust-cutback procedure for two climb gradients (not to scale).

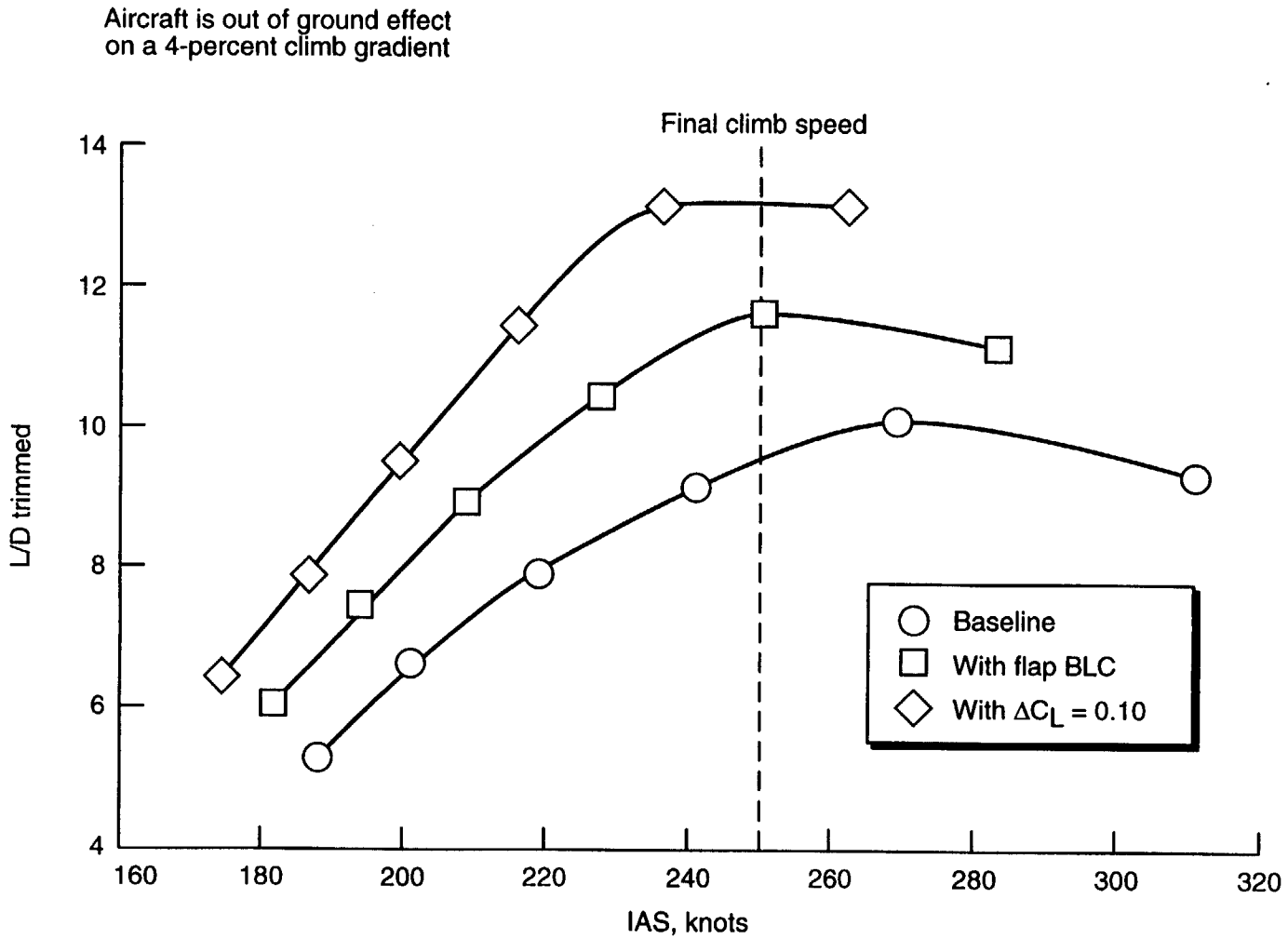

Figure 9. Trimmed *L/D* variation with airspeed for baseline configuration with and without high-lift aerodynamic improvements.

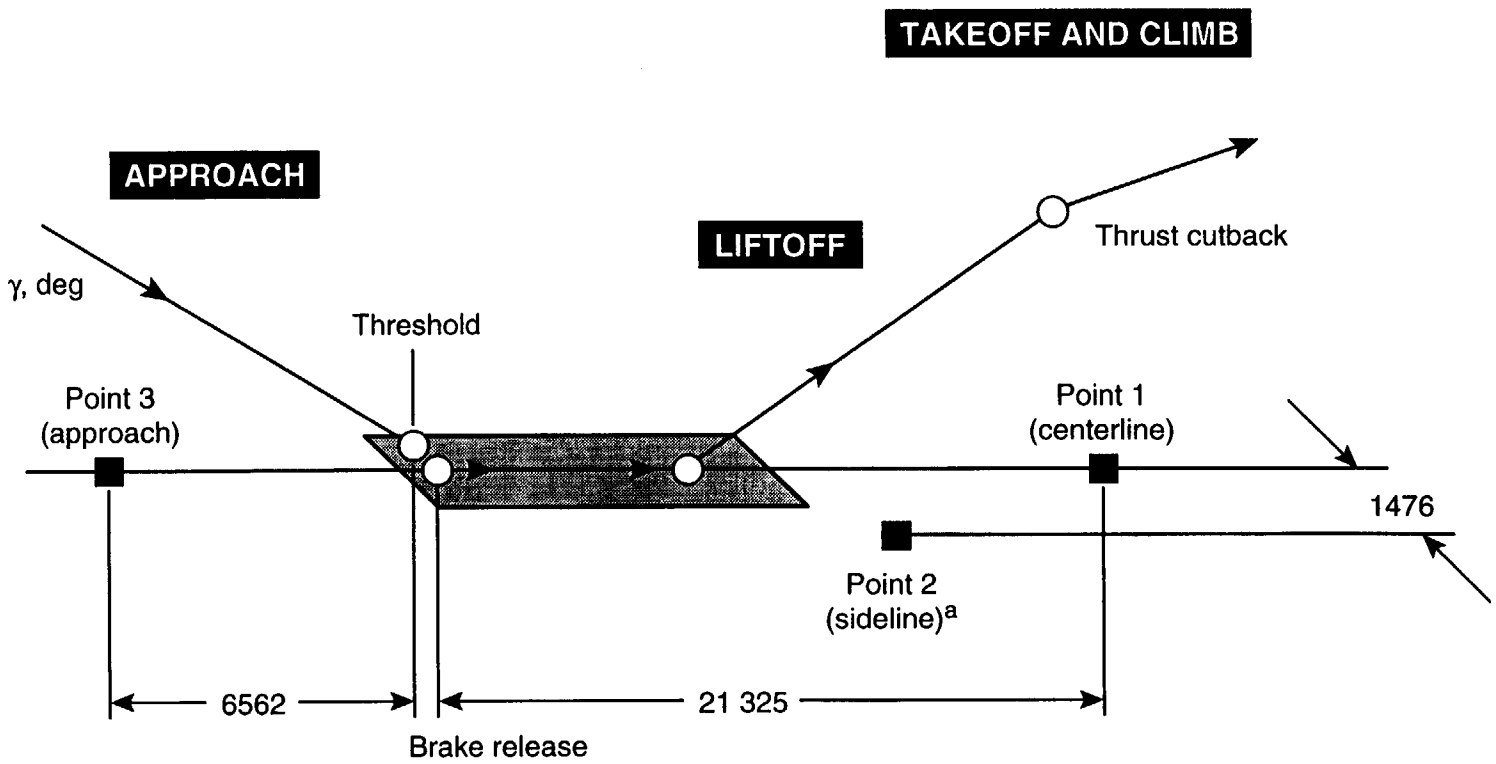

[a]Sideline noise is measured where noise level after liftoff is greatest.

Figure 10. FAR Part 36 noise certification measurement locations. All linear dimensions in feet.

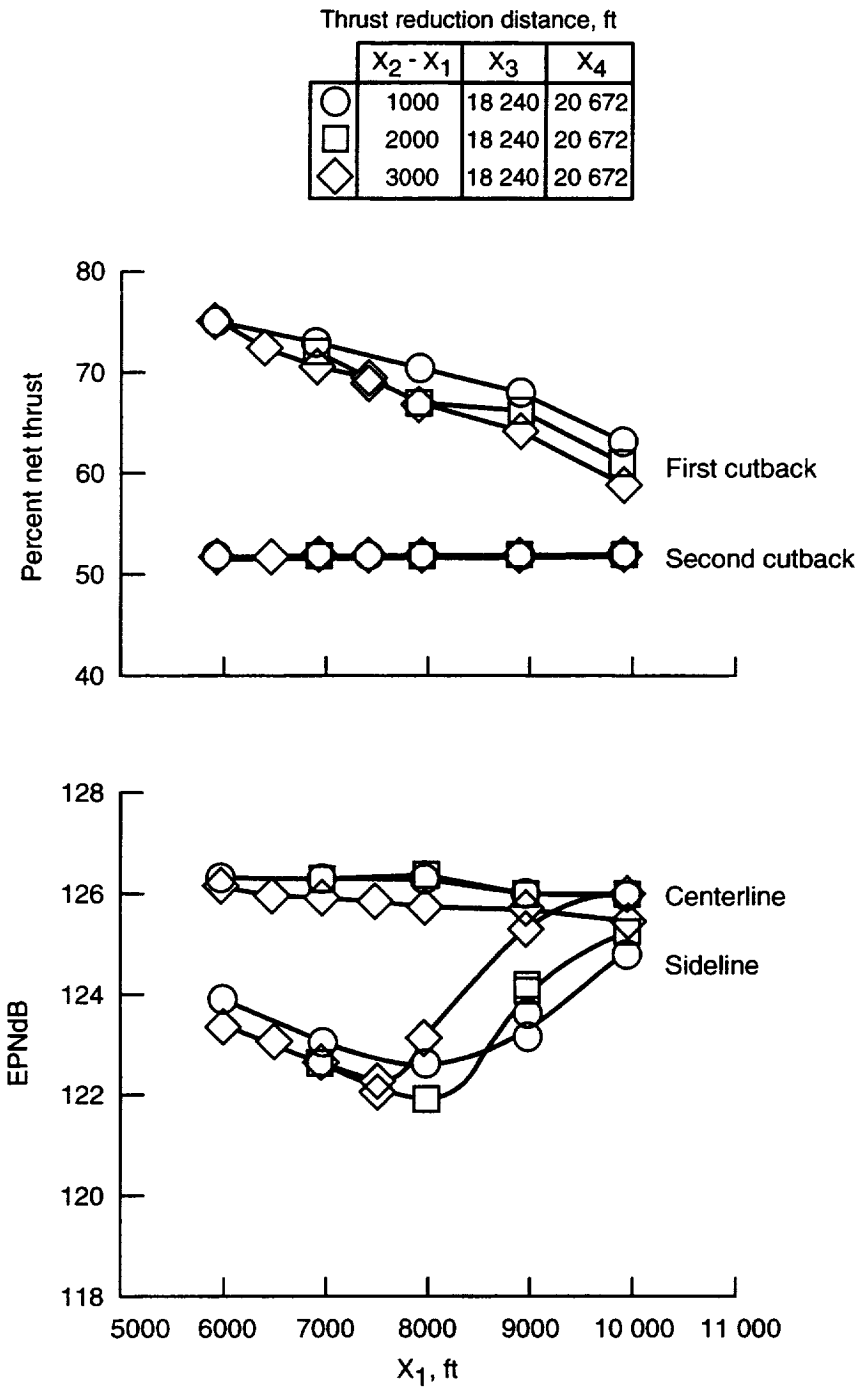

(a) Baseline configuration.

Figure 11. Effect of first thrust-cutback location on thrust and noise levels.

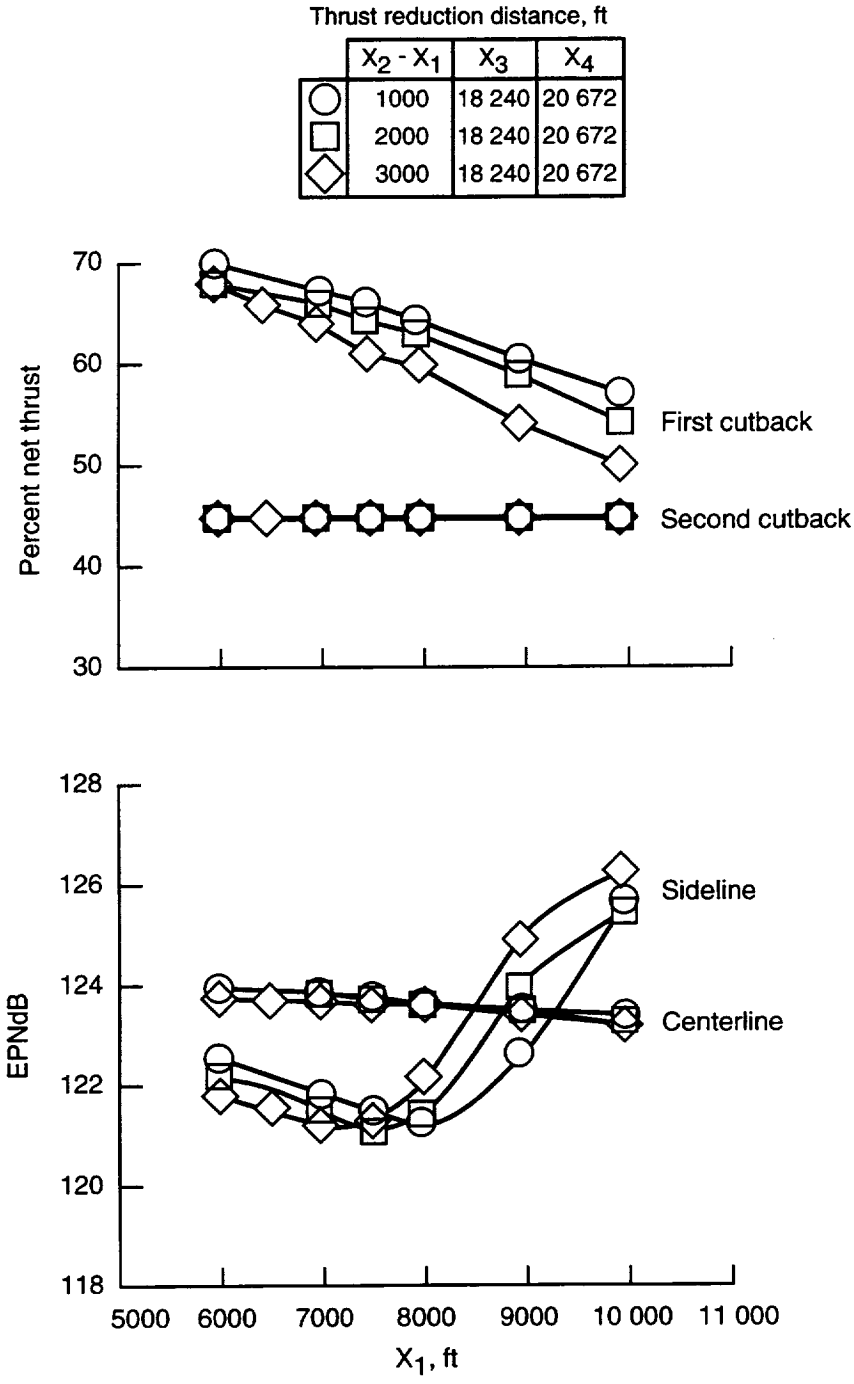

(b) Configuration with flap BLC.

Figure 11. Continued.

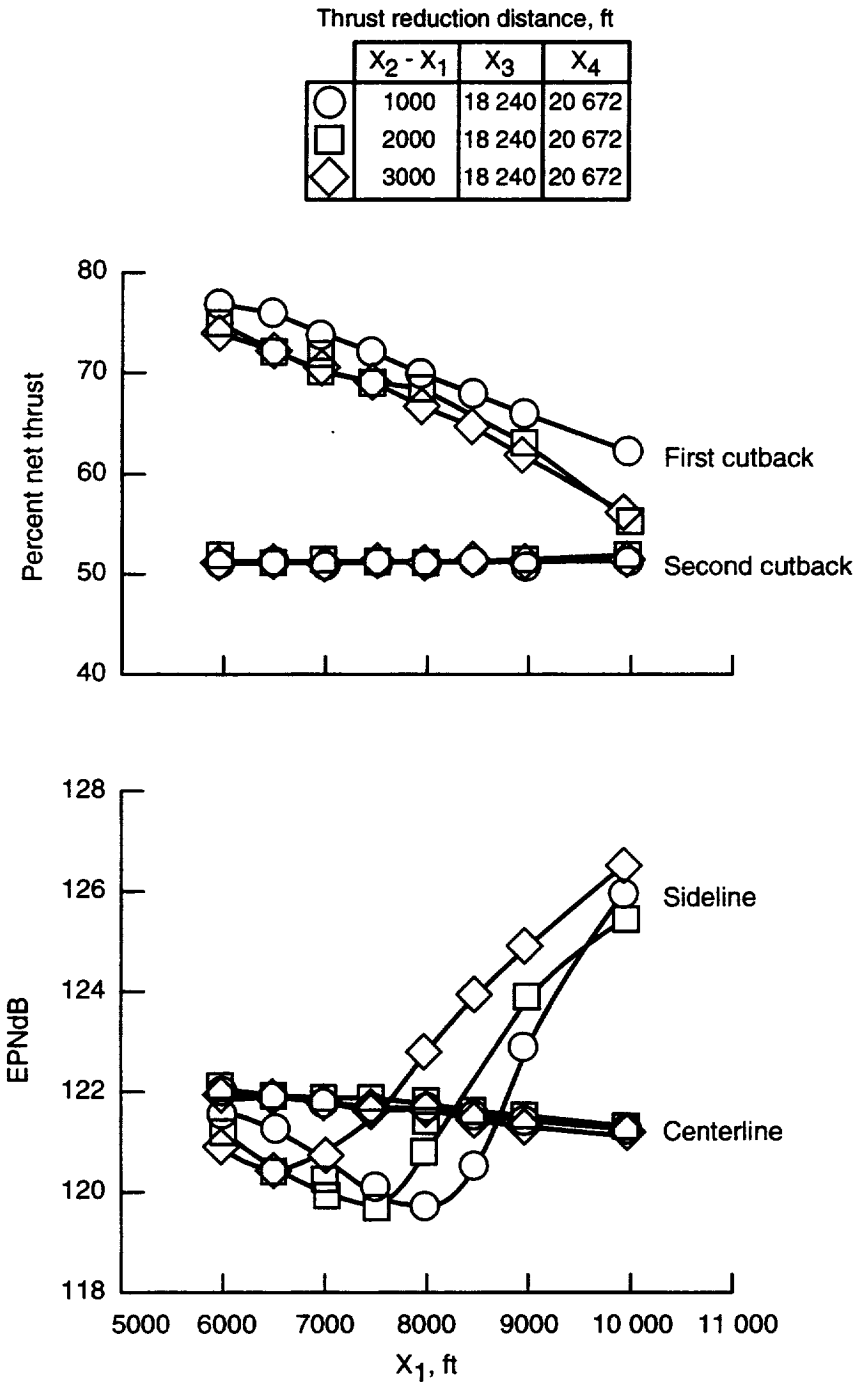

(c) Configuration with $\Delta C_L = 0.10$.

Figure 11. Concluded.

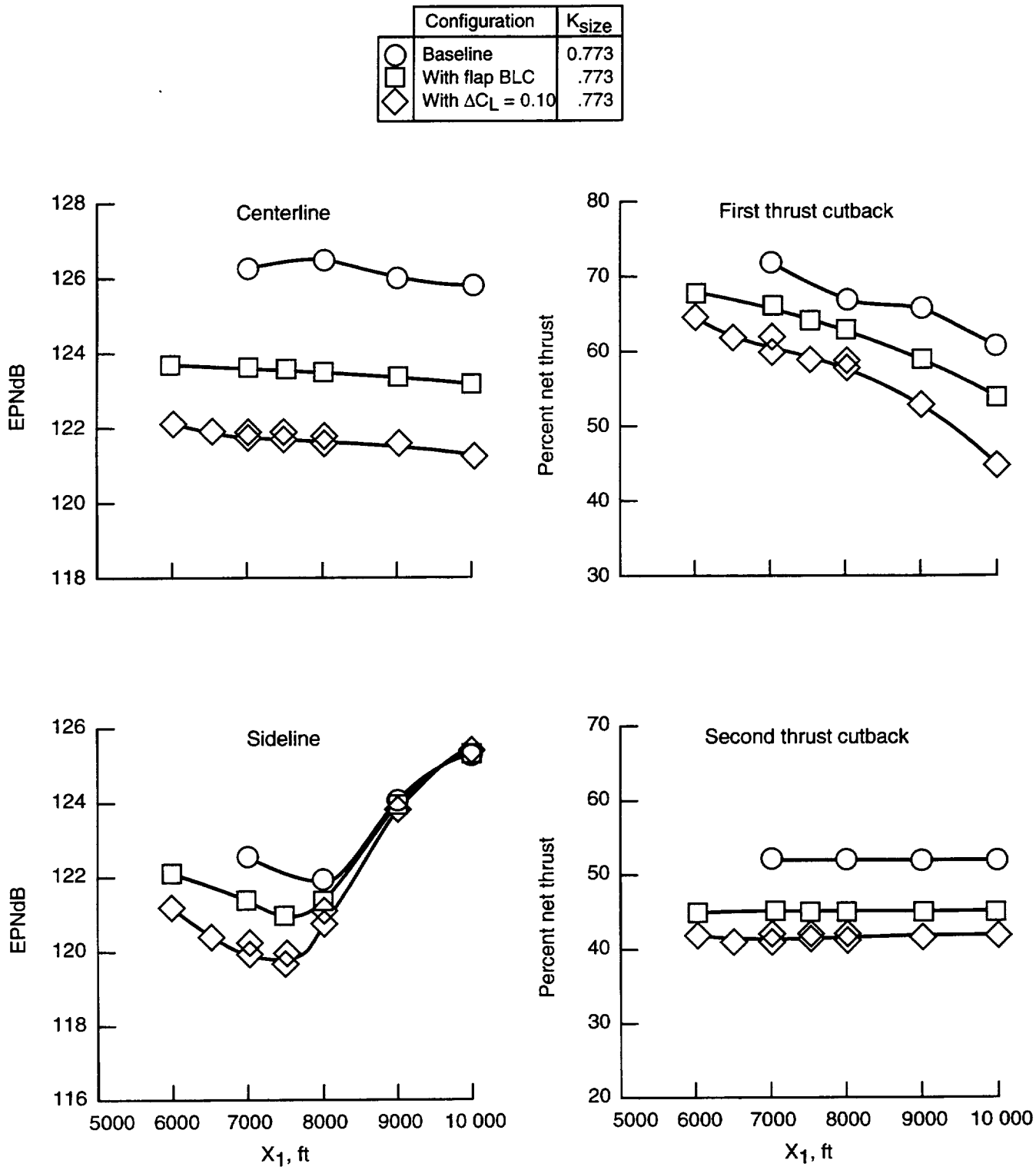

Figure 12. Effect of high-lift aerodynamics on thrust and noise levels with $X_2 - X_1 = 2000$ ft.

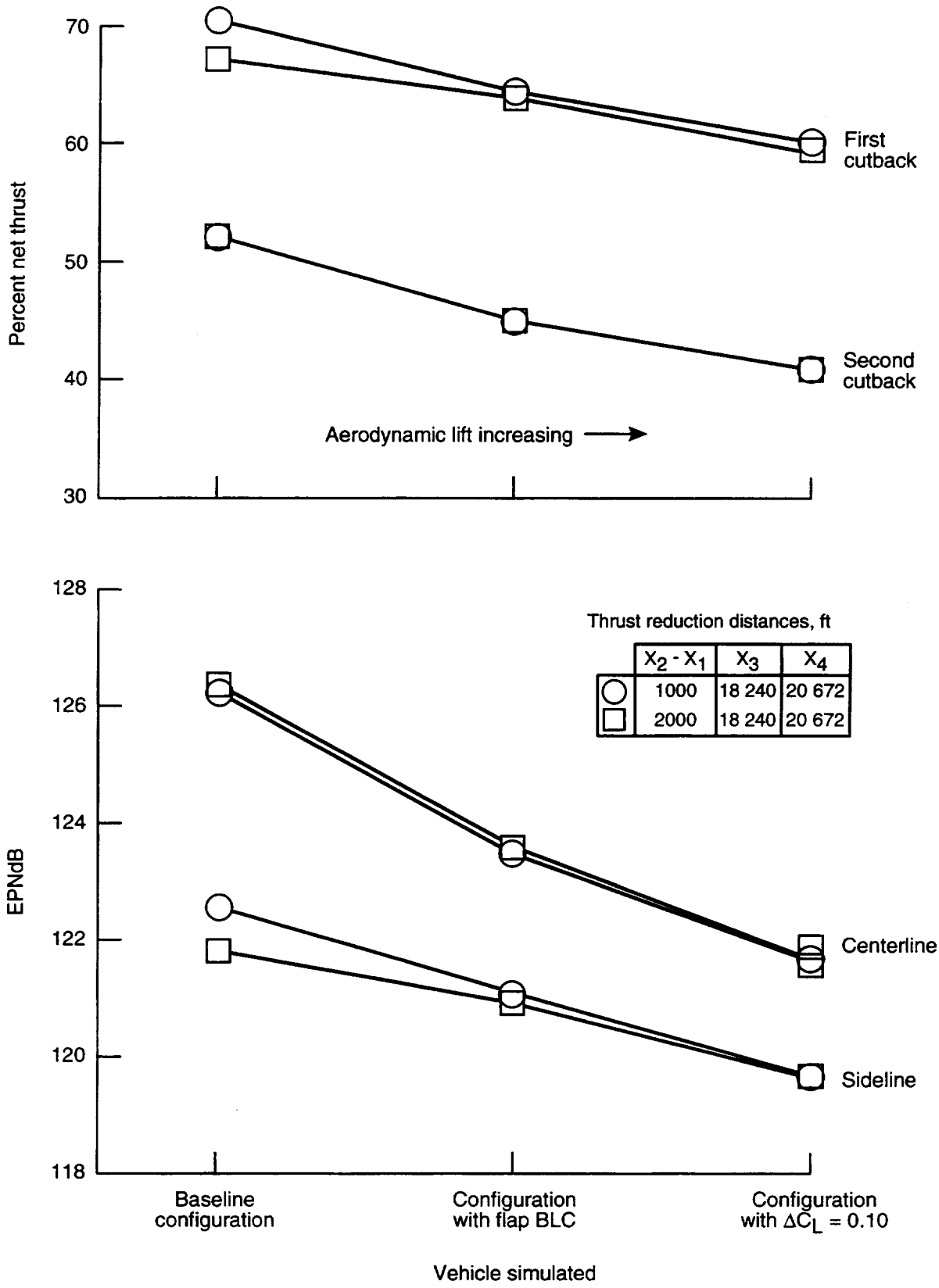

Figure 13. Effect of high-lift aerodynamics on thrust and noise levels when sideline noise levels are at a minimum.

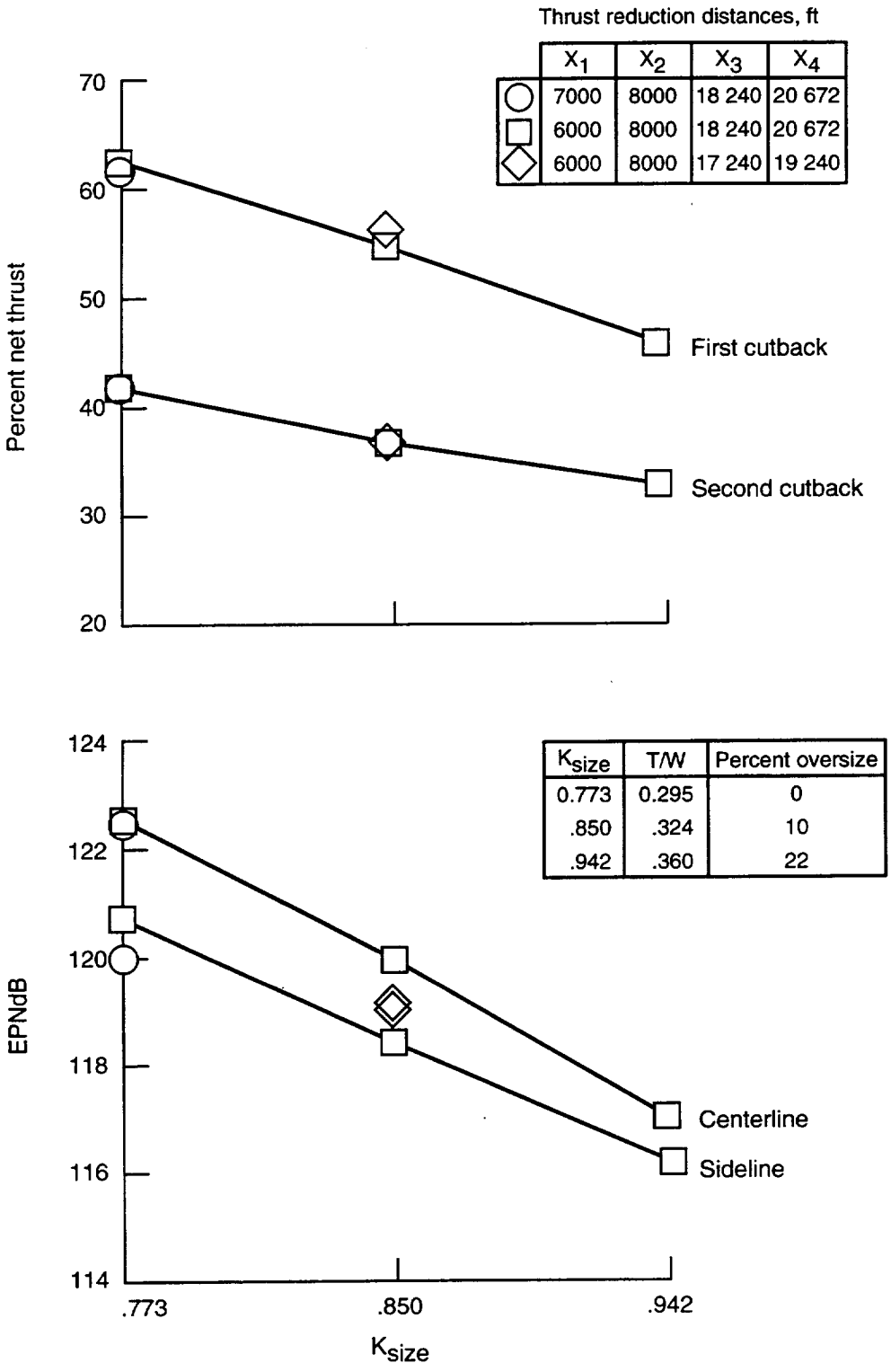

(a) Full thrust at brake release.

Figure 14. Effect of engine oversizing on thrust and noise levels for configuration with $\Delta C_L = 0.10$.

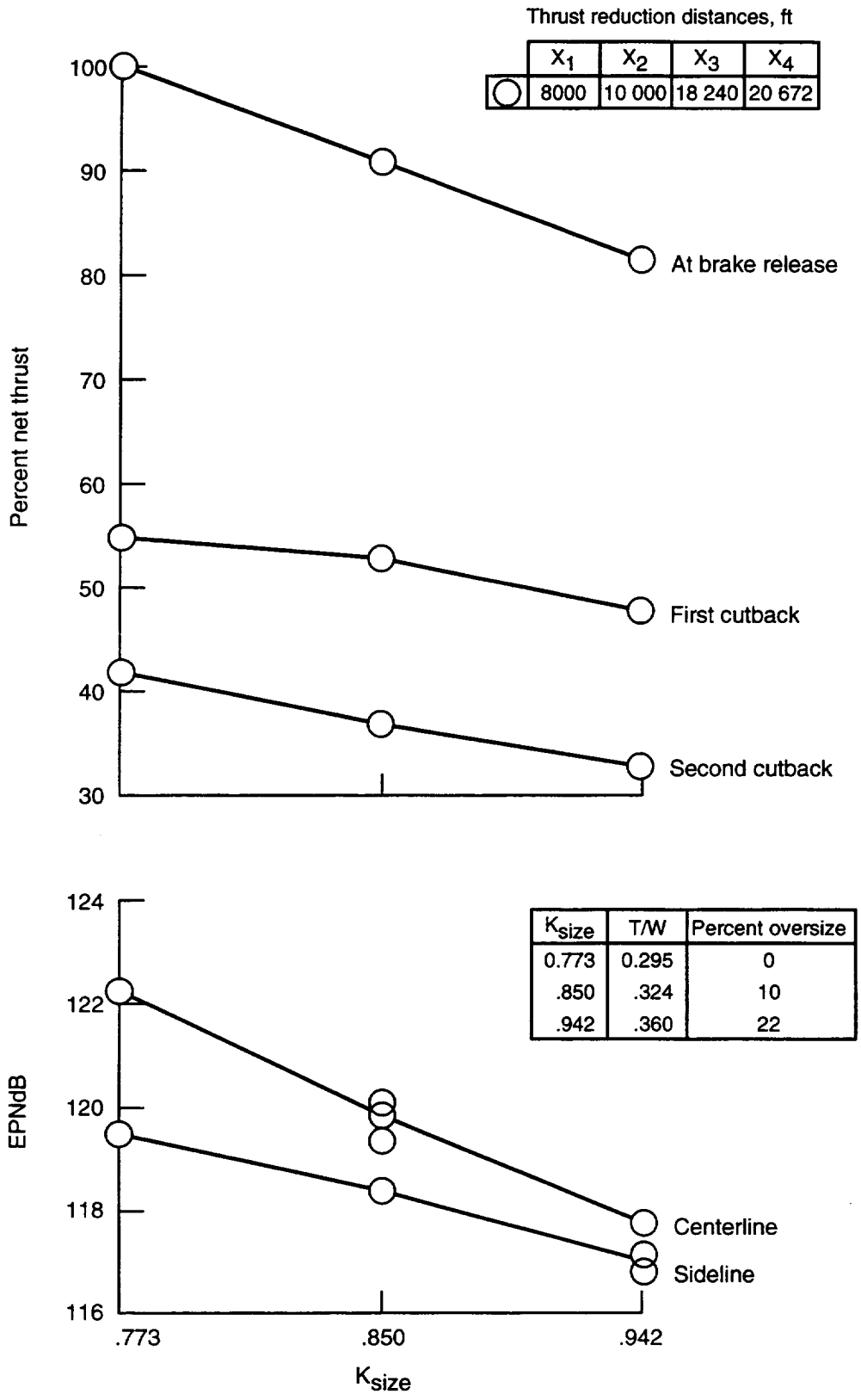

(b) Reduced thrust at brake release.

Figure 14. Concluded.

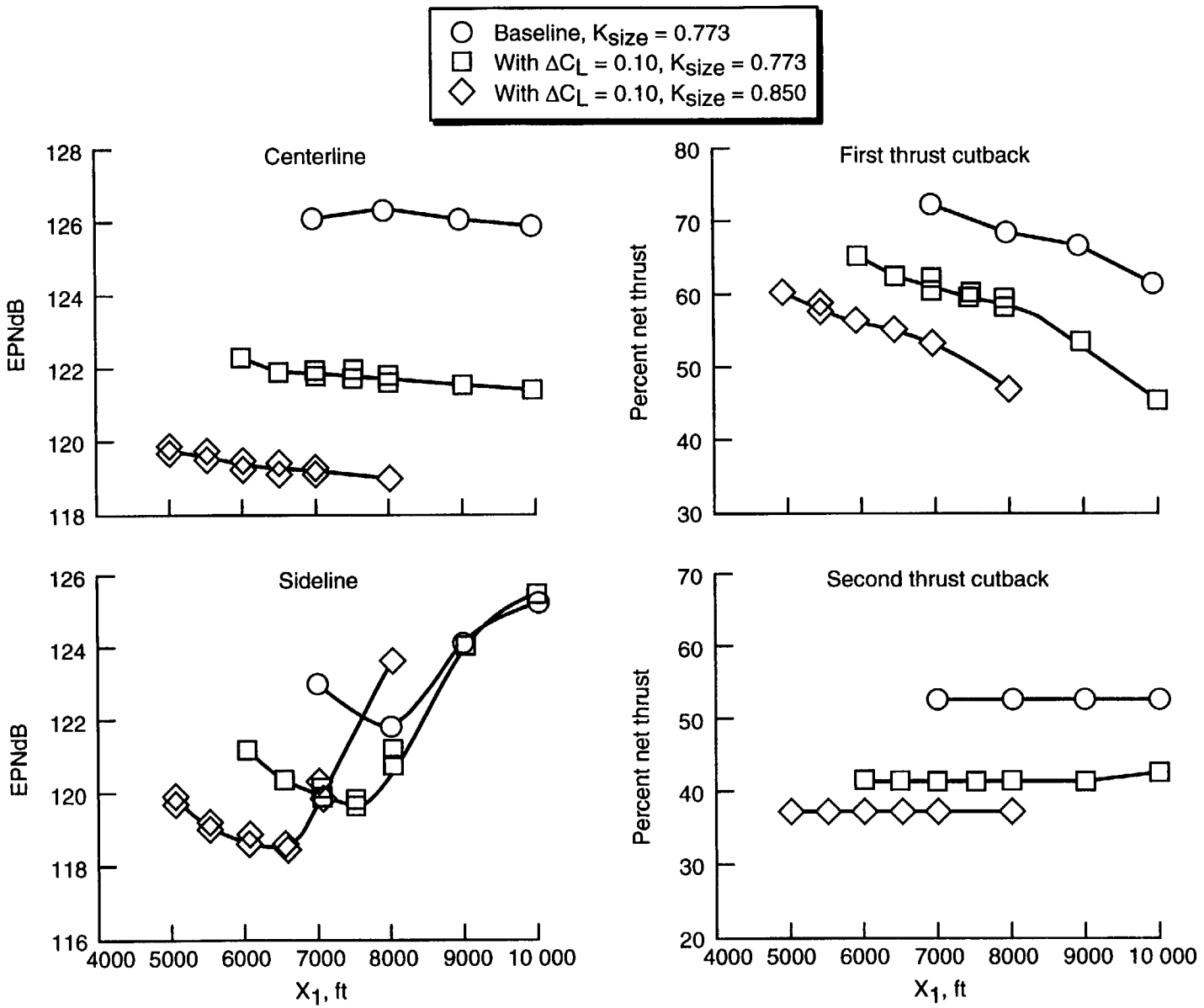

(a) Pilot G.

Figure 15. Effect of vehicle modifications on thrust and noise levels for $X_2 - X_1$ = 2000 ft.

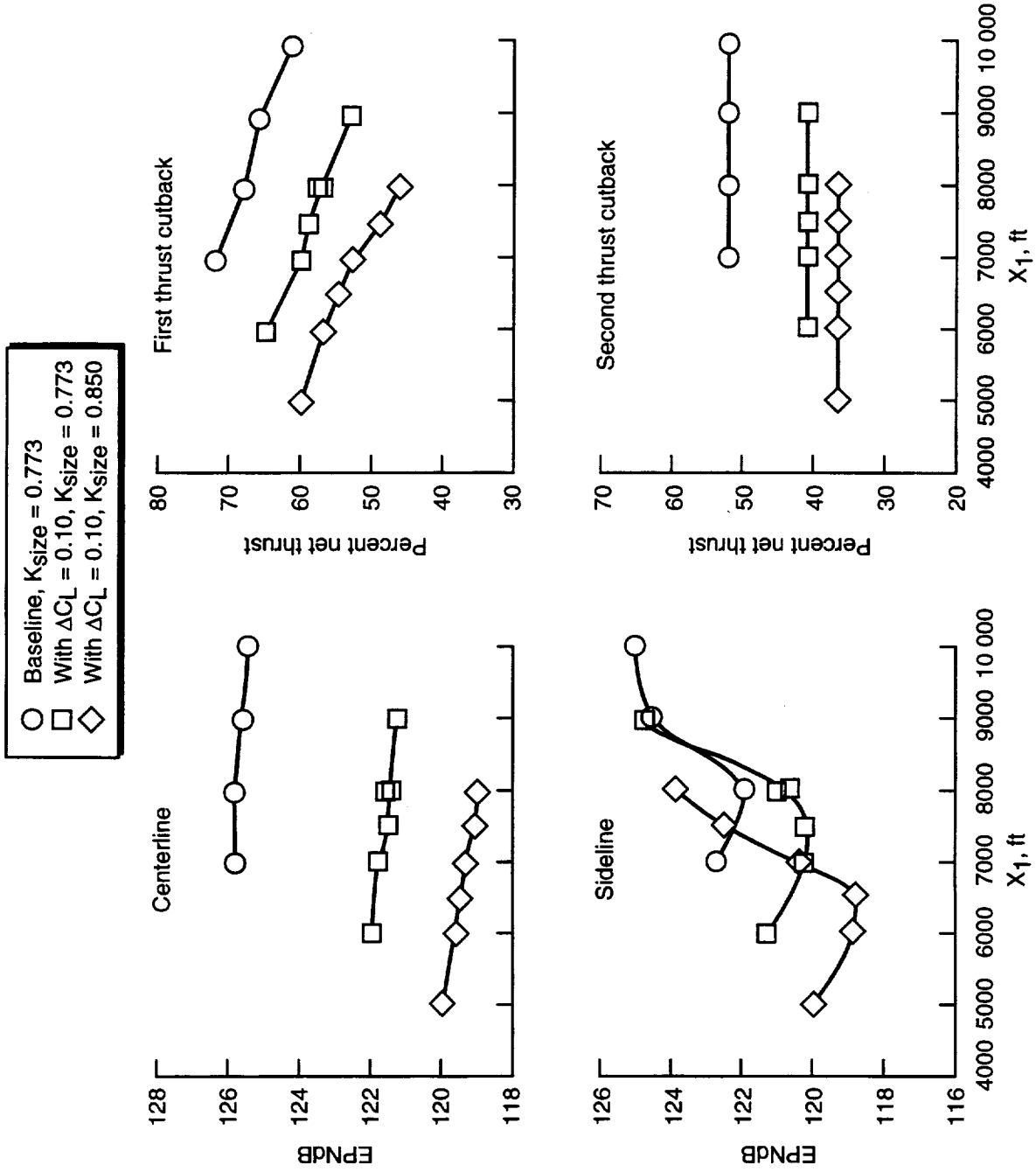

(b) Pilot B.

Figure 15. Concluded.

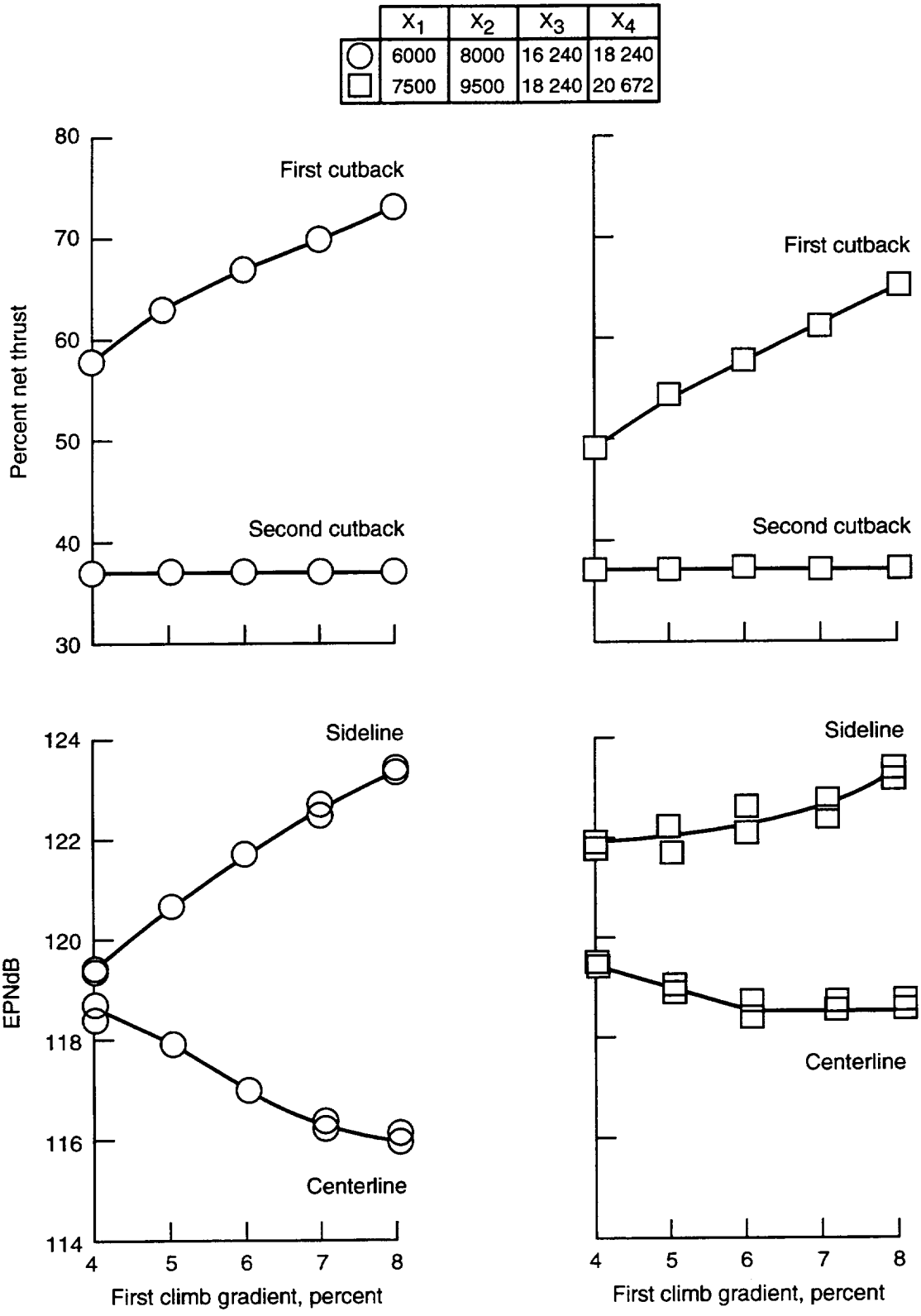

Figure 16. Effect of first climb gradient for configuration with $\Delta C_L = 0.10$ and 10-percent oversized engines.

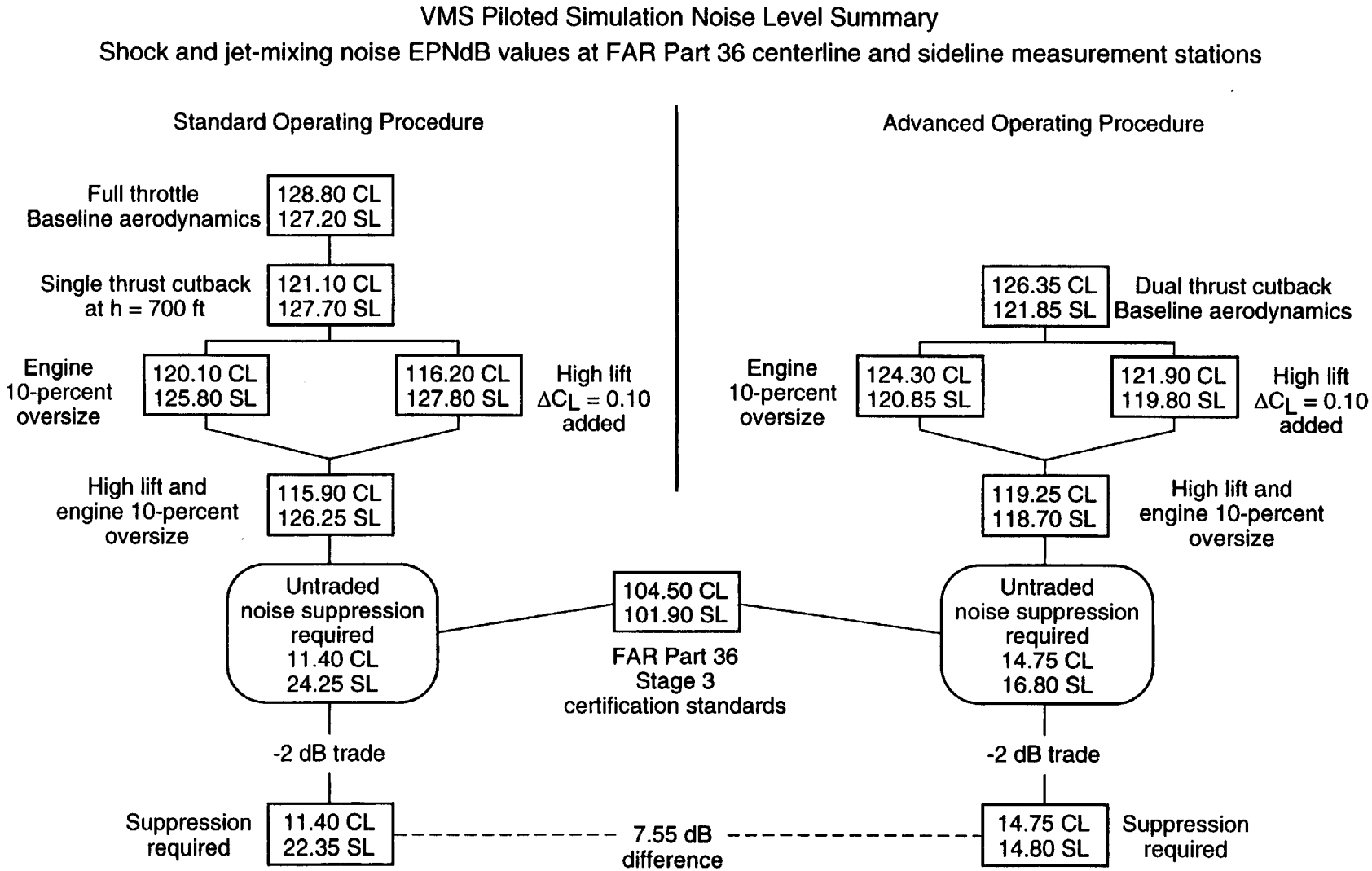

Figure 17. Noise assessment chart.

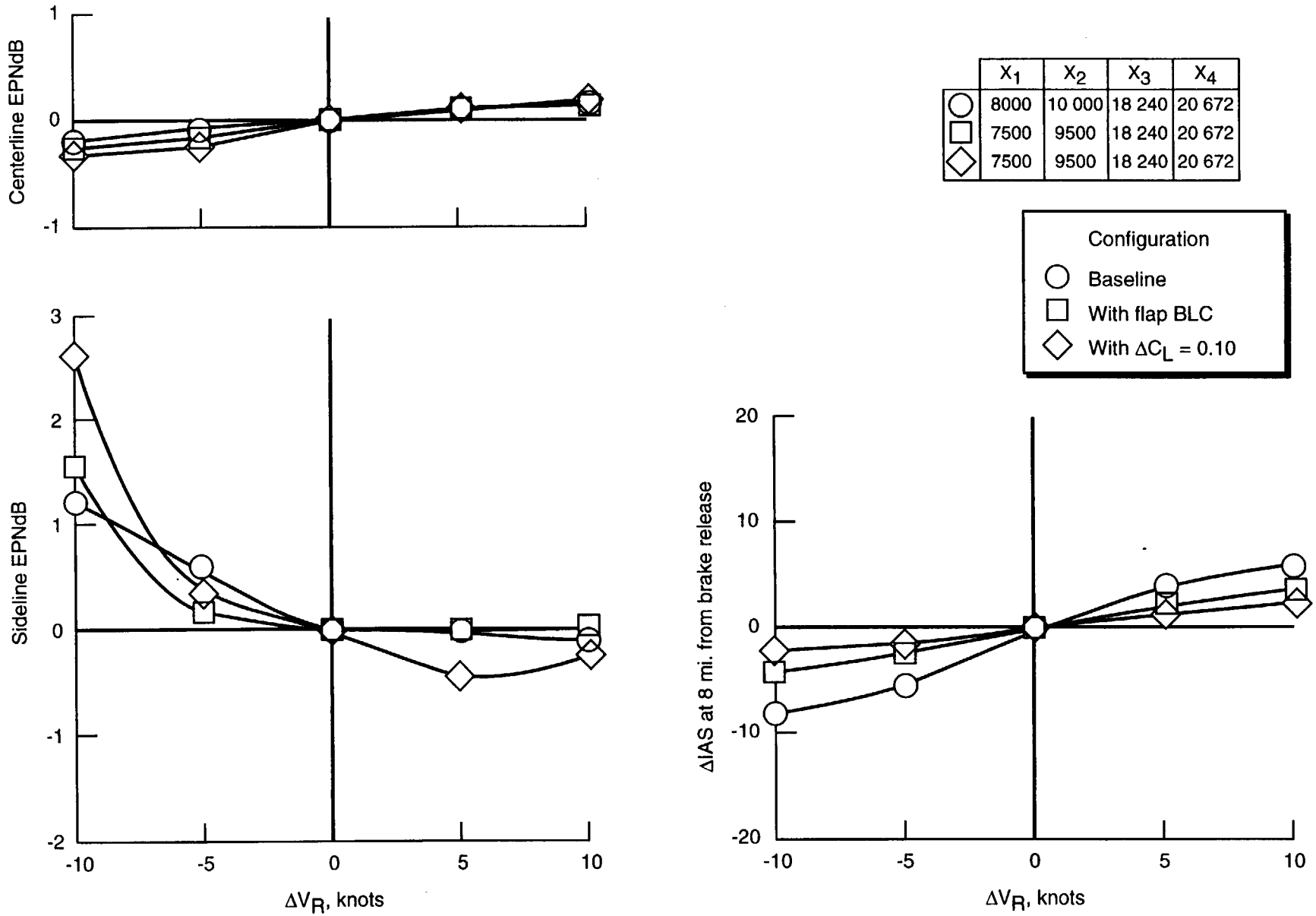

Figure 18. Sensitivity of sideline noise level, centerline noise level, and airspeed at run termination due to increments in rotation speed from desired 200 knots (pilot G).

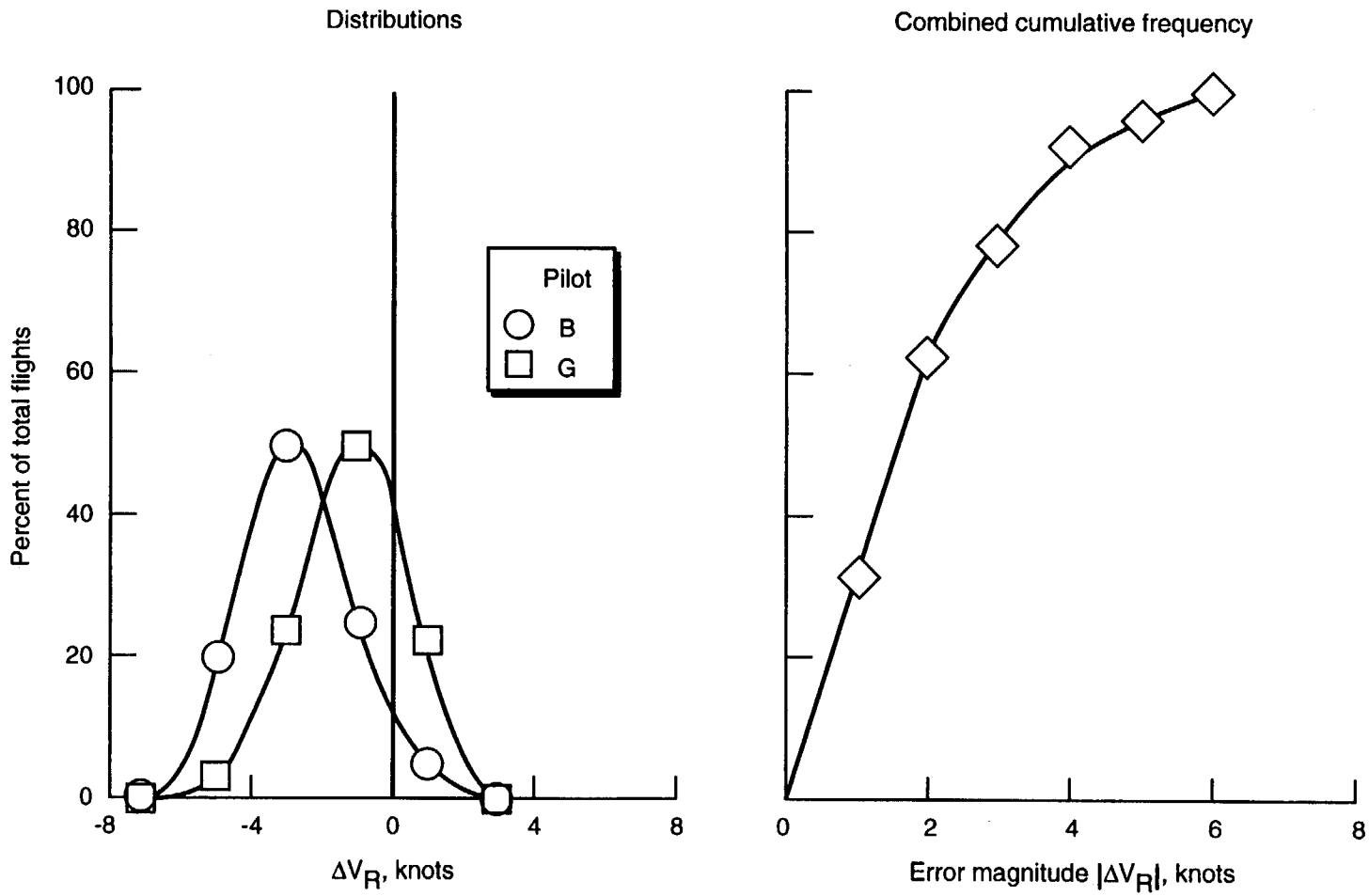

Figure 19. Rotation speed distributions and combined cumulative frequency results for 78 simulator flights.

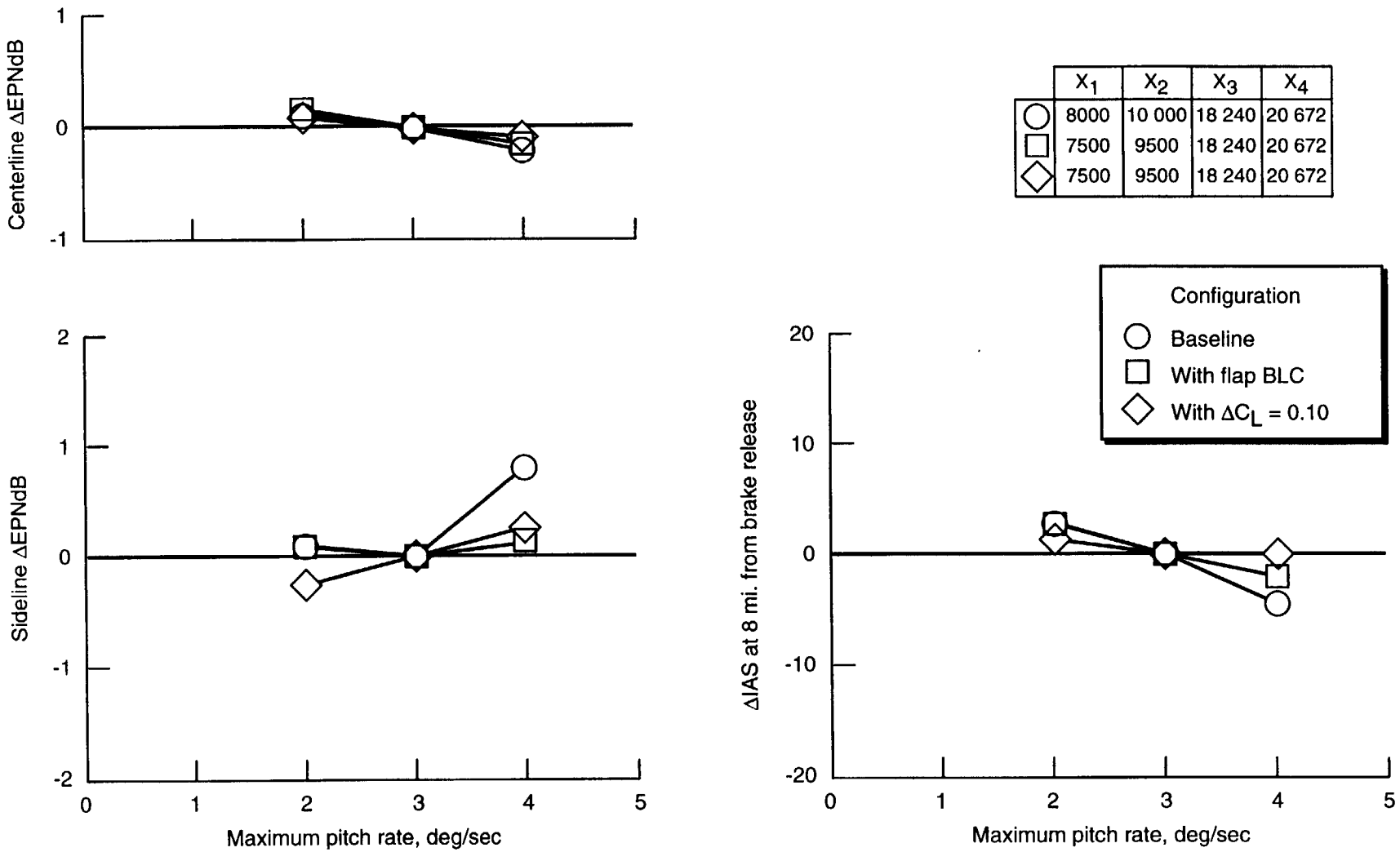

Figure 20. Sensitivity of sideline noise, centerline noise, and airspeed at run termination due to differences in maximum pitch rate from 3 deg/sec.

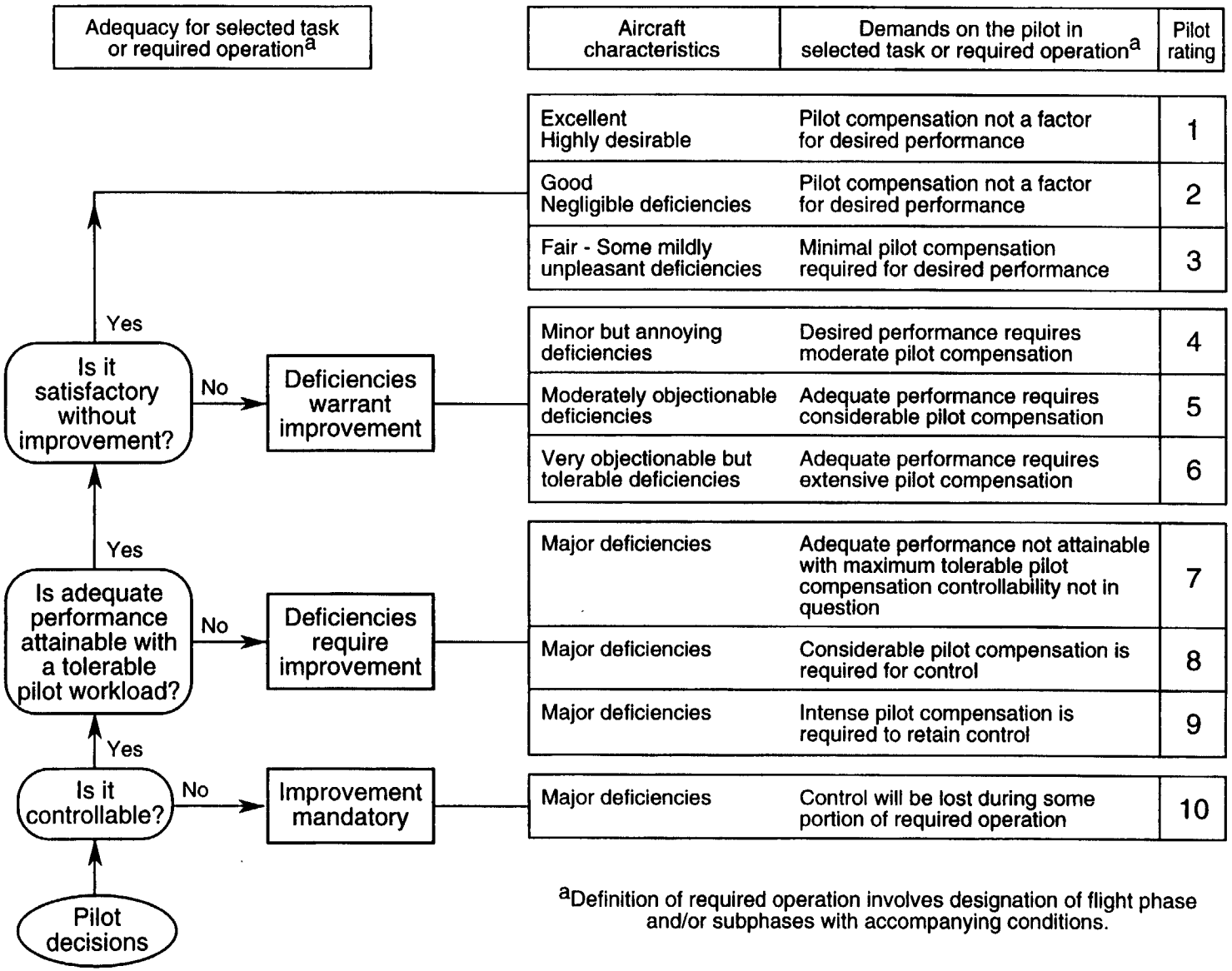

Figure 21. Cooper-Harper handling qualities rating scale.

Appendix A

Engine Information

Four single-stream turbine bypass engines with no noise suppression of any kind were used with the AST-105-1 configuration for the study reported herein. The engines were designated as TBE-M2.4, which indicates the engine design was optimized for the cruise condition at a Mach number of 2.4. A nominal data set giving gross thrust and ram drag values as a function of Mach number and altitude for full-throttle operation for a single engine is given in table A1.

Different engine sizes were obtained by reducing all thrust and ram drag values in table A1 by the size factor, K_{size}. Figure A1 presents the block diagram used in the simulation to adjust these scaled values for partial throttle operation and to incorporate associated engine dynamics. Figure A2 provides the power lever angle input-output relationship. Table A2 provides values of the bivariate function that scales the ram drag for partial throttle operation. Engine dynamics include scheduled gains and rate limiting, as indicated in figures A1 and A3. Values are provided in figure A3 only for throttle deflections above flight idle, although the program includes values for reverse thrust. For convenience, net-thrust values at full throttle as a function of Mach number and altitude for the baseline engine used herein are given in table A3.

The four engines were mounted on the airframe below the wings (fig. 2). The nozzles deflected downward 8° so that the thrust vectors would pass through the c.g. of the vehicle when the c.g. was at 60.1 percent of MAC, thus eliminating longitudinal trim changes with throttle operation. Because of the dominant influence of engine exhaust jet velocity on noise level magnitudes at the FAR noise certification locations, values of exhaust jet velocity V_j for full-throttle operation are given in figure A4 along with V_j variations for partial throttle operation at three Mach numbers.

Table A1. Gross Thrust and Ram Drag Values for Full-Throttle Operation of TBE-M2.4 Engine With K_{size} = 1.0

(a) Reference gross thrust, T_{GREF}

Mach number	Full-throttle reference gross thrust, lbf, at altitude of—				
	0 ft	1000 ft	2000 ft	5000 ft	10 000 ft
0	65 484.4	63 400.6	61 368.0	55 571.5	46 856.0
0.2	68 783.7	66 593.7	64 458.6	58 366.5	49 207.6
0.3	72 082.2	69 787.0	67 548.2	61 161.7	51 560.3
0.4	76 576.5	74 137.8	71 759.1	64 972.3	54 769.3
0.6	88 152.2	85 347.2	82 611.1	74 802.7	63 056.9

(b) Reference ram drag, $T_{DRAG_{REF}}$

Mach number	Full-throttle reference ram drag, lbf, at altitude of—				
	0 ft	1000 ft	2000 ft	5000 ft	10 000 ft
0	2.3	2.2	2.1	1.9	1.6
0.2	4759.4	4589.9	4425.4	3960.2	3273.5
0.3	7406.2	7142.4	6886.3	6162.3	5093.7
0.4	10 361.2	9992.2	9633.9	8620.9	7125.5
0.6	17 424.9	16 804.4	16 201.9	14 498.3	11 982.4

Table A2. Ram Drag Bivariate Function for Part Throttle Operation

(a) Mach number = 0

$\frac{T_{GROSS}}{T_{GREF}}$	$\frac{T_{DRAG}}{T_{DRAG_{REF}}}$
0.0635	0.5217
0.2836	0.7391
0.4245	0.8696
0.5547	0.9565
0.6635	1.0000
1.0000	1.0000

(b) Mach number = 0.2

$\frac{T_{GROSS}}{T_{GREF}}$	$\frac{T_{DRAG}}{T_{DRAG_{REF}}}$
0.0829	0.5257
0.2911	0.7283
0.4302	0.8507
0.5589	0.9587
0.6667	1.0000
1.0000	1.0000

(c) Mach number = 0.3

$\frac{T_{GROSS}}{T_{GREF}}$	$\frac{T_{DRAG}}{T_{DRAG_{REF}}}$
0.0976	0.4691
0.2973	0.7247
0.4348	0.8468
0.5620	0.9539
0.6694	1.0000
1.0000	1.0000

(d) Mach number = 0.4

$\frac{T_{GROSS}}{T_{GREF}}$	$\frac{T_{DRAG}}{T_{DRAG_{REF}}}$
0.1129	0.5196
0.3044	0.7196
0.4401	0.8414
0.5654	0.9472
0.6726	1.0000
1.0000	1.0000

(e) Mach number = 0.6

$\frac{T_{GROSS}}{T_{GREF}}$	$\frac{T_{DRAG}}{T_{DRAG_{REF}}}$
0.1372	0.5096
0.3164	0.7050
0.4490	0.8262
0.5700	0.9282
0.6785	1.0000
1.0000	1.0000

Table A3. Full-Throttle Net Thrust for TBE-M2.4 Engine With K_{size} = 0.77294.

Mach number	Full-throttle net thrust, lbf, at altitude of—				
	0 ft	1000 ft	2000 ft	5000 ft	10 000 ft
0	50 614.4	49 003.9	47 432.8	42 952.5	36 216.1
0.2	49 487.6	47 925.8	46 402.7	42 053.3	35 504.8
0.3	49 991.3	48 421.1	46 888.6	42 511.8	35 916.4
0.4	51 181.1	49 581.3	48 019.7	43 556.8	36 826.3
0.6	54 668.7	52 980.2	51 331.0	46 612.3	39 478.0

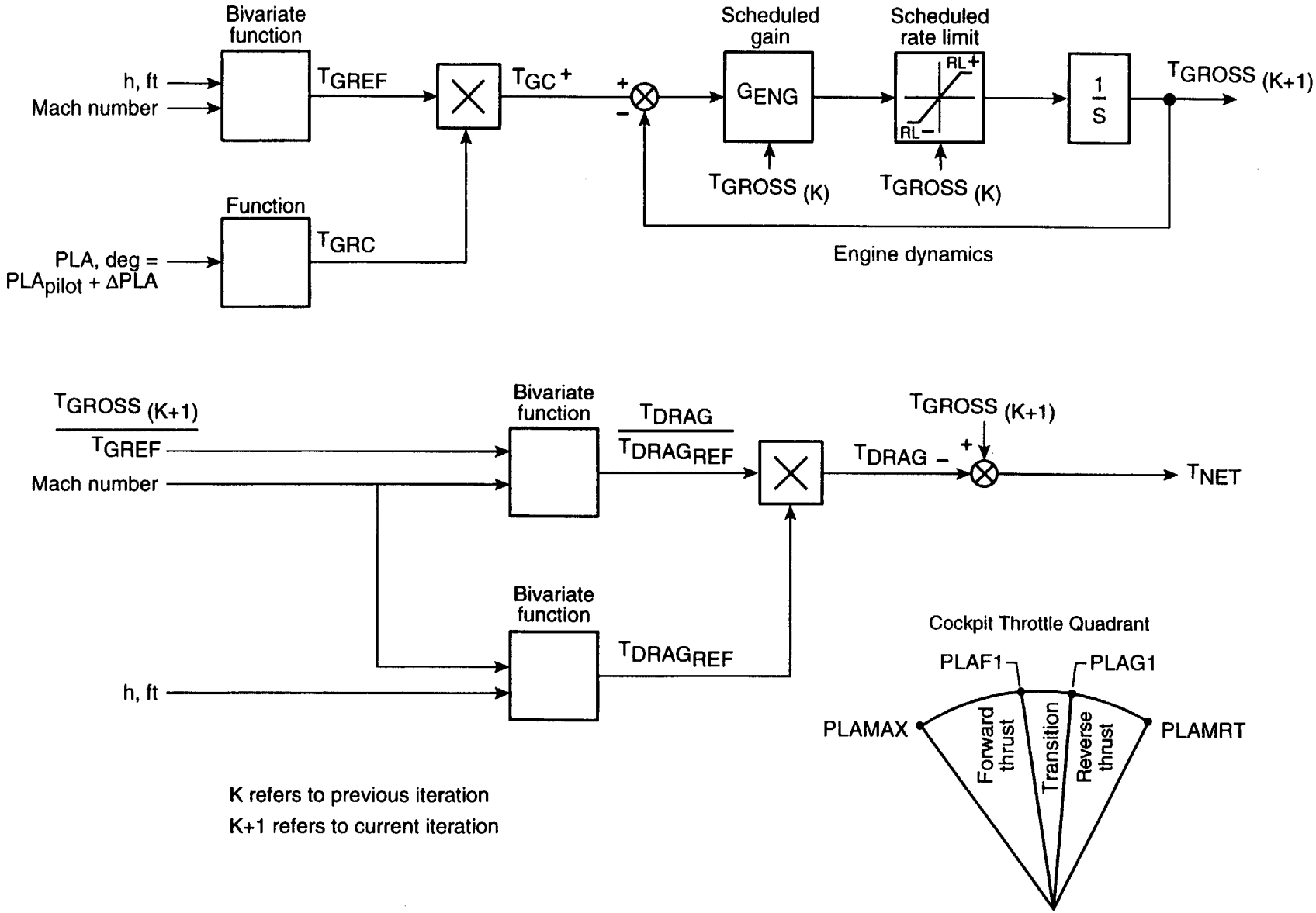

Figure A1. Engine block diagram. All forces in lbf.

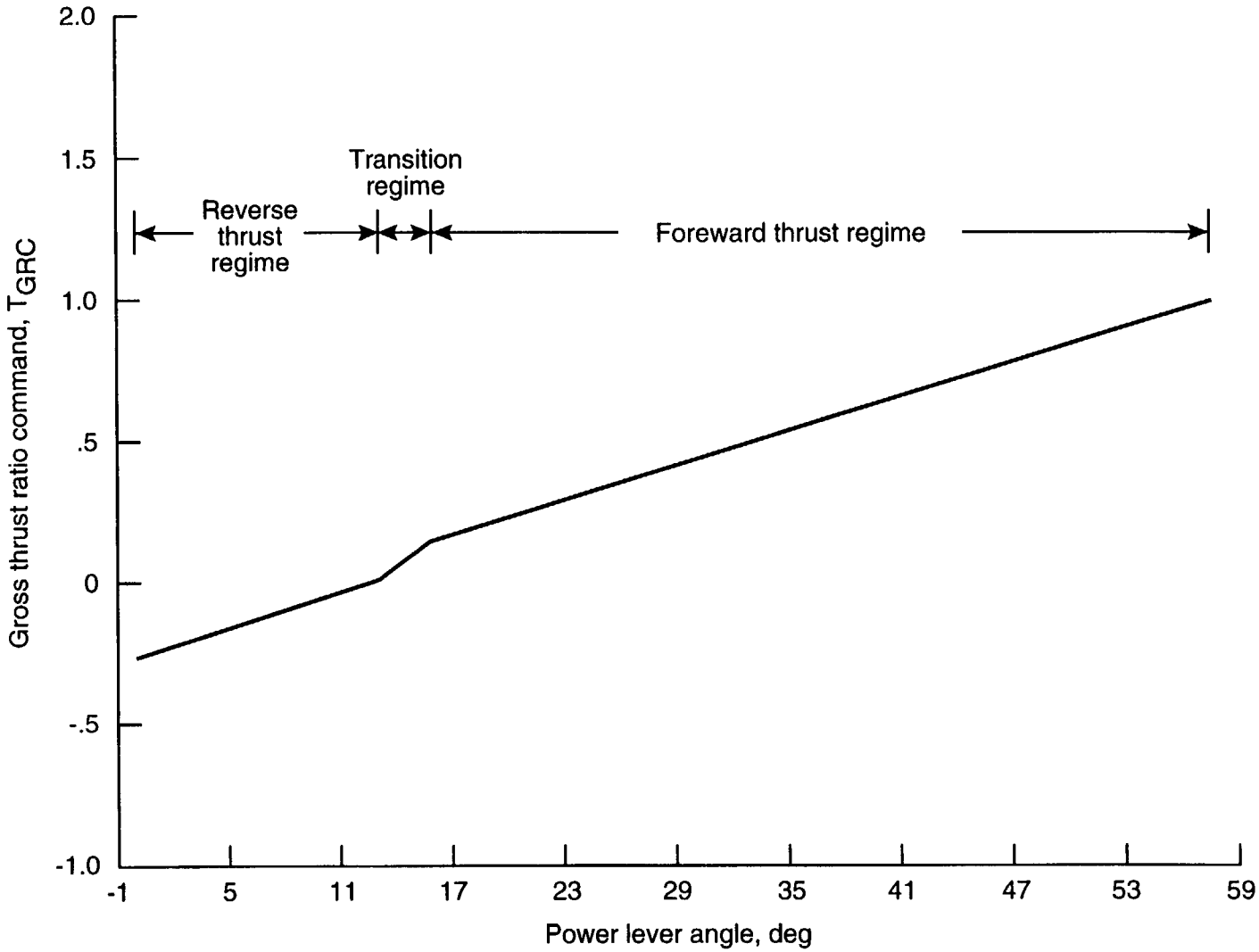

Figure A2. Throttle input-output diagram.

$T_{GMAX} \geq T_G \geq T_{GMIN}$ {forward}

(187) $T_1^* = 0.1$

(188) $T_2^* = 0.9$

(189) $G_{ENG_1} = 0.2$

(190) $G_{ENG_2} = 2.0$

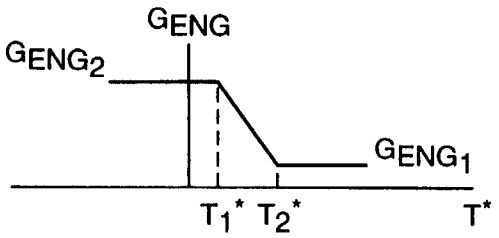

$$T^* = \frac{T_{GC} - T_G}{T_{GMAX} - T_{GMIN}}$$

(89) $T_1^{**} = 0.04$

(90) $T_2^{**} = 0.4$

(195) $R_{L_1}^+ = 3316$

(192) $R_{L_2}^+ = 28\,426$

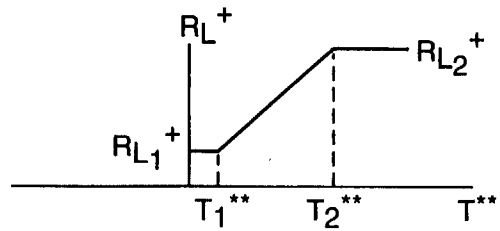

$$T^{**} = \frac{T_G - T_{GMIN}}{T_{GMAX} - T_{GMIN}}$$

Figure A3. Scheduled gains and limits for engine dynamics.

M	V_j, ft/sec, for full-throttle operation at altitude—				
	0 ft	1000 ft	2000 ft	5000 ft	10 000 ft
0	3116.66	3118.29	3119.85	3124.36	3130.75
.2	3149.06	3150.65	3152.24	3156.63	3162.84
.3	3180.10	3181.70	3183.24	3187.58	3193.70
.4	3220.00	3221.59	3223.13	3227.42	3233.56
.6	3312.07	3313.71	3315.30	3319.75	3325.99

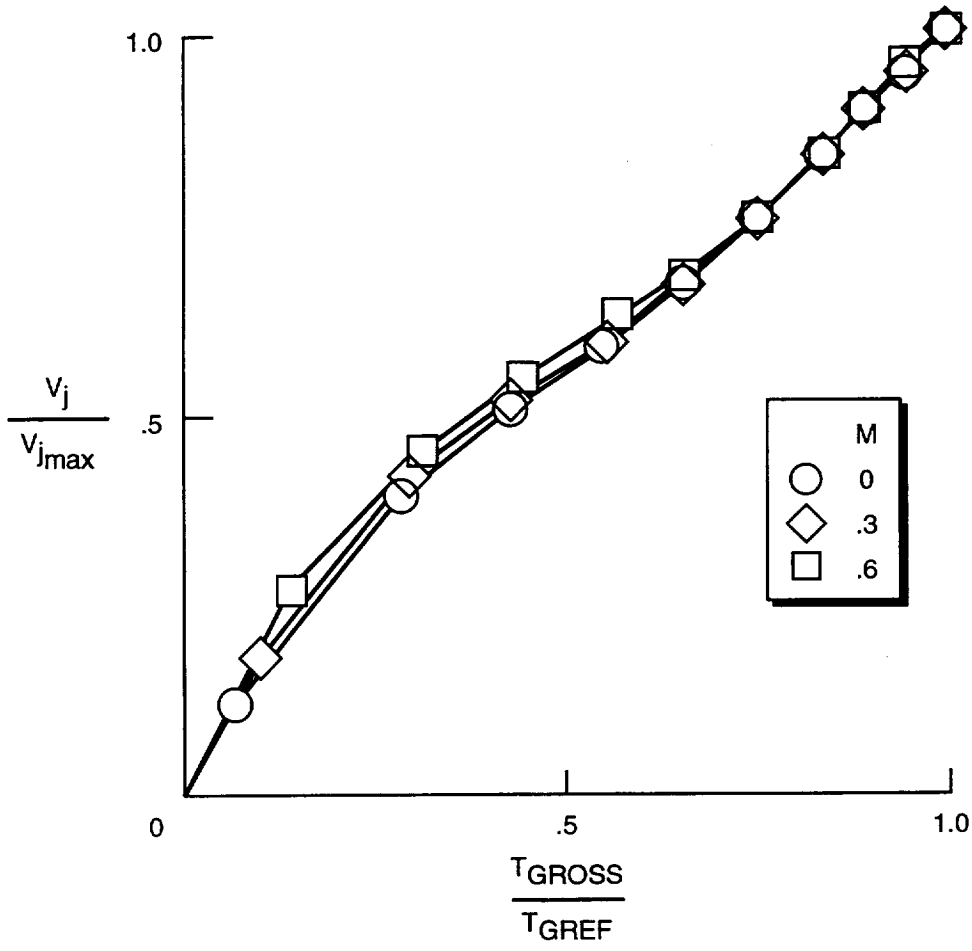

Figure A4. TBE-M2.4 engine exhaust jet velocity for full and part throttle operation.

Appendix B

Description of Pilot Controllers and Flight Control Systems

Force-deflection characteristics of the hand controller and the rudder pedals that were used in the simulation are given in figure B1. Hydraulic control loaders were used to provide the forces. A two-axis hand controller was mounted on the left side of the cockpit and used by the pilot for pitch and roll control inputs. The device was positioned so that an axis through the grip in the neutral position was tilted 10° inboard and forward 13° from the local vertical for pilot operating comfort. Rudder pedals were used for directional control. Breakout forces were used for all three axes and as indicated in figure B1 physical deadbands were not employed. Flight control system electrical inputs from the different pilot controller deflections are given in figure B2. Deadbands as illustrated in the sketch were employed in the computer program to eliminate inadvertent hand controller or rudder pedals inputs and/or unwanted coupled inputs when applying a single axis control input with the hand controller. Flight control system block diagrams for longitudinal, lateral, and directional axes are given in figures B3(a), B3(b), and B3(c), respectively. The mode of control was essentially a rate-command attitude-hold system. A wing leveler was incorporated in the lateral axis, and turn coordination in the directional axis.

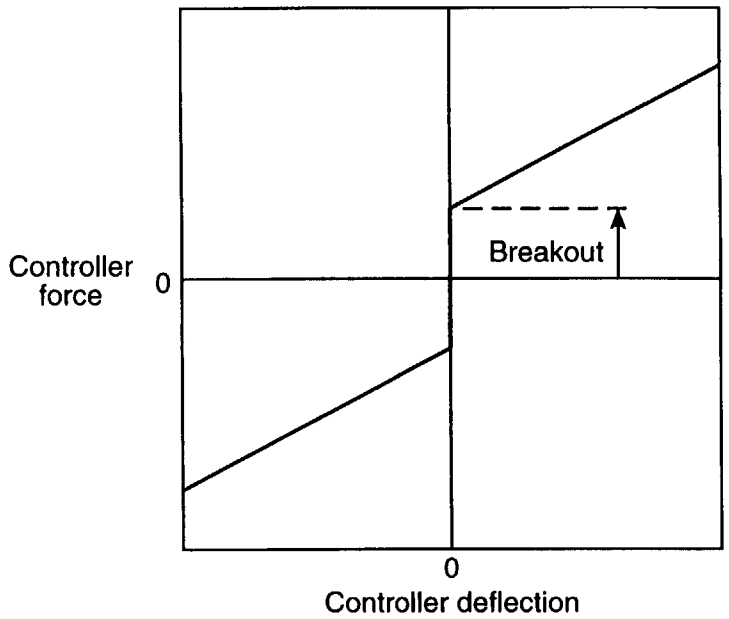

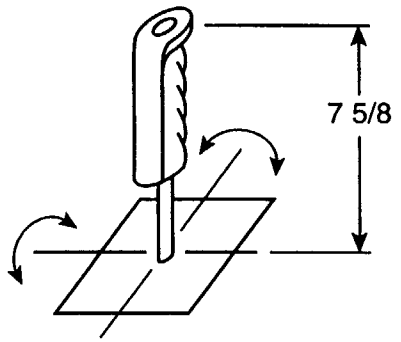

Hand controller details

Pilot control device	Axis	Breakout, lb	Force gradient	Neutral position	Maximum deflection
Hand controller	Pitch	±0.75	2.43 lb/deg	13° forward[a]	±12°
Hand controller	Roll	±0.75	1.27 lb/deg	10° inboard[a]	±12°
Rudder pedals	Yaw	±12	36 lb/in.	0 in.	±2.50 in.

[a]Measured from local vertical.

Figure B1. Force and deflection characteristics of hand controller and rudder pedals. Linear dimensions in inches.

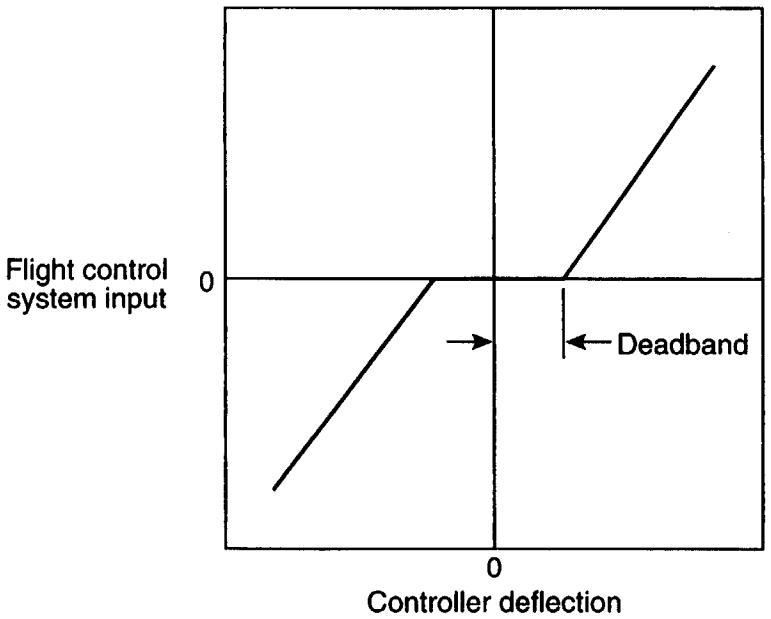

Pilot control device	Axis	Maximum deflection	Controller deadband	Control system input	Gradient	Maximum deflection
Hand controller	Pitch	±12°	±0.08°	δc_{pilot}, deg	4.1946 deg/deg	±50°
Hand controller	Roll	±12°	±0.50°	δw_{pilot}, deg	2.9522 deg/deg	±33.95°
Rudder pedals	Yaw	±2.5 in.	±0.05 in.	δ_{ped}, in.	1.1224 in./in.	±2.75 in.

Figure B2. Flight control system inputs for pilot controller deflections.

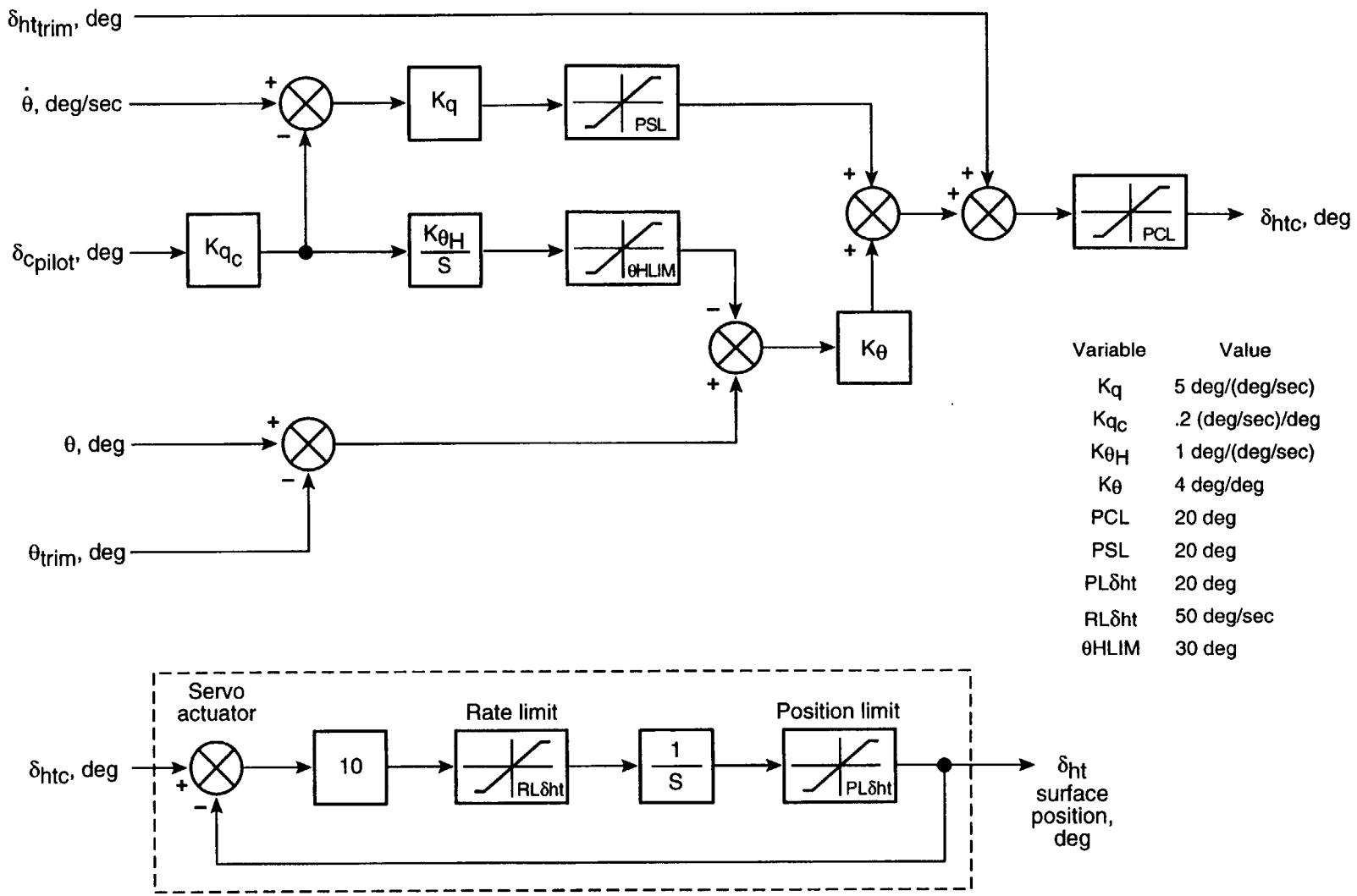

Variable	Value
K_q	5 deg/(deg/sec)
K_{q_c}	.2 (deg/sec)/deg
$K_{\theta H}$	1 deg/(deg/sec)
K_θ	4 deg/deg
PCL	20 deg
PSL	20 deg
PLδht	20 deg
RLδht	50 deg/sec
θHLIM	30 deg

(a) Longitudinal control system.

Figure B3. Flight control system block diagrams.

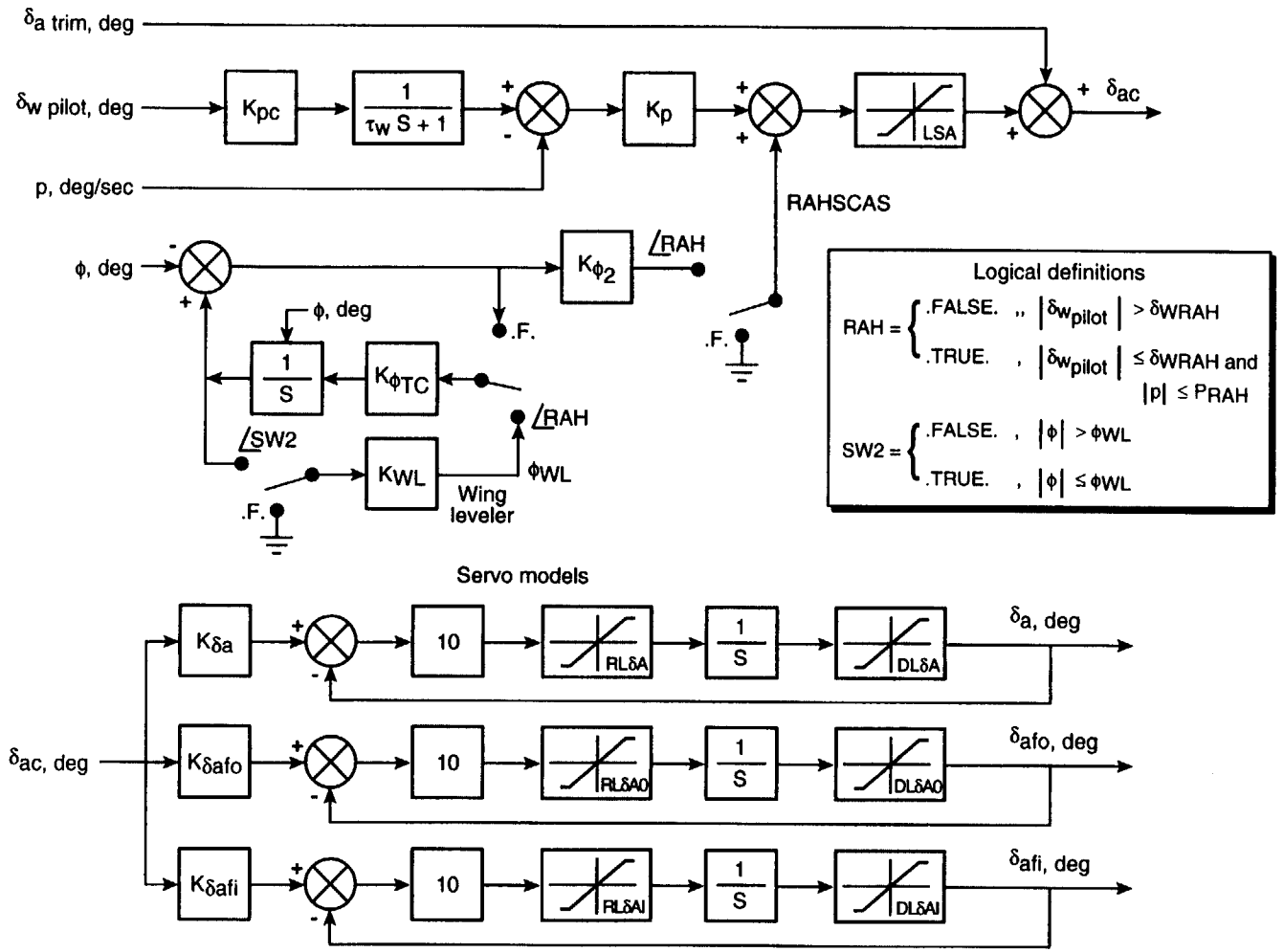

Variable	Value
K_{PC}	.35 (deg/sec)/deg
τ_W	.7 sec
K_p	6.5 deg/(deg/sec)
LSA	35 deg
K_{ϕ_2}	7.5 deg/deg
$K_{\phi_{TC}}$	-50 (deg/sec)/deg
K_{WL}	1 deg/deg
δ_{WRAH}	.3 deg
P_{RAH}	1 deg/sec
ϕ_{WL}	2 deg
$K_{\delta a}$	1 deg/deg
RLδA	70 deg/sec
DLδA	35 deg
$K_{\delta afo}$	.86 deg/deg
RLδAO	40 deg/sec
DLδAO	30 deg
$K_{\delta afi}$	.29 deg/deg
RLδAI	50 deg/sec
DLδAI	10 deg

(b) Lateral control system.

Figure B3. Continued.

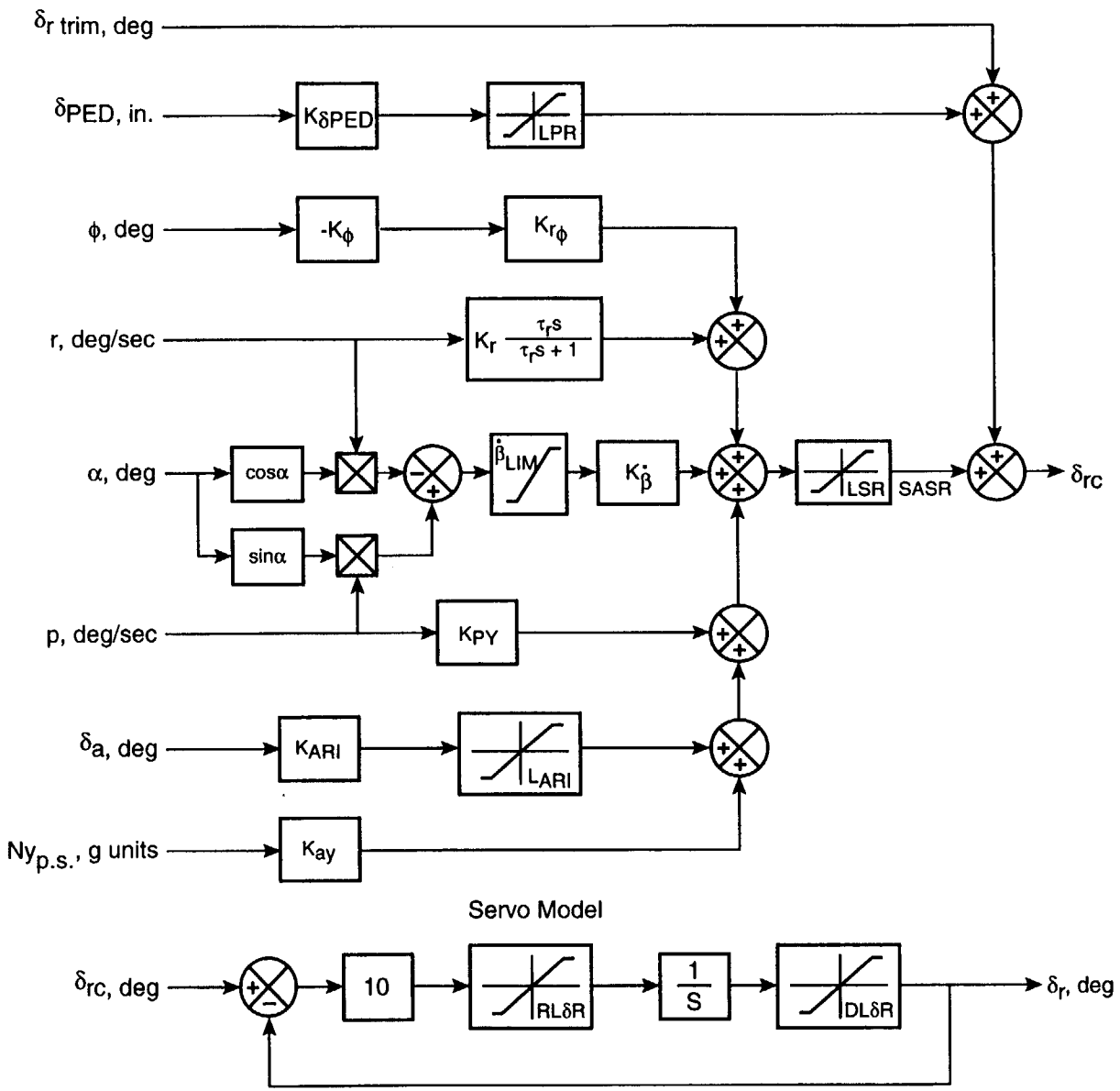

Variable	Value
$K_{\delta PED}$	-10 deg/in.
LPR	25 deg
K_{ϕ}	3 deg/deg
$K_{r_{\phi}}$	.14 deg/deg
K_r	-1 deg/(deg/sec)
τ_r	4 sec
$\dot{\beta}_{LIM}$	10 deg/sec
$K_{\dot{\beta}}$	-5 deg/(deg/sec)
K_{PY}	-.6 deg/(deg/sec)
LSR	25 deg
K_{ARI}	-.2 deg/deg
L_{ARI}	20 deg
K_{ay}	0 deg/g unit
RLδR	50 deg/sec
DLδR	25 deg

(c) Directional control system.

Figure B3. Concluded.

Appendix C

Some High Lift Considerations for Takeoff and Initial Climb-Out

To address the impact of HSCT operations on airport-community noise, the piloted simulation described herein explored various ways of reducing noise levels during takeoff flight phases. One way of reducing noise levels is to increase the lift and/or *L/D* of the configuration, and thus reduce the engine thrust required. One means of achieving an increase in lift is by applying BLC to the wing flaps. Because some information was already available from wind-tunnel tests of an identical wing-body-engine configuration performed in the early 1970's, this data was used in the analysis presented herein. Results of some brief calculations are presented to give an indication of what BLC on wing flaps can provide in terms of lift increment and thrust levels for the HSCT initial climb-out maneuver.

Figure C1 shows trimmed *L/D* values for the HSCT configuration (AST-105-1 simulation database) with the two inboard flaps on each wing semispan deflected 20° for takeoff. The *L/D* values are presented here as a point of reference because other studies have employed $(L/D)_{max}$ as a figure of merit. The lower curve on figure C1 corresponds to the values used during the study by Grantham, Smith, and Deal during the mid-1970's. This curve serves as a baseline condition (ref. 1). The curve labeled "with $\Delta C_L = 0.10$" contains an arbitrary increment in lift coefficient that was added to the aerodynamics of the baseline case and represents a potential improvement in the AST-105-1 configuration. Drag and pitching moment remained the same for the two curves. The middle curve corresponds to the baseline configuration with the addition of BLC over the upper surface of the two inboard flaps on each wing semispan with a blowing coefficient $C_\mu = 0.02$. (BLC results are from ref. 18.) The negative pitching moment increment due to flap lift from BLC is balanced by a positive pitching moment increment from a reduction in horizontal tail incidence angle. Drag results with and without BLC in reference 18 show identical values in the angle of attack range from 0° to 8°, which is the angle of attack range involved in takeoff trajectories. Therefore, no change in drag due to adding BLC was employed in the calculations.

It should be noted that the *L/D* values presented here are only due to aerodynamic effects—engine thrust components are not included. The simulation mathematical model of the AST-105-1 configuration incorporated a nozzle deflection angle of 8° on each engine for the specific purpose of directing the thrust vector of each engine through the aircraft c.g. Wind-tunnel test data have shown that power effects are not significant on the aerodynamic characteristics of this configuration.

The data in figure C1 indicate $(L/D)_{max}$ of the baseline occurs at an angle of attack of 2°. Also, a reasonable increase in all *L/D* values of the baseline occurs when BLC is applied. The increases shown in figure C1 would be larger if the down load on the horizontal tail to trim the BLC effect could be eliminated, possibly by using a jet or surface located forward of the c.g. Figure C2 presents $(L/D)_{max}$ values for these two additional trim schemes to illustrate possible *L/D* improvements.

One trim scheme employed a nose jet that was located on the fuselage lower surface and positioned longitudinally just forward of the nose wheels. The jet force was sized so that the pitching moment produced by the jet would balance the pitching moment due to flap BLC. For this scheme, the horizontal tail incidence used to trim the baseline configuration remained unchanged.

The second scheme replaced the nose jet with a canard at a fixed incidence relative to the fuselage. The canard was sized to balance the flap BLC effect at an angle of attack of 0°. When the vehicle angle of attack is increased, the additional canard lift force requires an increase in horizontal tail incidence angle to maintain trim conditions. For the simple estimate presented, the influence of the small canard on wing lift was neglected. Even with the jet or the canard modification, the value of $(L/D)_{max}$ is still slightly less than the value shown for the vehicle with the added $\Delta C_L = 0.10$ increment. The curve for the configuration with $\Delta C_L = 0.10$ in figure C1, however, would seem to be achievable with additional modifications to the configuration.

An analysis of steady climbing flight at constant velocity was made for the vehicle out of ground effect with the landing gear retracted. Figure C3 shows the force diagram and the equations used. As indicated, the thrust vector passed through the c.g., and thus, did not affect the pitching moment. The lift and drag values used in the analysis, however, correspond to trim condition and include adjustments to the horizontal tail incidence angle to null the aerodynamic pitching moment. Figure C4 provides the resulting C_T values as a function of IAS in knots. The calculated results are for a vehicle flight-path angle of 2.30° (4-percent climb gradient). As a ready reference, the corresponding *L/D* values are also provided in the figure. It is apparent from the C_T with IAS curves that providing increased lift at any speed (either by adding a ΔC_L or by applying BLC to the flaps) reduces engine thrust over that of the baseline configuration. At a speed of 250 knots, which is the maximum speed permitted by the FAA for flight operations below 10 000 ft, the reduction amounted to 6.5 percent with

BLC operating and approximately 10.0 percent with a lift addition of $\Delta C_L = 0.10$. An alternate interpretation from figure C4 is that the same C_T value can be employed at a lower speed when additional lift is supplied. It is of interest to note that in a steady climb on a 4-percent climb gradient with a speed of 250 knots, the vehicle with flap BLC is operating near its maximum value of *L/D*.

The additional C_T curve shown in figure C4 was generated with the full-throttle thrust values at 1000 ft and used in the simulation program for the TBE-M2.4 engine. The curve represents the total output of the four jet engines. It was included to permit a quick visual indication of the amount of thrust cutback available during initial climb out. A plot of C_T with flight-path angle for a climb speed of 250 knots is given in figure C5. Examination of the results shows that the engine thrust can be reduced by a constant percentage of the available thrust at any flight-path angle when flap BLC is employed. Engine thrust can be reduced by a larger percentage when the increment $\Delta C_L = 0.10$ is present. These additional thrust reductions will, of course, produce reductions in the airport-community noise levels due to jet engine source noise. The results shown in figure C5 indicate the thrust penalty for flight paths that exceed the 4-percent climb gradient mandated by the FAA.

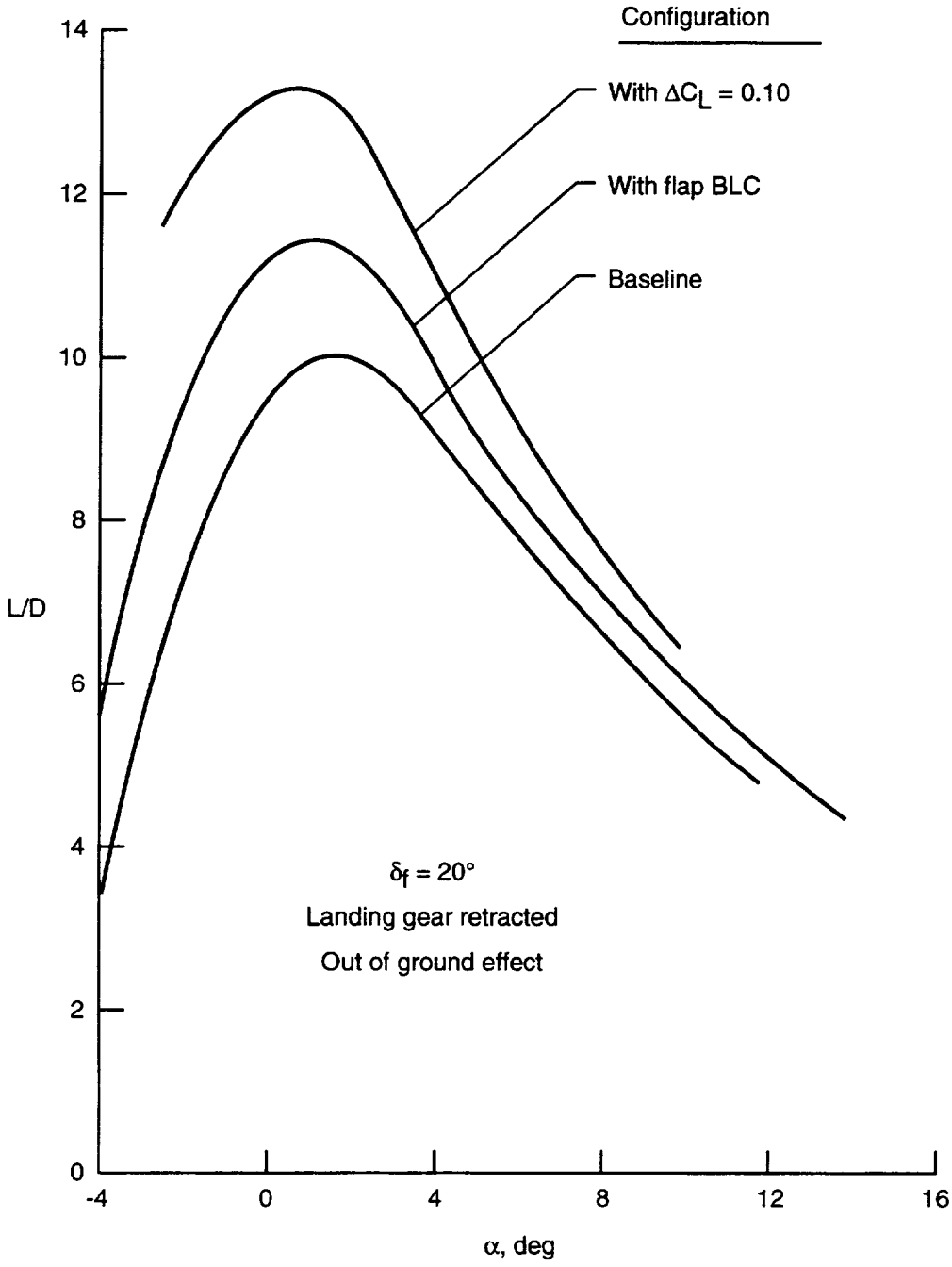

Figure C1. *L/D* values for trimmed aircraft configurations.

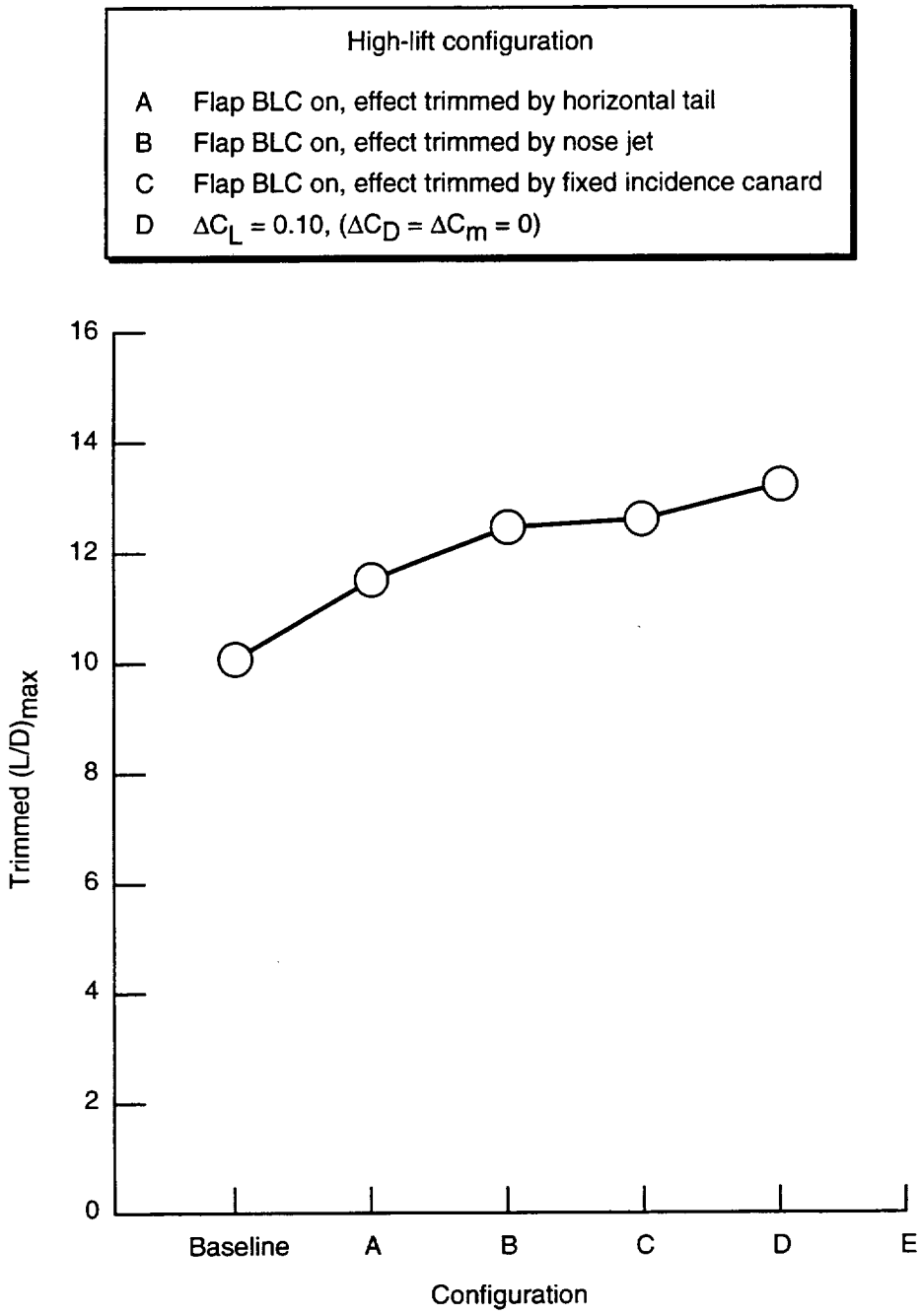

Figure C2. $(L/D)_{max}$ for trimmed baseline and high-lift configurations.

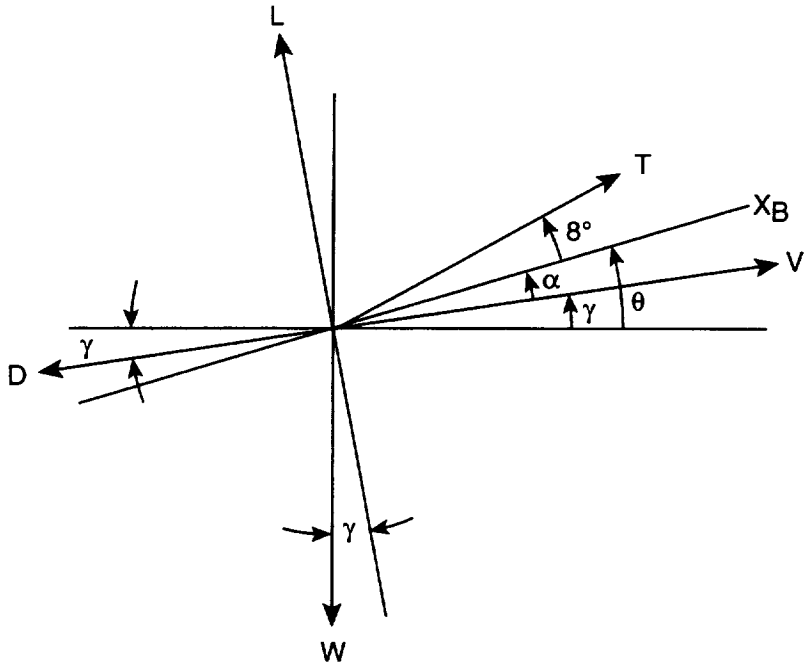

$$L + T \sin(\alpha + 8°) - W \cos\gamma = 0 \qquad (1)$$

$$D + W \sin\gamma - T \cos(\alpha + 8°) = 0 \qquad (2)$$

From (1) and (2)

$$\tan\gamma = \frac{T \cos(\alpha + 8°) - D}{T \sin(\alpha + 8°) + L} \qquad (3)$$

In coefficient form after rearranging

$$C_T = \frac{\tan\gamma\, C_L + C_D}{\cos(\alpha + 8°) - \tan\gamma \sin(\alpha + 8°)} \qquad (4)$$

Rewriting (1)

$$C_L + C_T \sin(\alpha + 8°) - \frac{W}{q_\infty S_W} \cos\gamma = 0$$

Solve for q_∞, then V

$$q_\infty = \frac{(W/S_W) \cos\gamma}{C_L + C_T \sin(\alpha + 8°)} \qquad (5)$$

Figure C3. Force diagram and equations for steady climbing flight.

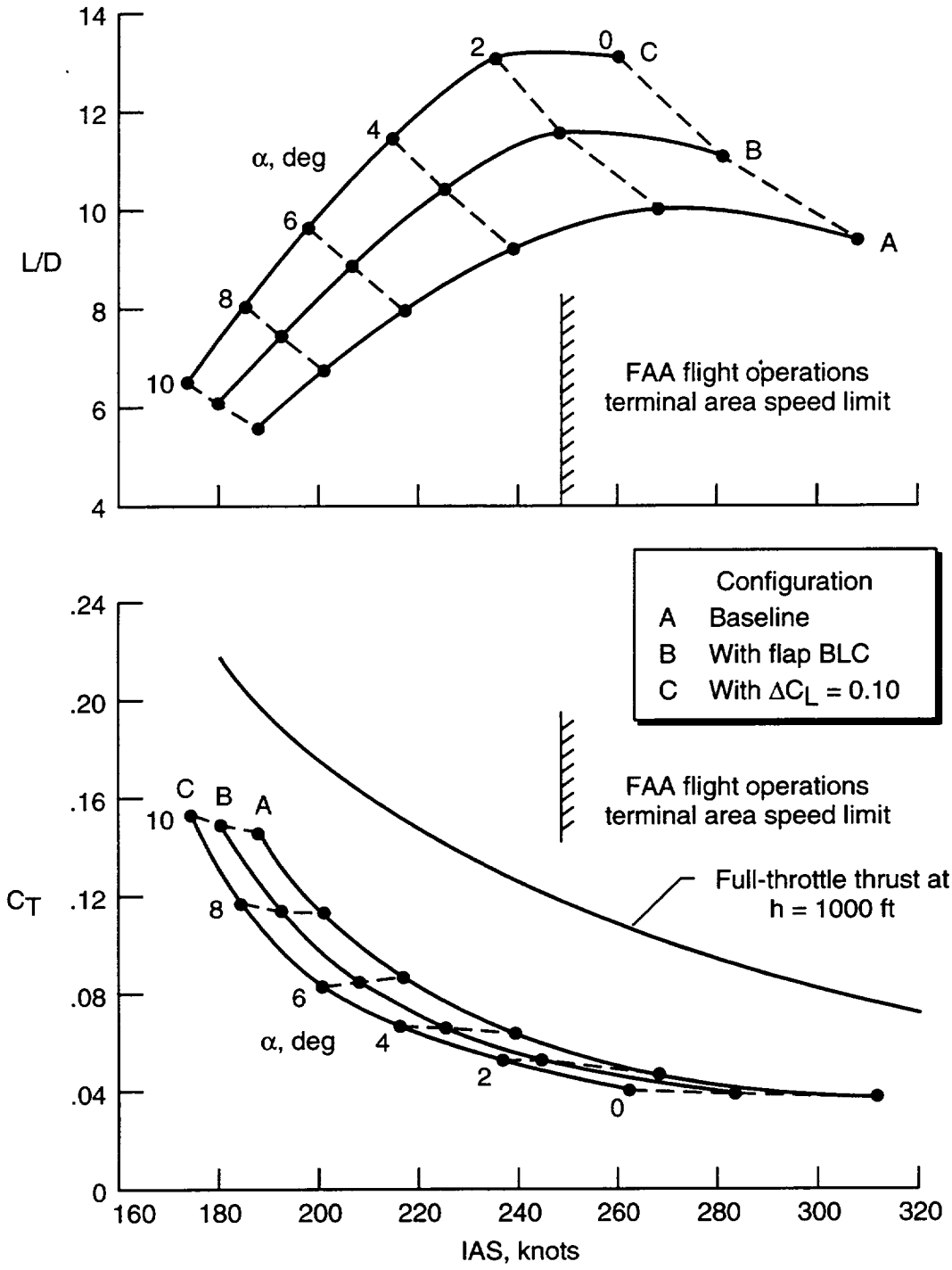

Figure C4. Values of thrust coefficient and lift-drag ratio for steady climbing flight on a 4-percent climb gradient with $\delta_f = 20°$, landing gear retracted, and out of ground effect.

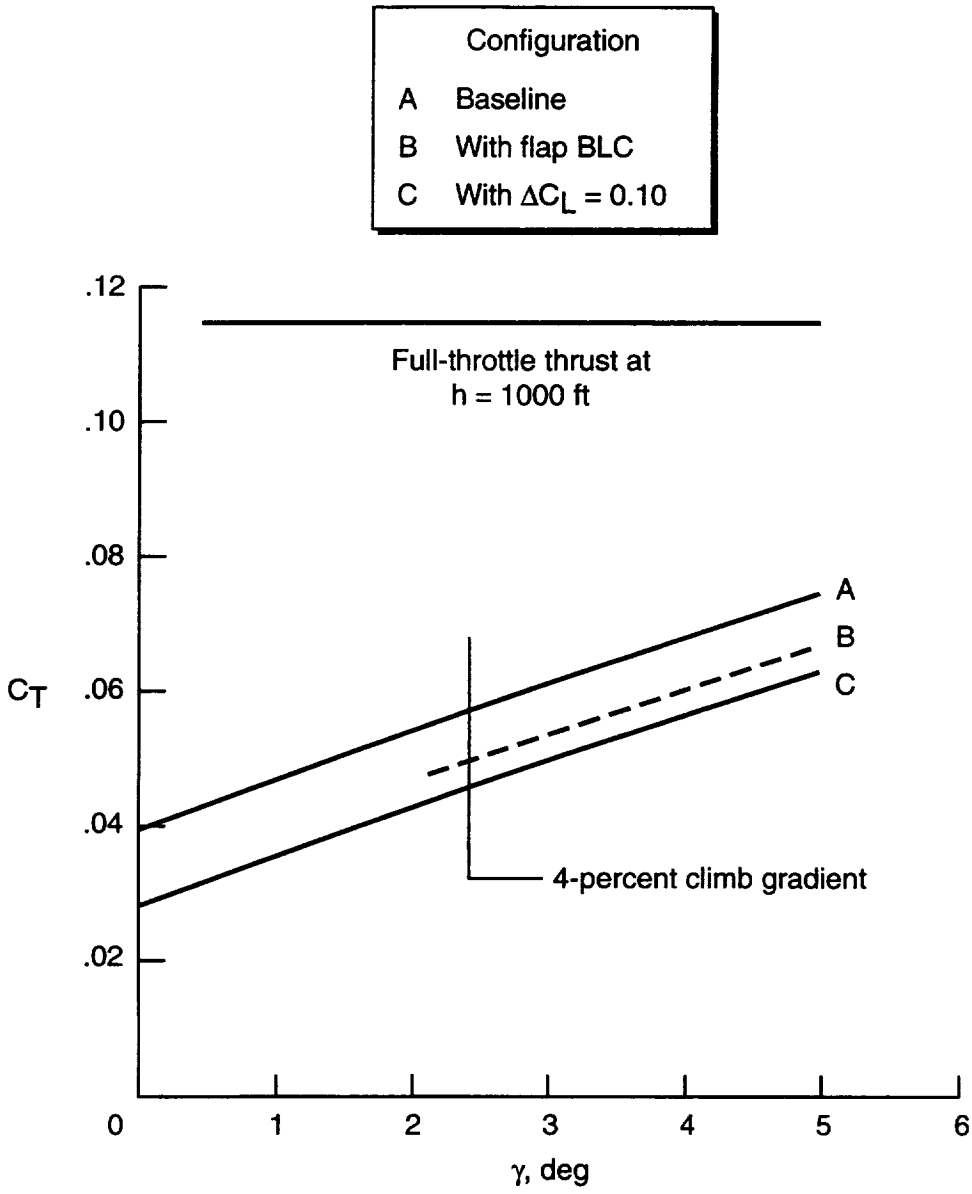

Figure C5. Thrust coefficient C_T with flight path angle γ for steady climbing flight at 250 knots with $\delta_f = 20°$, landing gear retracted, and out of ground effect.

Appendix D

Some Operational Considerations

During takeoff from the time the landing gear is fully retracted and until the aircraft reaches an altitude of 400 ft, FAR Part 25 specifies that the aircraft must be able to maintain a 3-percent climb gradient with one engine out. Above an altitude of 400 ft, the climb gradient requirement is reduced to 1.7 percent. A comparison of the engine thrust setting for the dual thrust-cutback procedure (all engines operating with the aircraft on a 4-percent climb gradient) with those required to trim the aircraft on a constant-speed 3-percent climb gradient with the critical engine (left outboard engine) inoperative is presented in figure D1. Results are presented for the baseline vehicle and with the two aerodynamic lift additions. The simulator thrust profiles presented are those producing the minimum sideline noise levels, which are shown in figure 11. An examination of the simulator flight data indicated that for all three lift cases, the aircraft reached an altitude of 400 ft with airspeeds between 240 and 245 knots. The curves in figure D1 indicate that the first thrust-cutback settings exceed the FAR Part 25 requirement over the airspeed range for the vehicle with either aerodynamic high-lift addition. The baseline configuration meets the requirement over most of the airspeed range and fails only very slightly for speeds between 224 and 229 knots. Except for this 5-knot speed interval, the results for the three lift cases indicate that sufficient thrust remains to maintain at least a 3-percent constant-speed climb gradient when an engine failure occurs. Thus, the programmed automatic throttles need not make an additional thrust adjustment in the first thrust-cutback level. The pilot must, however, reduce the climb gradient from 4 to 3 percent when the engine fails because the aircraft can no longer maintain the original 4-percent climb gradient at most airspeeds up to 240 knots without decelerating. Because the second thrust cutback occurs when the airspeed is about 250 knots and the vehicle altitude exceeds 400 ft, the 1.7-percent climb gradient requirement of FAR Part 25 applies for engine failures that occur after the second thrust cutback. The following table shows the net-thrust values of the dual thrust-cutback takeoff procedure that were used in the simulator and those of the FAR Part 25 for this flight region. Also shown are the engine net-thrust levels for straight and level flight with the critical engine inoperative.

Configuration	Single engine net-thrust settings for—		
	Dual thrust-cutback procedure,[a] percent	FAR Part 25 requirement,[b] percent	Level flight,[c] percent
Baseline	52	60	52
With flap BLC	45	52	44
With $\Delta C_L = 0.10$	42	47	38

[a]All engines operational and 4-percent climb gradient.
[b]One engine out and 1.7-percent climb gradient.
[c]One engine out and 0-percent climb gradient.

For all three configurations, net-thrust settings are below the requirement of FAR Part 25 for the 1.7-percent climb gradient with the critical engine inoperative. The net-thrust settings are, however, equal to or exceed those for maintaining straight and level flight with one engine out. Although this latter result eliminates a potential rate-of-descent condition from safety considerations, it appears that for an engine failure following second thrust cutback, engine throttle adjustments must be made to bring all configurations into compliance with the FAR 1.7-percent climb gradient requirement. Such thrust increases could be accomplished by using the computer driven automatic throttles and incorporating failure mode programming.

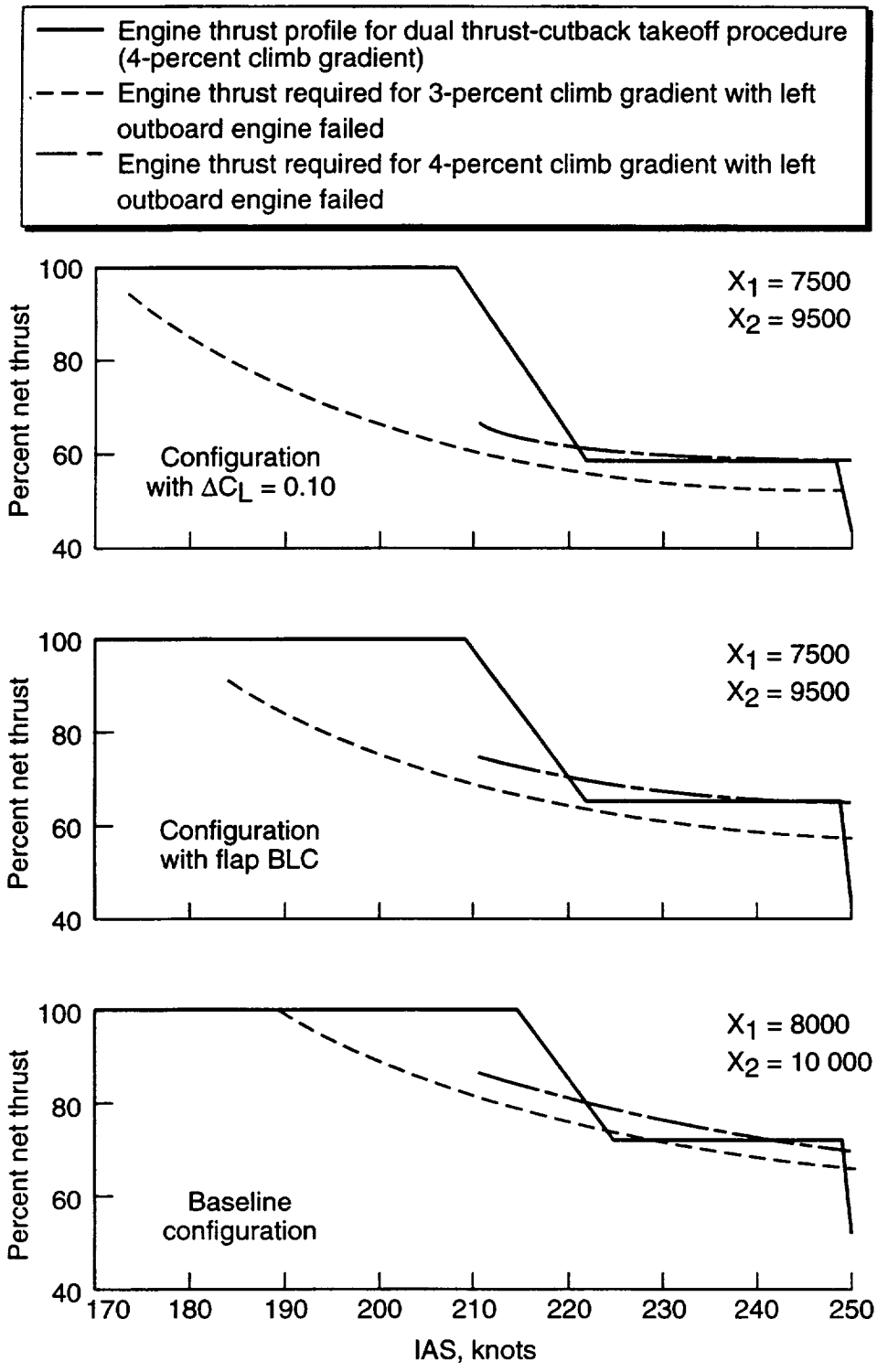

Figure D1. Engine thrust profiles for dual thrust-cutback procedure and FAR Part 25 engine failure requirements.

Appendix E

Further Noise Reductions and Operational Constraints

All noise data presented in figure 17 for the dual thrust-cutback procedure were obtained from simulator runs where the final climb speed was 250 knots. If the final climb speed for the configuration with $\Delta C_L = 0.10$ was chosen in the vicinity of $V_2 + 10$ (near 235 knots) rather than 250 knots, an additional improvement in sideline EPNdB levels could be obtained. By reducing the final climb speed from 250 to 235-knots, the level of thrust at first thrust cutback can be reduced because the acceleration level needed to reach the 235-knot final climb speed is reduced. A reduced-thrust level at first thrust cutback provides a reduction in sideline noise level. Centerline EPNdB noise values are also altered from those in figure 17 because of an increase in thrust setting that is required to maintain the slower constant-speed 4-percent climb gradient. Figure E1 presents the noise data and thrust levels for different climb speeds as a function of first thrust-cutback distance X_1. Results for the configuration with the standard engine and with the 10-percent oversized engine are provided. The data for $V_c = 250$ knots is that previously presented in figure 15(b). A comparison of the EPNdB values for each engine configuration indicates that sideline noise values can be reduced about 3 EPNdB by reducing the final climb speed to 235 knots. Centerline noise levels for the slower climb-speed data, however, show an increase of about 1/2 EPNdB over the data obtained with $V_c = 250$ knots. These takeoff noise results indicate a possible lower limit for the sideline EPNdB values. It should be noted that the thrust levels for the $V_c = 235$ knots are below those required for the critical condition of an inoperable engine, and thus, do not meet the requirements for FAR Part 25. To allow these low thrust levels to be used in flight operations, as well as for aircraft noise certification, would require the FAA to modify or grant exceptions to the FAR Part 25 regulations.

During takeoff from the time that the landing gear is fully retracted and until the aircraft reaches an altitude of 400 ft, FAR Part 25 specifies that the aircraft must be able to maintain a 3-percent climb gradient with one engine out. Above an altitude of 400 ft, the 3-percent gradient requirement is reduced to 1.7 percent. A comparison of the engine thrust setting for the aircraft on a 4-percent climb gradient with all engines operating (dual thrust-cutback procedure) with that required to trim the aircraft on a 3-percent climb gradient with the critical engine (left outboard engine) inoperative is presented in figure E2. Results are presented for the configuration with the $\Delta C_L = 0.10$ addition for both the standard and the 10-percent oversized engines. The simulator thrust profiles presented are those in figure E1 that had the minimum sideline noise levels. The results in figure E2 indicate that the first thrust-cutback settings are below those required to meet the FAR Part 25 requirement for critical engine-out operation. Likewise, the simulator thrust settings at second thrust cutback are below the 1.7-percent climb gradient of the FAR Part 25 requirement for critical engine-out operation. It is interesting to observe that the first thrust-cutback settings for the configuration with either engine are sufficient for the aircraft to maintain a 1.7-percent climb gradient, if at the time of the engine failure, the pilot reduces the climb gradient from 4 percent to 1.7 percent. Thus, although the 3-percent climb gradient requirement cannot be met, a positive rate of climb exists with the critical engine inoperative. Note that in the event of an engine failure, the thrust level at second thrust cutback can only maintain level flight with proper pilot pitch-down response. The results presented in figure E2 also indicate that automatic throttles under computer control for takeoff thrust will be required to incorporate engine failure programming that automatically increases the throttle settings, and thus, provides the thrust response necessary to achieve flight safety. Such procedures are not considered in the present FAR Part 25 regulations and would require the FAA to modify the regulations for HSCT type aircraft.

Figure E3 presents the thrust-velocity profiles for one configuration for takeoffs with final climb speeds of 235 and 250 knots. Also shown are the thrust trim curves for all engines operating and one engine out as detailed in FAA requirements FAR Part 36 and FAR Part 25. These three curves were obtained from computations using the simulation database and trim routine at a constant altitude and processed off-line in batch mode. The percentage levels shown can vary slightly because the TBE maximum thrust varies with altitude. The thrust-airspeed curve for all engines operating is provided because it establishes the lowest engine thrust setting that enables the aircraft to maintain a 4-percent climb gradient for a distance of 8.5 mi. From an examination of figure E3, a climb speed slightly less than 235 knots could provide a slightly lower thrust level at first cutback, and hence, a lower sideline EPNdB value. Unfortunately, a comparable thrust increase would be required to establish the final climb speed, and thus, produce a corresponding increase in the noise level at the centerline measurement location. As was indicated in the text, the minimum thrust level that establishes a 4-percent climb gradient occurs at an airspeed of 250 knots.

Noise levels for the two different climb speeds are presented in figure E4 for the configuration with

$\Delta C_L = 0.10$ both with and without 10-percent engine oversizing. The figure presents an evaluation of the noise suppression required by the TBE engines to meet FAR Part 36 Stage 3 requirements. Values with and without the −2 EPNdB trade available from the approach measurement are provided. The results with the 10-percent oversized engines and the −2 EPNdB traded value, shown on the right side of figure E4 indicate at least a 1 EPNdB reduction in the amount of required suppression occurred with the slower climb speed (235 knots) rather than the 250-knot climb speed. Note that the −2 EPNdB trade value is applied differently for the two cases. For the 250-knot data, the −2 EPNdB trade value is applied to reduce sideline noise; whereas, for the 235-knot data, the −2 EPNdB trade value is used to reduce the centerline noise level. Although adding noise suppressors to the jet engines to provide a 15 EPNdB reduction in noise level would qualify the aircraft for FAA noise certification at either climb speed, some flexibility in the takeoff (throttle setting and cutback distances) is available for the procedure with the slower climb speed. Note also that with some minor adjustments to the procedure for $V_c = 235$ knots, it may be possible to meet FAR Part 36 Stage 3 noise requirements with 15 EPNdB of noise suppression without engine oversizing.

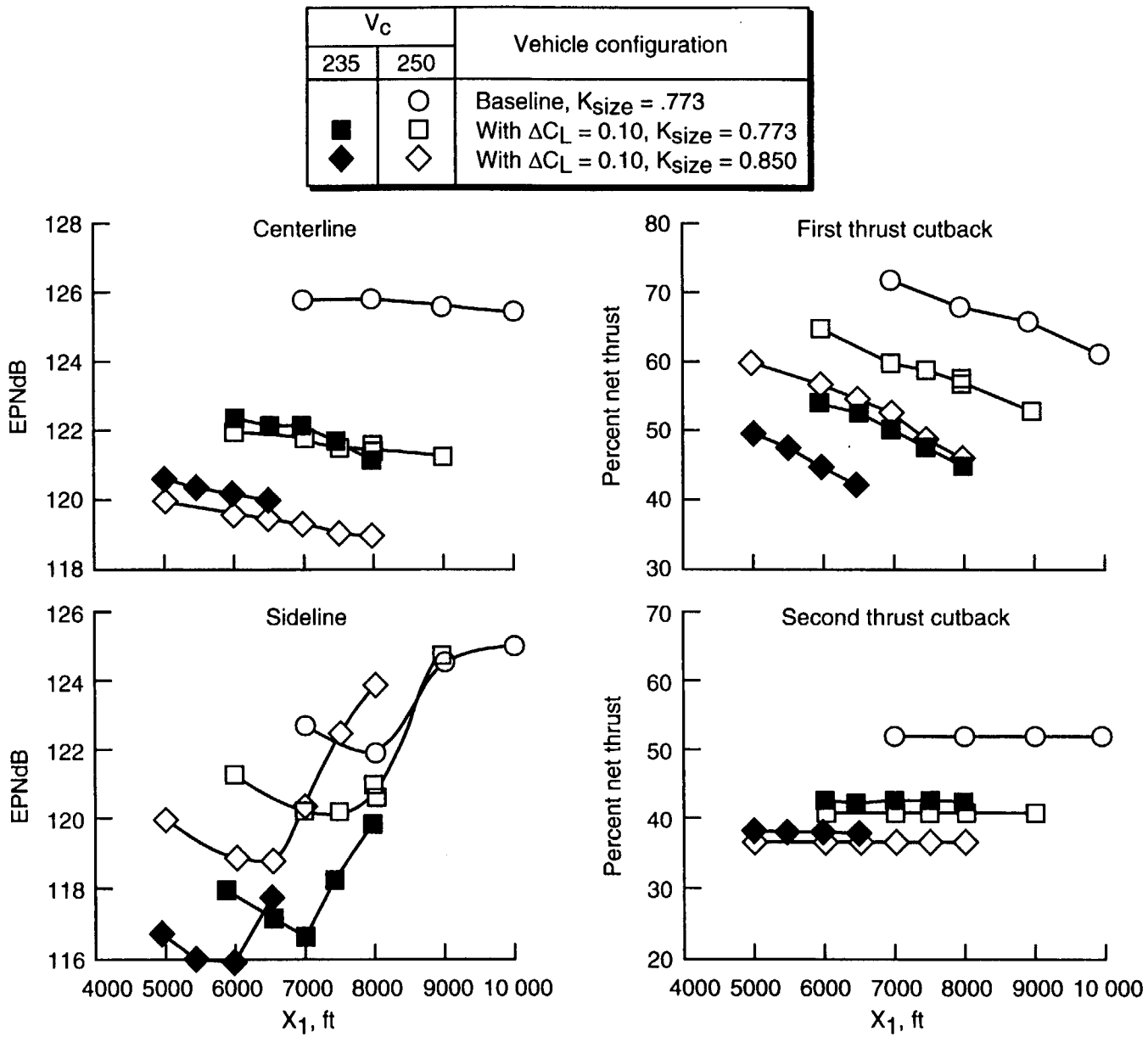

Figure E1. Effect of climb speed and vehicle configurations on thrust and noise levels.

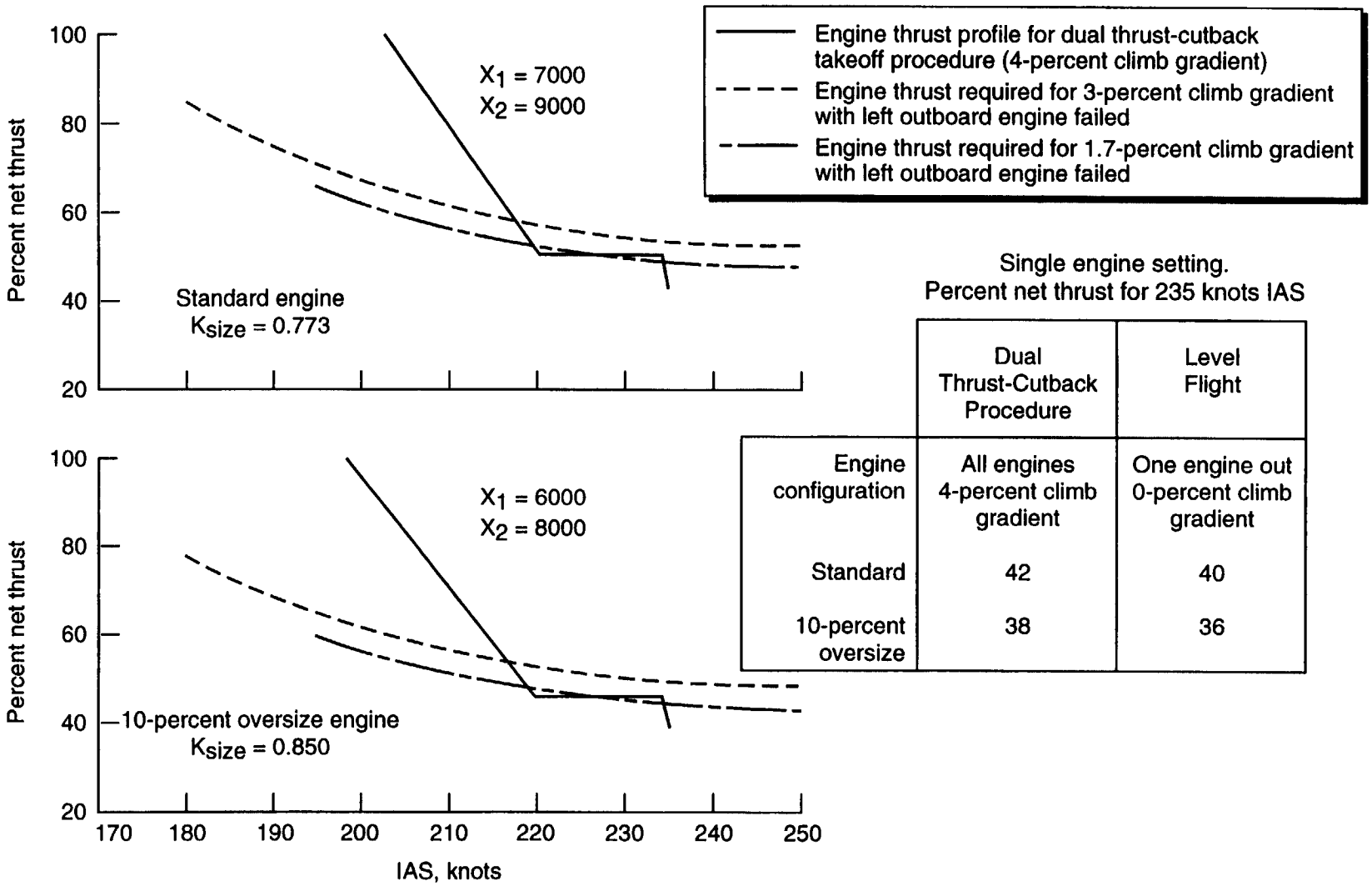

Single engine setting.
Percent net thrust for 235 knots IAS

Engine configuration	Dual Thrust-Cutback Procedure: All engines 4-percent climb gradient	Level Flight: One engine out 0-percent climb gradient
Standard	42	40
10-percent oversize	38	36

Figure E2. Engine thrust profiles for dual thrust-cutback procedure with final climb speed V_c of 235 knots and FAR Part 25 engine failure requirements for configuration with $\Delta C_L = 0.10$.

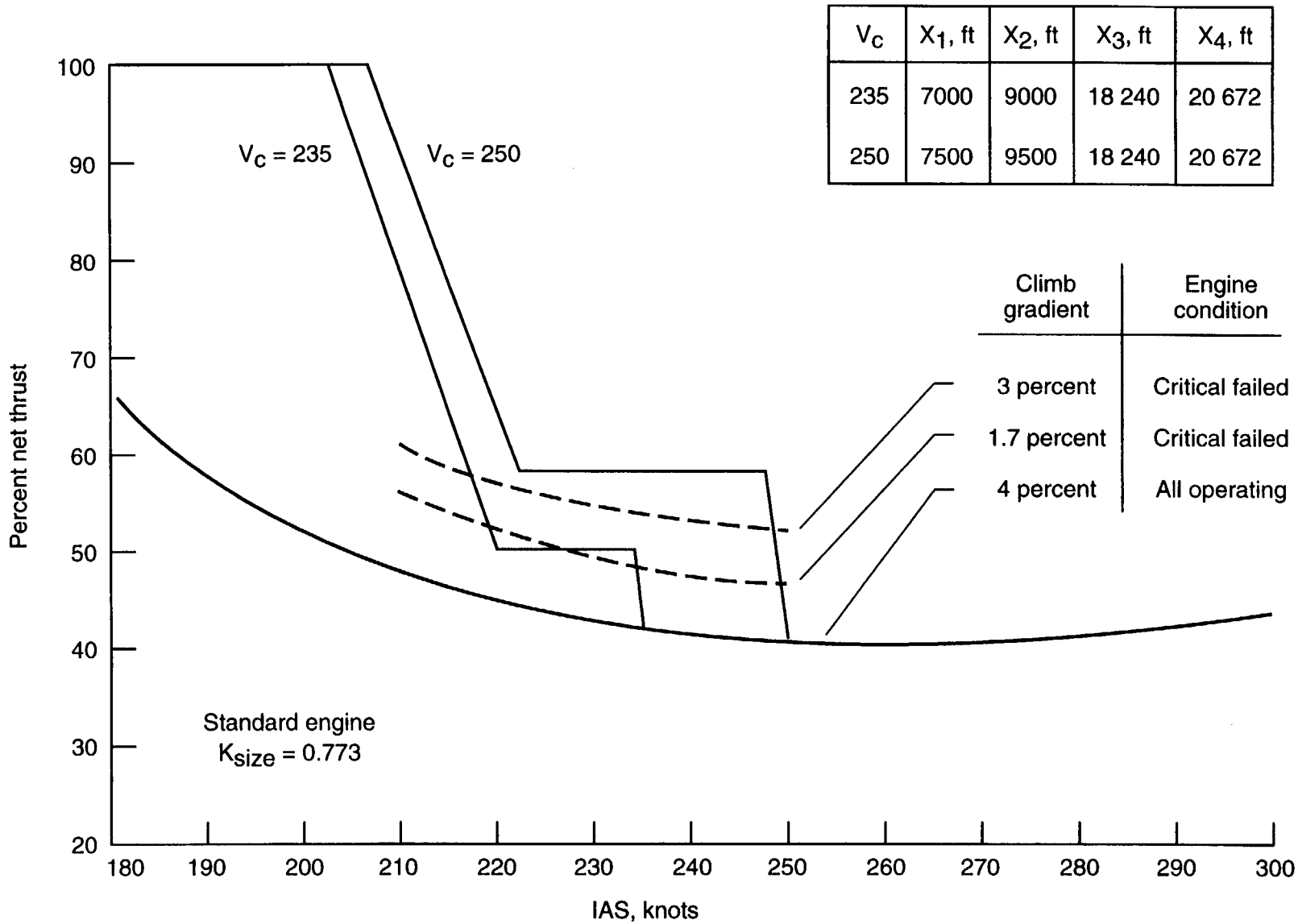

Figure E3. Engine thrust profiles for dual thrust-cutback procedure with final climb speeds of 235 and 250 knots and FAR requirements for configuration with $\Delta C_L = 0.10$.

Simulation Noise Level Comparison Summary

Shock and jet-mixing noise EPNdB values at FAR Part 36 centerline and sideline measurement stations

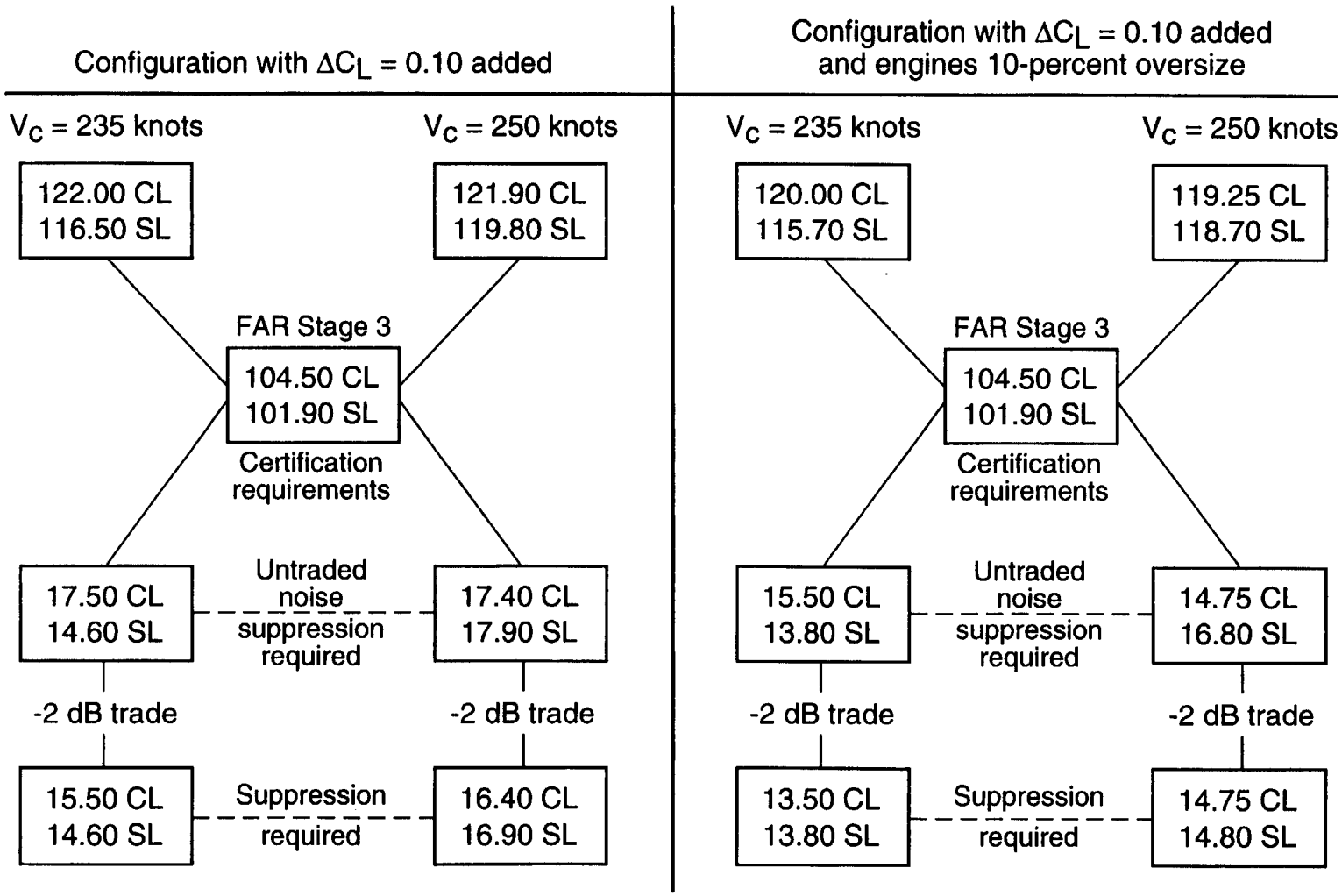

Figure E4. Noise level comparisons for piloted takeoffs with two final climb speeds.

References

1. Grantham, William D.; Smith, Paul M.; and Deal, Perry L.: *A Simulator Study for the Development and Evaluation of Operating Procedures on a Supersonic Cruise Research Transport To Minimize Airport-Community Noise.* NASA TP-1742, 1980.

2. Douglas Aircraft Co.: *New Commercial Programs: Study of High-Speed Civil Transports—Summary.* NASA CR-4236, 1990.

3. Boeing Commercial Airplanes: *High-Speed Civil Transport Study—Special Factors.* NASA CR-181881, 1990.

4. Glaab, Louis J.; Riley, Donald R.; Brandon, Jay M.; Person, Lee H., Jr.; and Glaab, Patricia C.: *Piloted Simulation Study of the Effect of High-Lift Aerodynamics on the Takeoff Noise of a Representative High-Speed Civil Transport.* NASA/TP-1999-209696, 1999.

5. Olson, E. D.: *Advanced Takeoff Procedures for High-Speed Civil Transport Community Noise Reduction.* SAE 921939, 1992.

6. Noise Standards: Aircraft Type and Airworthiness Certification. Code of Federal Regulations, Part 36, Title 14 (Parts 1 to 59), FAA, 1993, pp. 700–772.

7. Baber, Hal T., Jr.: *Characteristics of the Advanced Supersonic Technology AST-105-1 Configured for Transpacific Range With Pratt and Whitney Aircraft Variable Stream Control Engines.* NASA TM-78818, 1979.

8. Fishbach, Laurence H.; and Caddy, Michael J.: *NNEP—The Navy NASA Engine Program.* NASA TM X-71857, 1975.

9. Dieudonne, James E.; Parrish, Russell V.; and Bardusch, Richard E.: *An Actuator Extension Transformation for a Motion Simulator and an Inverse Transformation Applying Newton-Raphson's Method.* NASA TN D-7067, 1972.

10. Parrish, Russell V.; Dieudonne, James E.; Martin, Dennis J., Jr.; and Copeland, James L.: *Compensation Based on Linearized Analysis for a Six-Degree-of-Freedom Motion Simulator.* NASA TN D-7349, 1973.

11. Parrish, Russell V.; Dieudonne, James E.; and Martin, Dennis J., Jr.: *Motion Software for a Synergistic Six-Degree-of-Freedom Motion Base.* NASA TN D-7350, 1973.

12. Parrish, Russell V.; Dieudonne, James E.; Bowles, Roland L.; and Martin, Dennis J., Jr.: Coordinated Adaptive Washout for Motion Simulators. *J. Aircr.*, vol. 12, no. 1, Jan. 1975, pp. 44–50.

13. Martin, D. J., Jr.: *A Digital Program for Motion Washout on Langley's Six-Degree-of-Freedom Motion Simulator.* NASA CR-145219, 1977.

14. Zorumski, William E.: *Aircraft Noise Prediction Program Theoretical Manual.* NASA TM-83199, Parts 1 and 2, 1982.

15. Anon.: *Gas Turbine Jet Exhaust Noise Prediction.* SAE ARP 876, Mar. 1978.

16. Harper-Bourne, M.; and Fisher, M. J.: *The Noise From Shock Waves in Supersonic Jets. Noise Mechanisms.* AGARD-CP-131, Mar. 1974.

17. Tanna, H. K.; Dean, P. D.; and Burrin, R. H.: *The Generation and Radiation of Supersonic Jet Noise. Volume IV—Shock-Associated Noise Data.* AFAPL-TR-76-65, Vol. IV, U.S. Air Force, Sept. 1976. (Available from DTIC as AD A032 883.)

18. Coe, Paul L., Jr.; McLemore, H. Clyde; and Shivers, James P.: *Effects of Upper-Surface Blowing and Thrust Vectoring on Low-Speed Aerodynamic Characteristics of a Large-Scale Supersonic Transport Model.* NASA TN D-8296, 1976.

REPORT DOCUMENTATION PAGE

Form Approved
OMB No. 0704-0188

1. AGENCY USE ONLY *(Leave blank)*	2. REPORT DATE	3. REPORT TYPE AND DATES COVERED
	December 1999	Technical Publication

4. TITLE AND SUBTITLE
Piloted Simulation Study of a Dual Thrust-Cutback Procedure for Reducing High-Speed Civil Transport Takeoff Noise Levels

5. FUNDING NUMBERS
WU 537-03-22-08

6. AUTHOR(S)
Donald R. Riley, Louis J. Glaab, Jay M. Brandon, Lee H. Person, Jr., and Patricia C. Glaab

7. PERFORMING ORGANIZATION NAME(S) AND ADDRESS(ES)
NASA Langley Research Center
Hampton, VA 23681-2199

8. PERFORMING ORGANIZATION REPORT NUMBER
L-17431

9. SPONSORING/MONITORING AGENCY NAME(S) AND ADDRESS(ES)
National Aeronautics and Space Administration
Washington, DC 20546-0001

10. SPONSORING/MONITORING AGENCY REPORT NUMBER
NASA/TP-1999-209698

11. SUPPLEMENTARY NOTES
Riley, Brandon and Person: Langley Research Center, Hampton, VA; Glaab, L. J.: Lockheed Engineering & Sciences Company, Hampton, VA; Glaab, P. C.: Unisys Corporation, Hampton, VA.

12a. DISTRIBUTION/AVAILABILITY STATEMENT
Unclassified–Unlimited
Subject Category 02 Distribution:Nonstandard
Availability: NASA CASI (301) 621-0390

12b. DISTRIBUTION CODE

13. ABSTRACT ***(Maximum 200 words)***
A piloted simulation study was performed for the purpose of indicating the noise reduction benefits and piloting performance that could occur for a typical 4-engine High-Speed Civil Transport (HSCT) configuration during takeoff when a dual thrust-cutback procedure was employed with throttle operation under direct computer control. Two thrust cutbacks were employed with the first cutback performed while the vehicle was accelerating on the runway and the second cutback performed at a distance farther downrange. Added vehicle performance improvements included the incorporation of high-lift increments into the aerodynamic database of the vehicle and the use of limited engine oversizing. Four single-stream turbine bypass engines that had no noise suppression of any kind were used with this configuration. This approach permitted establishing the additional noise suppression level that was needed to meet Federal Air Regulation Part 36 Stage 3 noise levels for subsonic commercial jet aircraft. Noise level results were calculated with the jet mixing and shock noise modules of the Aircraft Noise Prediction Program (ANOPP).

14. SUBJECT TERMS	15. NUMBER OF PAGES
Piloted simulation; Takeoff; High lift; Airport-community noise; Noise certification; HSCT; ANOPP	72
	16. PRICE CODE: A04

17. SECURITY CLASSIFICATION OF REPORT	18. SECURITY CLASSIFICATION OF THIS PAGE	19. SECURITY CLASSIFICATION OF ABSTRACT	20. LIMITATION OF ABSTRACT
Unclassified	Unclassified	Unclassified	UL